PAPER BASED LATERAL FLOW BIOSENSOR FOR DETECTION OF CONTAMINANT AND INFECTION

YEW CHEE HONG @ TAKAHIRO

FACULTY OF ENGINEERING
UNIVERSITY OF MALAYA
KUALA LUMPUR

2018

PAPER BASED LATERAL FLOW BIOSENSOR FOR DETECTION OF CONTAMINANT AND INFECTION

YEW CHEE HONG @ TAKAHIRO

DISSERTATION SUBMITTED IN FULFILMENT OF THE REQUIREMENTS FOR THE DEGREE OF MASTER OF ENGINEERING SCIENCE

FACULTY OF ENGINEERING
UNIVERSITY OF MALAYA
KUALA LUMPUR

2018

UNIVERSITY OF MALAYA

ORIGINAL LITERARY WORK DECLARATION

Name of Candidate: **YEW CHEE HONG @ TAKAHIRO**

Matric No: **KGA140081**

Name of Degree: **MASTER OF ENGINEERING SCIENCE BY RESEARCH**

Title of Dissertation:

PAPER BASED LATERAL FLOW BIOSENSOR FOR DETECTION OF CONTAMINANT AND INFECTION

Field of Study: **BIOMEDICAL ENGINEERING**

I do solemnly and sincerely declare that:

(1) I am the sole author/writer of this Work;
(2) This Work is original;
(3) Any use of any work in which copyright exists was done by way of fair dealing and for permitted purposes and any excerpt or extract from, or reference to or reproduction of any copyright work has been disclosed expressly and sufficiently and the title of the Work and its authorship have been acknowledged in this Work;
(4) I do not have any actual knowledge nor do I ought reasonably to know that the making of this work constitutes an infringement of any copyright work;
(5) I hereby assign all and every rights in the copyright to this Work to the University of Malaya ("UM"), who henceforth shall be owner of the copyright in this Work and that any reproduction or use in any form or by any means whatsoever is prohibited without the written consent of UM having been first had and obtained;
(6) I am fully aware that if in the course of making this Work I have infringed any copyright whether intentionally or otherwise, I may be subject to legal action or any other action as may be determined by UM.

Candidate's Signature Date:

Subscribed and solemnly declared before,

Witness's Signature Date:

Name:

Designation:

PAPER BASED LATERAL FLOW BIOSENSOR FOR DETECTION OF CONTAMINANT AND INFECTION

ABSTRACT

Conventional diagnostic methods for detecting toxicity in water and mosquito-borne infections are very accurate, yet they are expensive to carry out as they require complicated procedures, sophisticated instrumentation and highly-skilled personnel, limiting their application in areas with poor resources. Recently, paper-based sensors, like lateral flow assays (LFA) and paper-based gas sensors have been developed to tackle the limitations of conventional diagnostic methods by leveraging the modifiability, light weight and capillary properties of paper materials. However, paper-based sensors for chemicals still suffer from the need for large instruments and complex circuitry, and the sensitivity of LFA is challenged by the low amount of target in the samples. Therefore, this study aims to develop and enhance the sensitivity of paper-based sensors for diagnostic purposes. A simple lateral flow paper-based capacitive sensor (PCS) was developed for identification and quantification of chemical liquids with the dependence of an easily obtainable cheaper multimeter. The geometry of the sensor and the conditions during application of the sensor were optimized. With an optimized geometry, PCSs, with and without pre-drying conditions, both were able to distinguish small volumes (70 µL) of liquids and quantify solutions, i.e. ethanol-water and nitrate salt solutions based on a capacitance measurement that reflects their dielectric parameters. The developed PCS was able to detect Fe (III) ions up to 1mM, a concentration too low for the naked eye to detect. The sensitivity of a paper-based LFA was enhanced by realizing fluidic control through the induction of coating on the nitrocellulose (NC) membrane with hydrophobic electrospun polycaprolactone (PCL) nanofibres. FESEM and wettability analyses were performed to study the structural morphology and the hydrophobicity of the electrospin-

coated NC membrane, respectively. The modified LFA was able to detect 0.5 nM of synthetic Zika virus DNA, a 10-fold of signal enhancement relative to the unmodified LFA. As a proof of concept, the developed PCS and electrospin-coating method demonstrate great potential for sensitive detection of toxicity and infection in paper-based lateral flow diagnostic platforms.

Keywords: Paper-based lateral flow sensor, capacitive sensor, electrospinning, sensitivity, diagnostic detection

ALAT BIO-PENGESAN ALIRAN SISI BERDASARKAN KERTAS UNTUK PENGESANAN BAHAN CEMAR DAN JANGKITAN

ABSTRAK

Kaedah-kaedah diagnosis konvensional bagi mengesan kadar racun dalam air dan jangkitan bawaan nyamuk adalah sangat tepat, namun kos adalah mahal kerana melibatkan prosedur yang rumit, instrumen yang canggih, pengendali yang mahir; ini mengehadkan penggunaannya di kawasan mempunyai sumber terhad. Kebelakangan ini, alat pengesan berasaskan kertas, seperti ujian aliran sisi (LFA) atau alat pengesan gas berasaskan kertas telah dihasilkan untuk mengatasi kelemahan dalam cara-cara diagnosis konvensional dengan memanfaatkan sifat-sifat kertas seperti kebolehubahsuaian, ringan dan kapilari. Namun, alat pengesan berasaskan kertas untuk bahan kimia memerlukan instrumen yang besar, reka litar yang rumit dan kepekaan, dan LFA pula masih diterhadkan oleh kepekatan sasaran yang rendah dalam sampel. Oleh yang demikian, kajian ini bertujuan untuk membina dan mempertingkatkan kepekaan alat pengesan berasaskan kertas bagi kegunaan diagnostik. Alat pengesan kapasitif aliran sisi berasaskan kertas (PCS) yang ringkas telah dibina untuk pengenalpastian dan kuantifikasi cecair kimia dengan menggunakan multimeter yang mudah didapati dan murah. Geometri dan keadaan semasa penggunaan alat pengesan tersebut telah dioptimumkan. Dengan geometri yang optimum, PCS, dengan atau tanpa pra-pengeringan, dapat membezakan cecair dan menyukat kepekatan larutan berisipadu kecil (70 µL), seperti etanol-air dan larutan garam nitrat berdasarkan pengukuran kapasitans yang mencerminkan parameter dielektrik. PCS yang dihasilkan mampu mengesan ion Fe (III) sehingga 1 mM, di mana kepekatan ini adalah terlalu rendah untuk pemerhatian mata kasar. Selain itu, kepekaan LFA telah dipertingkatkan dengan realisasi kawalan fluidik melalui pengenalan salutan nanoserat elektrospin hidrofobik polikaprolakton (PCL) pada

lembaran nitroselulosa (NC). FESEM dan analisis kebolehlembapan dijalankan untuk mengkaji struktur morfologi dan hidrofobisiti lembaran NC bersalut-elektrospin. LFA yang diubahsuai dapat mengesan 0.5 nM DNA sintetik virus Zika, iaitu pencapaian 10-kali ganda peningkatan isyarat berbanding dengan LFA yang tidak diubahsuai. Sebagai bukti konsep, PCS dan kaedah salutan-elektrospin berpotensi besar untuk mengesan kadar racun dan jangkitan dengan lebih peka pada platform diagnostik aliran sisi.

Kata kunci: Alat pengesan aliran sisi berasaskan kertas, alat pengesan kapasitif, elektrospinning, kepekaan, pengesanan diagnostik

ACKNOWLEDGEMENTS

Firstly, I would like to express my sincere gratitude to my supervisor at the University of Malaya, Associate Prof. Ir. Dr. Belinda Pingguan-Murphy for her advice, support and guidance throughout my studies.

I would also like to thank Prof. Dr. Feng Xu, all the team members of point-of-care group, especially Jie Hu and others in Bioinspired Engineering and Biomechanics Center, Xi'an JiaoTong University, PRC for the opportunity to learn and discover new things beyond my basic knowledge in biotechnology. They have encouraged me to open my mind towards a more critical understanding of research. The gratitude is extended to Dr. Ming Liu and his students who provided the usage of LCR meter for testing for free during my attachment in Xi'an JiaoTong University.

I would like to express my gratitude to the post-doctoral fellow in Tissue Engineering Lab, University of Malaya, Dr. Pedram Azari for giving me guidance and support on the electrospinning methods and publication. Also, the gratitude should be extended to all the lab members in Tissue Engineering Lab who have given help and support on the experiments and material preparation.

Last but not least, I am always in debt to my parents and my brother for their endless love and care. I appreciate all the help and support from all of you that I couldn't mention. Thank you very much.

TABLE OF CONTENTS

LIST OF FIGURES

LIST OF TABLES

LIST OF ABBREVIATIONS

AC	:	Alternating current
AcOH	:	Acetic acid
Ag	:	Silver
ASSURED	:	Affordable, Sensitive, Specific, User-friendly, Rapid and robust, Equipment-free, and Deliverable
Au	:	Gold
AuNP-DP	:	Gold nanoparticle
BSA	:	Gold nanoparticle-detecting probe conjugate
CANF	:	Cellulose acetate nanofibres
$Cd(NO_3)_2$	:	Cadmium(II) nitrate
cDNA	:	Complementary DNA
CDS	:	Coding DNA sequence
CH_2Cl_2	:	Dichloromethane
CHCl3	:	Chloroform
Cr(NO3)3	:	Chromium(III) nitrate
Cu	:	Copper
DEG	:	Diethylene glycol
DMF	:	N, N-dimethylformamide
DMSO	:	Dimethyl sulfoxide
DNA	:	Deoxyribonucleic acid
E. coli	:	Escherichia coli
EA	:	Ethyl acetate
EG	:	Ethylene glycol

EIS	:	Electrochemical impedance spectroscopy
ELISA	:	Enzyme-linked immunosorbent assay
ETA	:	Ethanolamine
EtOH	:	Ethanol
Fe	:	Iron
$Fe(NO_3)_3$	:	Iron (III) nitrate
FESEM	:	Field emission scanning electron microscope
H_2O_2	:	Hydrogen peroxide
HBV	:	Hepatitis B virus
Hg	:	Mercury
iPrOH	:	Isopropyl alcohol
KB	:	$Polystyrene_{8K}$-block-poly(ethylene-ran-butylene)$_{25K}$-block-$polyisoprene_{10K}$-Brij76
KNO_3	:	Potassium nitrate
LFA	:	Lateral flow assay
LOD	:	Limit of detection
LSPR	:	Localized surface plasmon resonance
MeOH	:	Methanol
$Mn(NO_3)_2$	:	Manganese(II) nitrate
MO	:	Mineral oil
N_2H_4	:	Hydrazine
$Na_2B_4O_7$	:	Sodium borate
$Na_2C_{10}H_{16}N_2O_8$ ($EDTANa_2$)	:	Disodium ethylenediaminetetraacetate
$Na_2C_2O_4$	:	Sodium oxalate
Na_2HPO_4	:	Disodium hydrogen phosphate
Na_2SO_4	:	Sodium suphate

$Na_3C_6H_5O_7$	:	Trisodium citrate
Na_3PO_4	:	Trisodium phosphate
NaCl	:	Sodium chloride
NaH_2PO_4	:	Sodium dihydrogen phosphate
$NaHCO_3$	:	Sodium bicarbonate
$NaNO_3$	:	Sodium nitrate
NC	:	Nitrocellulose
NH_3	:	Ammonia
OA	:	Oleic acid
OD	:	Optical density
$Pb(NO_3)_2$	:	Lead (II) nitrate
PBS	:	Phosphate buffer saline
PCL	:	Poly(ε-caprolactone)
PCR	:	Polymerase chain reaction
PCS	:	Paper-based capacitive sensor
PDMS	:	Poly(dimethylsiloxane)
PEG	:	Poly(ethylene glycol)
PLA	:	Poly(lactic acid)
POC	:	Point-of-care
PPy	:	Poly(pyrrole)
PVC	:	Poly(vinyl chloride)
qPCR	:	Quantitative polymerase chain reaction
RH	:	Relative humidity
SDS	:	Sodium dodecyl sulphate
SSC	:	Saline sodium citrate
THF	:	Tetrahydrofuran

UPW	:	Ultrapure water
USEPA	:	United States Environmental Protection Agency
WHO	:	World Health Organisation

LIST OF SYMBOLS

A	:	Overlapping area under the conducting plates
A_c	:	Capacitance area
A_p	:	Area of filter paper
C_a	:	Capacitance of air
C_{a*}	:	Capacitance of air after drying
C_c	:	Capacitance of cellulose
C_f	:	Capacitance of filter paper
C_p	:	Capacitance of PCS
C_{s1}	:	Capacitance of sample fluid
C_{s2}	:	Capacitance of sample solute
D	:	Capacitance of double-sided tape
d	:	Pore diameter
d_p	:	Distance between the conducting plates
d_t	:	Thickness of filter paper
h or L	:	Wicking liquid front height
K	:	Permeability
L_c	:	Length of conducting plates
L_l	:	Length of loading region
R	:	Effective pore radius
S	:	Wicking speed
t	:	Time
$tan\ \delta$	:	Dissipation factor or dielectric loss
V_p	:	Volume of filter paper
V_{void}	:	Void volume

W_c	:	Width of conducting plates
W_l	:	Width of loading area
W_s	:	Width of PCS
ε_0	:	Dielectric constant of free space
ε_c	:	Dielectric constant of cellulose
ε_p	:	Dielectric constant of filter paper
ε_r	:	Relative permittivity or dielectric constant
ε_t	:	Dielectric constant of double-sided tape
η	:	Effective porosity of filter paper
η^*	:	Modified effective porosity of filter paper
θ	:	Contact angle
μ	:	Viscosity
σ or γ	:	Interfacial tension

LIST OF APPENDICES

CHAPTER 1: INTRODUCTION

1.1 Background

Human health can deteriorate by diseases which are caused by toxicity and infections. When toxic chemical contamination of food and water, e.g. high concentration of heavy metal ions or organic liquid goes undetected and consumed, it may cause acute symptoms like gastrointestinal upset, coma and death (Bernhoft, 2012; Friberg & Vostal, 1972) and stunted growth in long term. Apart from chemicals, infection like mosquito-borne diseases, e.g. dengue, Zika, chikungunya, etc. could also impair foetal growth and brings deaths to people, especially from tropical countries. There have been 1,950 cases of microcephaly out of 1,673,272 cases of Zika infection in Brazil during 2015-2016 (de Oliveira et al., 2017), while 20,000 lives are claimed by dengue fever every year globally (Carabali, Hernandez, Arauz, Villar, & Ridde, 2015). Despite being highly sensitive and accurate, conventional methods like flame atomic absorbance spectrometry for heavy metal analysis, liquid chromatography coupled with mass spectrometry for organic chemical analysis and quantitative polymerase chain reaction (qPCR) for nucleic acid analysis require expensive, bulky, and heavy instruments and skilled personnel for operations (Jane Ru Choi et al., 2017; Dasbasi, Sacmaci, Ulgen, & Kartal, 2015; Tobin, Walsh, Garvey, & Larkin, 2014). These operations are time, energy and resource consuming, labour intensive, lab centralized and therefore unsuitable for *in situ* applications in remote areas, like rural villages where resources are limited. Hence, to address and treat toxicity and infections associated diseases, it is of high priority to develop an affordable, rapid and sensitive method for toxicity and clinical screening at point-of-care (POC).

Advances in the development of microfluidics and nanotechnology have resolved several problems in the conventional methods while retaining comparable sensitivity and

specificity (Sun, Xianyu, & Jiang, 2014). These methods implement nanoparticles properties into miniaturized microfluidic devices that use a small volume of reagents and process a small volume of sample (D. Liu, Wang, & Jiang, 2011; Zeng, Baillargeat, Ho, & Yong, 2014). However, the usage of laboratory instruments for analysis and complex fabrication of chip-based microfluidic devices (integration of many functional units like shunts and pumps) may reduce their suitability of POC diagnostic purpose (Hawkins & Weigl, 2010). Meanwhile, dielectric properties that are specific to the innate electronic configurations of a particle and its resistance to an external field (Kirkwood, 1939; Lide, 2004) may be represented by capacitance as capacitance is directly proportional to the dielectric constant. Chemical and biological targets such as water, organic compounds, proteins, and nucleotides can be detected by the capacitive measurement of dielectric performance (Berney et al., 2000; Han, Kim, Li, & Meyyappan, 2012; Patel et al., 2003; Qureshi, Niazi, Kallempudi, & Gurbuz, 2010). However, the complex design of the device circuitry, refined modifications and preparation of chemicals limit its application in POC diagnostics. Therefore, the development of a low-cost, readily disposable, and simplified device to identify a substance is still needed.

Paper-based platforms for diagnostics, when compared to other methods, are simpler to apply (Liana, Raguse, Gooding, & Chow, 2012). Paper test strips such as dipsticks, test strips for specific metal ions and immunoglobulins, lateral flow assay (LFA) and blood glucose test kits are commercialised in the market, therefore indicating its public interest in POC (Yetisen, Akram, & Lowe, 2013). However, many commercial paper test strips for heavy metals do not fulfil the demand of lowest limit of detection (LOD) set by international regulators. In addition, the low levels of targets in limited biological samples volume restricts the direct application of paper-based assays for disease diagnosis, unless high sensitivity can be achieved (Posthuma-Trumpie, Korf, & van Amerongen, 2009).

Recent efforts to enhance sensitivity in paper-based sensors and assays are based on signal amplification by additional probe, label aggregation, sample pre-concentration and flow control (Choi, Liu, et al., 2016; J. Hu et al., 2013; Lan et al., 2016; Tang et al., 2016). Flow control on a paper-based platform may be realized through the addition of a barrier to impede capillary action or lengthen the time for reactions (Sajid, Kawde, & Daud, 2015). However, most of them requires multi-steps procedures and costly equipment to function. Structurally similar to paper, electrospun nanofibres have many biomedical applications (Thenmozhi, Dharmaraj, Kadirvelu, & Kim, 2017). A few applications of electrospun nanofibres modified with biological probes enable specificity towards detection of biomolecules during lateral flow (D. P. Li, Frey, & Baeumner, 2006; Reinholt, Sonnenfeldt, Naik, Frey, & Baeumner, 2014). Perhaps because hydrophobicity obstruct wetting, many have overlooked this property of electrospun nanofibres for sensitivity enhancement in lateral flow sensors or assays.

This study proposes a proof of concept to realize a simple detection of potential toxic chemicals in contaminated water, such as various organic liquids and ions, by a low-cost parallel plate paper-based capacitive sensor (PCS) with the utilization of an affordable and easily obtainable multimeter. Due to the distinct dielectric characteristics of every substance, the combination of paper and dielectric performances enables identification and quantification of liquid chemical substances with PCS. Furthermore, flow manipulation is applied on the paper material by introducing hydrophobicity to increase the sensitivity of existing paper-based assays. Here, LFA is used as a model to realize flow manipulation by coating poly(caprolactone) (PCL) nanofibres onto nitrocellulose (NC) membrane with electrospinning. The impact of electrospin-coating on the membrane surface structure and sensitivity of standard LFA are observed. Such a method is suggested to improve sensitivity in other paper-based platforms as well.

1.2 Aim and Objectives

This study aims to develop and enhance paper-based lateral flow sensors for diagnosis and testing. The specific objectives are as follows:

i. To develop and optimize a paper-based capacitive sensor (PCS) for the identification and quantification of chemical fluids
ii. To enhance the sensitivity of paper-based assays, *i.e.* LFA, with electrospinning for biomedical application

1.3 Dissertation's outline

The following enlists the brief description of the chapters in this dissertation.

Chapter 1 presents the introduction of this dissertation that overviews the background, aim, objectives and research question of the study. The outline of this dissertation is also described in this chapter.

Chapter 2 provides the critical literature reviews of this study. Factors of disease manifestation, which divided to chemical toxicity and infection, are discussed at first. The conventional approach and the development of paper-based sensors for diagnosis and testing are then discussed. Based on the idea of a sensor for POC testing, paper-based and capacitance-based method are further discussed. Following the ever-growing demand of sensitivity in development of paper-based sensor, the application and advantage of electrospinning are also discussed.

Chapter 3 describes the simple development of a user-friendly, low-cost PCS as a proof of concept to identify and quantify toxic chemical liquid or solution by capacitance measurement using multimeter and LCR meter.

Chapter 4 presents a method to manipulate liquid flow by electrospin-coating NC membrane as an approach to ameliorate the sensitivity of LFA for nucleic acid testing.

Chapter 5 concludes the findings of the dissertation, the arising challenges during the study, and the suggestions for possible future study.

CHAPTER 2: LITERATURE REVIEW

2.1 Public health concerns

The war between disease and vitality is never-ending. Developments in medicine and technology may help to reduce the burden of disease. Yet, the rise of new diseases may occur due to *de novo* mutations in humans, parasites and microbes (Acuna-Hidalgo, Veltman, & Hoischen, 2016). Many diseases exist as manifestations of chemical toxicity, pathogenic infection and parasitic infestation (Karlsson, Kwiatkowski, & Sabeti, 2014).

Chemical toxicity is generally caused by excessive intake of substances which the body cannot not make use of or repel efficiently. Despite water being essential for life, uncontrolled human activities following urbanization has often caused contamination of clean freshwater (Kumar Reddy & Lee, 2012). In Malaysia, notable cases before 2014 were due to oil spillage and high ammonia (NH_3) levels (Kamsari, 2014). In 2015, iron (Fe) and bauxite dust from mining activities was washed away by rainwater to the river and sea near Kampung Selamat, Pahang, causing contamination to the water (Tariq, 2015) and the level of heavy metals in the water exceeded the allowable limit set by the corresponding authority (Karim & Shah, 2015). Common acute symptoms of heavy metal poisoning may manifest as gastrointestinal upset (Bernhoft, 2012; G. Z. Lin, Wu, Yan, Li, & Liu, 2012) while higher severities result in coma and death (Friberg & Vostal, 1972). In another example, lead toxicity causes stunted growth in children (Needleman & Bellinger, 1991), anaemia in pregnant women and teratogenicity in foetuses (Shannon, 2003). As a secondary contaminant, Fe toxicity causes metabolic acidosis, hypovolemic shock and even physiologic immaturity of developing organs (Valentine, Mastropietro, & Sarnaik, 2009). Heavy metals may also damage DNA (Dieguez-Acuna et al., 2004), leading to cell death (Pieper et al., 2014) and carcinogenesis (Goyer, 1990) by

complicating gene expressions. The United States Environmental Protection Agency (USEPA) has regulated the maximum contaminant level of Fe and lead in drinking water to 0.3 mg L^{-1} and 0.015 mg L^{-1}, respectively (USEPA, 2017a, 2017b).

Organic chemical toxicity happens when excessive organic chemicals are metabolised in the body. For instance, the metabolism of ethanol (EtOH) produces acetaldehyde and reactive oxygen species that induce cell apoptosis and steatosis in hepatocytes (Louvet & Mathurin, 2015), and impose injury and degeneration to the mature and foetal neural cells (de la Monte & Kril, 2014). Another example shows that extreme toluene intake through an intoxication inhalant results in dyspnoea and severe academia, a consequence of profound metabolic acidosis (Dickson & Luks, 2009). While the lethal dose of ethylene glycol (EG) for a human is around 100 mL kg^{-1} body weight (Freidman, Greenburg, Merrill, & Dammin, 1962), excessive intake causes acidosis, elevated anion gap and osmolality gap, rapid respiration, cold skin, vomiting, blood-tinged urine, confusion, and finally stupor and prostration. Victims could die within two days of ingestion depending on the amount of ingestion and the rate of treatment received (Freidman et al., 1962).

Pathogenic infections are mainly caused by transmission of pathogens, such as viruses, viroids, bacteria, fungi, etc. that emerge or re-emerge from adaptive genetic changes (Karlsson et al., 2014). These mutations often result in stronger pathogens that defy the body's immune system, and the existing antimicrobial effect of drugs (Hassell, Begon, Ward, & Fevre, 2017). In Malaysia, dengue, chikungunya and malarial fever are the most common and imperishable mosquito-borne infectious diseases at present (Shafie, Roslan, Ngui, Lim, & Sulaiman, 2016). Globally, dengue fever has taken around 20,000 lives each year (Carabali et al., 2015). Meanwhile, the recent infamous Zika virus infection outbreaks in central and south America, especially Brazil, have been related to microcephaly cases in foetuses. The Asian serotype which was first discovered in Pahang,

Malaysia is believed to have spread to other parts of the peninsula and Borneo island (Jamal, Sam, Chan, Vythilingam, & Sulaiman, 2016). Zika often cannot be differentiated from dengue and chikungunya due to similar transmission vectors, early symptoms, and serological conditions that result in cross-reactivity and false diagnosis (Waggoner & Pinsky, 2016). Currently, there are no vaccines for dengue and Zika virus infections.

In addition to the diseases, clinical or medical services often lack access, especially in rural or remote areas in underdeveloped and developing countries, due to limited infrastructure, resource, skilled practitioner and healthcare management. Many deaths are avoidable if early rapid diagnosis and suitable treatments are given. Therefore, simple, portable and affordable diagnostic platforms are needed to develop and augment healthcare by controlling and monitoring disease and toxicity in water and food.

2.2 Conventional Diagnostic Platform

Conventional methods often give highly sensitive and specific results from the analysis for detection. These methods are studied to improve their accuracy, and combined with on-line sample pre-treatment steps to enhance the tracing process.

For instance, atomic absorption spectrometry (Alothman, Unsal, Habila, Tuzen, & Soylak, 2014), inductively coupled plasma emission spectrometry (Y. A. Zhang et al., 2015), and potential stripping (Jagner, 1978) are used for heavy metal ion determination and analysis. For organic chemicals, methods like liquid chromatography and gas chromatography combined with tandem mass spectrometry (Tobin, 2014), and high-performance liquid chromatography combined with water or solid phase extraction (Watanabe, Kobara, Baba, & Eun, 2013) are used to detect several pesticide residues in vegetables. Despite having very high detection limits, i.e. 3.48 ng L^{-1} to 5.2 µg L^{-1}, these methods require large equipment and complicated operational setting (Alothman et al., 2014; Hocevar, Wang, Deo, & Ogorevc, 2002; Y. A. Zhang et al., 2015). The whole

preparation, detection and analysis process may take hours as shown in the potentiometric stripping analysis, with more than 1 hour of plating (Jagner, 1978). The working concept of the instruments is important, but preparations are normally tedious, complex and dangerous to carry out, as it sometimes requires mercury (Hg) film and organic solvents (Jagner, 1978).

Bacterial and viral infection can be determined through selective culture media and biomolecular analysis like polymerase chain reaction (PCR) and enzyme-linked immunosorbent assay (ELISA) (Delbeke et al., 2015; Fongaro et al., 2013; Waggoner & Pinsky, 2016). In fact, the recommended practice for identification of Shiga-toxin producing *E. coli* infection is to have simultaneous culture and non-culture assays for Shiga-toxin that follows with molecular characterizations (Gould, 2012). Despite the combination of qPCR and ELISA being the gold standard to detect infectious agents like viruses and bacteria, skilled personnel are needed to handle large, heavy and expensive instruments that can only be established in a heavily secured laboratory (Peeling et al., 2010). For instance, qPCR, ELISA and culture for infectious agents need to be done in an aseptic environment to avoid cross-contamination while instruments are needed to accommodate the reactions. In addition, the bacterial culture and plague assays takes up 3 – 7 days while further biochemical or molecular tests for positive result confirmation would take an extra 2 – 3 days (Bhunia, 2014). Meanwhile, PCR needs several hours to amplify the genes of interest. Along with the time taken for sample pre-treatment, these methods result in delayed diagnosis, even though a high sample volume is required. Development of simpler, small-sample volume, and rapid diagnostic methods for assessing chemical toxicity and detecting disease is therefore highly important.

2.3 Sensor Diagnostic Platform

According to WHO, the criteria of an ideal point-of-care (POC) sensor are affordable, sensitive and specific, user-friendly, rapid and robust, equipment-free, and deliverable (ASSURED). Methods are explored to deliver an all-round sensor that can carry out qualitative and quantitative analysis of chemical and biochemical compounds in a remote area (Cordeiro, Ferreira Carlos, Pedrosa, Lopez, & Baptista, 2016).

Electrochemical sensors have been developed for chemical, biochemical and biological detection. Chronoamperometry (Castaneda, Alegret, & Merkoci, 2007), anodic stripping voltammetry (Nie et al., 2010), cyclic voltammetry (S. J. Liu, Nie, Jiang, Shen, & Yu, 2009), differential pulse voltammetry (Rajawat, Srivastava, & Satsangee, 2012), square wave voltammetry (Zhu et al., 2009) and electrochemical impedance spectroscopy (EIS) (Z. Lin, Li, & Kraatz, 2011) are some analyses that characterise a target detection. Despite the simplification of procedures and enhancement of the sensing part compared to conventional methods, electrochemical sensors still require a separate step with an extra instrument. Therefore, professional personnel are needed to fulfil the detection and analysing steps, as well as translating the information to an end-user.

Apart from electrochemical sensors, the visual changes in optical sensors, i.e. fluorometry, colourimetry or luminescence, enable direct judgement during the detection process. In fluorometric detection, quantum dots (Jiao, Zhang, Liang, Peng, & Lin, 2014) and fluorescent dyes (Chatterjee et al., 2009) may be modified for the detection of heavy metals, biomolecules and pathogens. The detection method may be referred to an induction (Chatterjee et al., 2009) or quenching of fluorescence (Huang et al., 2016; Jiao et al., 2014). Meanwhile, a colourimetric sensor utilises chemical probes for chromogenic detection of chemicals (H. N. Kim, Ren, Kim, & Yoon, 2012) and biological molecules (Piriya et al., 2017). For example, the presence of Hg^{2+} produces a bluish colour from

colourless solutions in a reusable chromofluorogenic chemodosimeter at a concentrations as low as 2 ppb (Ros-Lis, Marcos, Martinez-Manez, Rurack, & Soto, 2005). Gold nanoparticles (AuNPs) are frequently used in the detection of ions and organic molecules (D. Liu et al., 2011), especially in biosensors due to their surface properties which facilitate reaction with metallic ions and nucleic acid (He, Liu, Wang, Cai, & Jiang, 2011). Moreover, it can be functionalized for more specific biomolecular targeting (Cordeiro et al., 2016). Combining with localized surface plasmon resonance (LSPR), the heavy metal ion can alter the surrounding or the surface of the AuNPs, thus making detection feasible by measuring the change in wavelength (Park, Byun, Yim, & Kim, 2016). However, the main drawback of the fluorometric and colourimetric method is the lack of a simplified procedure, as most reactions require multiple steps to acquire the final results.

2.3.1 Dielectric or capacitance-based detection

A substance can be affected by an external field based on their kinetic, magnetic and electrical properties. An external electrical field would render the particles in a medium to displace from its original position based on its polarity and interactions with neighbouring molecules (Kirkwood, 1939). The dielectric constant or relative permittivity relates to this ability of a substance relative to free space, as a medium to interact with the external electric field.

Applications of the dielectric constant in sensors involve assessing changes to the dielectric properties caused by chemical reactions between the sensor and target. Capacitance is in turn related to the dielectric properties. The dielectric constant can be derived automatically in an instrument, or manually calculated from capacitance measurement. Existing application of detection or examination methods has been shown beneficial in fields like biomedicine (Dawan et al., 2011; Shrestha, Yeung, Mills, Lewington, & Tsang, 2007), microbiology (Samanman, Kanatharana, Chotigeat,

Deachamag, & Thavarungkul, 2011), chemical hazard control (Patel et al., 2003; Shuster, Baltianski, Tsur, & Haick, 2011) and environmental condition measurement (Han et al., 2012; Mraovic, Muck, Pivar, Trontelj, & Pletersek, 2014). For instance, integration of a radio frequency identification chip on a package surface identifies the surrounding relative humidity (RH) wirelessly at 23 °C but the reproducibility of the sensor is poor (Mraovic et al., 2014). To recognize bio-targets, antibodies (Dawan et al., 2011; Samanman et al., 2011) or single-stranded DNA (Shrestha et al., 2007) are used as recognizing probes. Chemiselective materials are used as the dielectric material or integrated with the electrode to selectively and sensitively react with the chemical targets (Han et al., 2012; Patel et al., 2003; Shuster et al., 2011). Paper, as a hygroscopic porous material can also be utilized to measure moisture content in the air or RH based on the change in relative permittivity (Han et al., 2012; Mraovic et al., 2014; Shuster et al., 2011).

Although non-paper-based dielectric or capacitive sensors have been developed to detect various substances with a high limit of detection, many complex designs of circuitry and integration of other electronic devices may render high cost and complex fabrication (Lötters et al., 2015). The necessity of an external large instrument for analysis involves sophisticated procedures and thus it can only be managed by skilled personnel. The design of the sensor in terms of the functionality and material should be simplified for easier usage.

2.3.2 Paper-based sensors

Paper-based biosensors are affordable, miniaturised and portable due to the low cost, light weight and modifiability of paper (J. Hu et al., 2014). While normal assays involve sophisticated in-tube procedures and multiple steps for sample preparation and analysis, paper-based assays leverage the porous structure of paper that enables wicking of fluid to

carry out the automated delivery of reagents with capillary action (Jane Ru Choi et al., 2017). Manipulation of fluidics is realized on the paper-based sensor by creating patterns or channels with wax patterning (H. Liu, Li, & Crooks, 2013; H. Wang et al., 2014) or photolithography (Nie et al., 2010). Manually, a paper origami sensor can also be folded to realize fluid manipulation for transfer and reaction (W. Li et al., 2016). Paper-based assays have been applied to various detections, such as pathogens (Bruno, 2014), proteins (Ge, Wang, Song, Ge, & Yu, 2012), nucleic acids (Choi, Hu, Tang, et al., 2016), chemicals (Xing et al., 2015), drugs (Taranova et al., 2013) and heavy metals (M. Li et al., 2015). These assays may include paper-based microfluidic sensors (Y. Zhang, Zuo, & Ye, 2015), LFA (Bruno, 2014; Xing et al., 2015) or even sensors that makes use of "patterned" paper as a supporting substrate (Feng et al., 2013; M. Li et al., 2015). Colourimetry (M. Li et al., 2015), fluorometry (Feng et al., 2013) or electrochemistry (M. Zhang et al., 2013) are some principles used for detection of paper-based sensors.

Electrochemical paper-based sensors commonly employ a three-electrode system where the three electrodes can be screen-printed, inkjet-printed or drawn on the paper with inexpensive conductive ink or pencil (Hossain & Brennan, 2011; Z. D. Li et al., 2016; Wu et al., 2015). Other than changing the electrolyte or the platform design, the detection's sensitivity and specificity can be enhanced through modification or usage of different electrodes (Allibai Mohanan, Kacheri Kunnummal, & Biju, 2016; Apilux et al., 2010; Govindhan, Lafleur, Adhikari, & Chen, 2015). Like conventional electrochemical methods, paper-based electrochemical sensors are still unable to avoid the usage of large electrochemical workstations or electroanalytical instruments. Despite the detection methods being greatly simplified, they are still limited to lab-centralized applications.

Paper-based optical sensors can rely either only on lateral flow (Hossain & Brennan, 2011) or on both lateral and vertical flows (Ge et al., 2012) of fluid on a paper material.

Paper-based immunoassays, such as immunodot-blot and slip-pad are analysed based on the colourimetric changes of the assays (H. Liu et al., 2013; Wong, Cabodi, Rolland, & Klapperich, 2014). Although many paper-based optical assays have high LOD, and good sensitivity and specificity, many still require separate sample addition to the testing region (M. Li et al., 2015). While some require complicated paper folding and washing steps, the signals do not last long under the light (Ge et al., 2012).

Therefore, there is a need for a simple paper-based sensor. Meanwhile, lateral flow assay (LFA), a commercial paper-based assay, is easy to fabricate and only requires one step to carry out detection.

2.4 Lateral flow assay

LFA has been employed as a pre-clinical diagnostic tool at POC for many infectious diseases and chemicals. It is a paper-based assay that is assembled by different paper materials on a piece of single-sided adhesive backing card, i.e. glass fibre as the conjugating and sample pad, NC membrane for target capturing and detection, and cellulose card as the absorbent pad (J. Hu et al., 2014). A control line and a test line are generated on a NC membrane by dispensing control probes and capture probes while label-tagged detecting probes are dispensed onto the conjugation pad. Metal nanoparticles, especially gold (Yang, Duan, Li, Wang, & Guo, 2012) and coloured latex particles (Posthuma-Trumpie et al., 2009), are commonly used as label particles in the LFA. The surface of the labels can be modified with detecting probe, *i.e.* antibodies, nucleotides or other elements to facilitate interactions and detection. As the sample is applied to the assay, the target in the sample will interact with the label-tagged detecting probe on the conjugation pad while wicking to the NC membrane, where it will be captured on the test line or control line (Sajid et al., 2015). The mode of detection in LFA is often colourimetric (Tang et al., 2017), but extra equipment could extend to

electrochemical detection (Luo et al., 2012). For colourimetric analysis, image processing of the test line's colour on the assay can be done using a smartphone camera and imaging applications (Yu et al., 2015). Detection of inorganic chemicals (Fang et al., 2010) and biomolecules (Peng et al., 2016) has been feasible using LFA.

2.4.1 Advancement of LFA sensitivity

A low cost, simple to use and rapid assay like LFA could become an alternative to conventional assays like ELISA, which take more than 1 hr to process and analyse. Due to the low concentration of targets in a limited volume of sample, the results from current commercial LFAs alone are still less credulous for further clinical action. Such issues have stimulated many studies to increase the sensitivity of the assay, an enhancement which may be achieved by physical and molecular methods.

To enhance the sensitivity of LFA by the molecular approach, the surface of the label molecules can be treated to acquire an increment of signal intensity. For example, a metallic shell of noble metals like silver (Ag^0) and gold (Au^0) is deposited on the surface of AuNPs due to the reduction of their ions, Ag^+ and Au^{3+}. The deposition increases the size and density of AuNPs, therefore changing its wine-red colour to darker tones. This visible colour change is a result of LSPR effect that is affected by the density of the nanoparticles and the refractive index of the solution (Cordeiro et al., 2016). For instance, the use of Ag enhancement in lateral flow immunoassay boosts the sensitivity of detection for ochratoxin A (Anfossi, Di Nardo, Giovannoli, Passini, & Baggiani, 2013) and prostate-specific antigen (Rodriguez, Covian, Garcia, & Blanco-Lopez, 2016) by 10-fold and 3-fold, respectively. Other than noble metals, the surface of AuNPs can also be modified with ligands to aid in signal amplification. The amplification is based on aggregation of AuNPs that is connected by the ligands. This connection can be facilitated by specific bonding like antigen-antibody, enzyme-substrate and complementary nucleic

acid hybridization. For example, detection of *E. coli* O157: H7 in milk and casein has been boosted 100-fold and 1000-fold using antigen-antibody and enzyme-substrate approaches, respectively (M. Chen et al., 2015; Cho, Bhunia, & Irudayaraj, 2015). In another approach, the nucleic acid hybridization-based method has also increased the sensitivity of human immunodeficiency virus type 1 DNA and Cu^{2+} ion detection for 2.5-fold and 80-fold, respectively (J. Hu et al., 2013; Y. Wang et al., 2017). Nevertheless, molecular approaches are not cheap due to the additional AuNP usage, the noble value of Au and Ag, and the high cost of ligand synthesis. The protein-based ligands require complicated preparation steps and are unstable due to heat and pH sensitivity, batch-variations and prone to cross-reactivity issue.

On the other hand, the physical methods may involve installation of additional devices onto the assay for sample pre-treatment purpose or an equipment to carry out detection in a conditioned environment. For instance, heating plates, which requires a power supply, generate heat to evaporate samples at one end of the paper strip. The long evaporation process concentrates tuberculosis biomarkers in the urine sample at the heating region for higher sensitivity in immuno-dot blot assay (Wong et al., 2014). Similarly, isotachophoresis is an electrokinetic method that requires an electric circuit and external power supply to generate an electric field for sample separation and pre-concentration (Moghadam, Connelly, & Posner, 2015). In another study, Tang et. al. integrated a poly(ethylene glycol) (PEG)-contained dialysis-based filter device in front of the sample pad of LFA to pre-concentrate the sample more than fourfold due to PEG absorbing water and saline ions (Tang et al., 2016). Choi et. al. has manipulated the environmental conditions, *i.e.* temperature and RH using electrically powered equipment, so that the interaction between probe and target can be optimised to acquire higher sensitivity (Choi, Hu, Feng, et al., 2016). However, making and using such equipment would require higher cost and additional complicated steps to operate.

Another way of physically enhancing the assay sensitivity is through flow control. While the speed of flow is maintained in the NC membrane, Parolo et. al has increased the width of the pads in LFA threefold to augment the number of reacting target molecules through the NC membrane. This raised the interaction rate and achieved an 8-fold improvement of sensitivity to IgG (Parolo, Medina-Sanchez, de la Escosura-Muniz, & Merkoci, 2013). The disadvantages of this method, however, include the demand for a higher volume of sample and AuNP solution, and the fact there is no commercially available cassette suitable for the modified LFA strip. On the other hand, a decrease in flow rate can be rendered by adding a shunt to LFA to provide a longer period for the binding reactions between target and probes. Toley et. al. has demonstrated that the attachment of a cellulose shunt on a NC strip amplified the detection of malaria protein *PfHRP2* through flow delay (Toley et al., 2013). Later, Choi et. al. has proposed tuning the porous properties of the inserted glass fibre-agarose shunt to render reduction of flow rate, which has increased the sensitivity of dengue DNA detection by approximately tenfold with a flow delay of 178 s (J. R. Choi et al., 2017). Tang et. al. adjusted the geometry and surface energy of the sponge shunt to achieve a delayed flow of 90 s and tenfold enhancement of sensitivity towards nucleic acid testing of hepatitis B virus (HBV) (Tang et al., 2017). Meanwhile, flow can be resisted by creating shunts on the NC membrane. When wax pillars were applied onto NC membrane of LFA as barriers, the flow delay rendered 3-fold improvement of sensitivity towards human IgG (Rivas, Medina-Sanchez, de la Escosura-Muniz, & Merkoci, 2014). Alternatively, the combination of poly(dimethylsiloxane) (PDMS) barriers on NC membrane and glass-fibre shunt increases sensitivity towards HBV by 10-fold with about 255 s of flow delay (Choi, Liu, et al., 2016). Despite a shunt generating sensitivity enhancement, it may require labour-extensive fabrication. Moreover, the wax shunt is highly sensitive to heat

and might completely block the capillary if melted. Therefore, a simpler automatic method or a more stable material is in need to enhance the sensitivity of detection.

2.5 Electrospinning

Electrospinning is a top-down method that draws submicron and nanofibers from a polymeric solution by making use of electrostatic repulsion force. The process was first patented in 1900 by Cooley and Morton (Thenmozhi et al., 2017). The repeatable process, the various choices of polymeric materials that are soluble in the volatile solvent and the controllable fibre properties have led to opportunities for industrialization. The setup of electrospinning involves a high voltage electric supply, a conductive collector plate and a needle with a continuous feed of electrospinning dope by a pump. The main steps of electrospinning commence with droplet generation at the tip of the capillary (needle) due to feeding before an electric field is applied (Deitzel, Kleinmeyer, Harris, & Tan, 2001). As high voltage is applied to the collector plate and needle, the droplet elongates to form a cone-shaped structure that is known as Taylor's cone due to charge movement in the droplet (Yarin, Koombhongse, & Reneker, 2001). As it reaches a critical voltage, the surface tension of the droplet would be overcome by the electric charge. A jet of the polymer solution will be initiated and ejected due to the tendency of spreading the charge over the expanded surface area (Subbiah, Bhat, Tock, Parameswaran, & Ramkumar, 2005). During ejection, the jet elongates in a straight course towards the collector plate according to the axial component of the surface electrostatic charges under the electric field (Reneker & Yarin, 2008). As the jet continues to stretch and thin due to charge accommodation, the elongation becomes destabilised and bends to reduce the charge density on its surface, which looks like whipping (Reneker, Yarin, Fong, & Koombhongse, 2000). With the increased surface area of the jet during whipping instability, the solvent will evaporate faster and causes the jet to dry up and solidify before

it hit the collector plate. The fibre obtained from the collector plate under optimum conditions would be circular in cross-section, bead-free and free from structural deformation (Tripatanasuwan, Zhong, & Reneker, 2007).

The polymer to be electrospun is often dissolved in a solvent as the preparation steps using molten polymer are complicated (Reneker & Yarin, 2008). The physical properties of electrospun fibres are affected by several parameters associated with the solution properties, process conditions and environmental factors (Thenmozhi et al., 2017). Each of the parameters is interdependent and may be affected by changing one of them. Some essential solution properties to be considered include the solubility (Wannatong, Sirivat, & Supaphol, 2004), conductivity (Subbiah et al., 2005) and volatility (Megelski, Stephens, Chase, & Rabolt, 2002) of solvent, the viscosity (Thenmozhi et al., 2017) and concentration of the solution, and the molecular weight of the polymer (Gupta, Elkins, Long, & Wilkes, 2005). Process conditions such as the applied voltage (Reneker et al., 2000), the feeding rate (Zuo et al., 2005), the distance between the needle and collector (Buchko, Chen, Shen, & Martin, 1999), and the diameter of needle (S. Zhao, Wu, Wang, & Huang, 2004) also affect the outcome of the electrospun fibres. During the process, environmental factors like temperature (C. H. Kim et al., 2006) and relative humidity (Tripatanasuwan et al., 2007) can influence the volatility and viscosity, thus changing the properties of the resultant fibres. When the viscosity of the polymer solution is too low, the jet cannot hold together due to insufficient chain entanglements of the polymer, and so it breaks into droplets instead of complete fibres (Gupta et al., 2005).

Due to adjustability of the parameters in electrospinning, electrospun fibres of various features can be produced to suit many applications, e.g. filtration (Makaremi, De Silva, & Pasbakhsh, 2015), protective clothing (Peterson, Lu, & Epps Iii, 2017), tissue engineering (Rozila et al., 2016), drug delivery (Akhgari et al., 2017), cells (Hao et al.,

2013), catalysts, and sensors. Apart from the prior applications, Arslan et. al. also fabricated a multifunctional electrospun Nylon 6,6 polymeric nanofibrous mat with silicon quantum dots, zinc oxide nanoparticles and palladium nanocubes that could catalyse the reduction of paranitrophenol or decomposition of methylene blue, and sense trinitrotoluene in aqueous solution (Arslan & Uyar, 2017). The following section elaborates the applications of electrospinning in sensor making.

2.5.1 Electrospinning in sensor applications

Sensors containing electrospun nanofibres are widely applied in agricultural and food safety, biomolecular detection and diagnostic testing. They can be modified with ligands, e.g. polymers, proteins and nucleic acids to facilitate detection of the target molecule. The high surface area-to-volume ratio in electrospun fibres benefit by hosting a higher number of target-binding ligands, therefore achieving a higher sensitivity of the sensor. Some examples of applications are described below.

A thickness shear mode sensor coated with poly-lactic acid-co-glycolic acid polymeric nanofibers is able to differentiate hydrophilic and hydrophobic liquids based on shift in resonant frequency and detect benzene gas based on signal attenuation, respectively, which relate to the change in viscoelasticity of the nanofiber (Kwoun, Lec, Han, & Ko, 2001). Zhao et. al. measures blood pulse through electrical current signals generated by push-release movements on a piezoelectrical sensor made of poly(L-lactic acid) electrospun nanofibers (G. R. Zhao et al., 2017).

When integrated with an electrode, processed electrospun fibres can be combined with nanoparticles to improve electrochemical interactions. For instance, Chen et. al. improves the electrocatalysis of glucose oxidation and detection of glucose by spreading carbonized electrospun carbon nanofibers with nickel(II) hydroxide nanoplatelets on glass carbon electrode (L. Chen et al., 2017). Also, Macagnamo et.al. has deposited electrospun fibrous

titania with AuNPs embellishment on the interdigitated electrodes of a conductive sensor. The modified electrodes entrap and detect the concentration of trace gaseous Hg in the air, with a LOD of 1.5 ppb. The electrospun titania was using polyvinylpyrrolidone-titanium isopropoxide mixture and further processed in a muffled furnace to remove polyvinylpyrrolidone and crystallize the metal oxide (Macagnano et al., 2017).

Electrospun nanofibres can also be modified with fluorescent materials to generate fluorescent changes when activated by target molecules. A mixture of electrospun nanofibres containing a fluorescent polymer, poly(acrylic acid)-poly(pyrene methanol) and polyurethane latex is able to detect Fe^{3+}, Hg^{2+}, and 2,4-dinitrotoluene based on fluorescence quenching. The detection was enhanced roughly 2-3 orders of magnitude when compared to previous thin film sensors (X. Y. Wang et al., 2002). Wang et. al. fabricated electrospun cellulose acetate nanofibres (CANF) with mercapto-groups that bind with DNA oligonucleotide-conjugated AuNPs. The CANF based sensor detects BRCA I gene fragment DNA by replacing the prior DNA oligonucleotide and turning on the fluorescent reporter probe on the replaced DNA oligonucleotide (H. Wang et al., 2013). Another study demonstrated the integration of dye-intercalated DNA dendrimers into an electrospun poly(styrene-co-maleic acid) nanofiber platform to facilitate a sandwiched assay for beta thalassemia gene fragment, thrombin protein and HeLa cells (H. M. Wang et al., 2015). Modification of electrospun nanofibres is also done to facilitate binding of the target in colourimetric detection. Hosseini et. al. combined far-field electrospinning and free-radical polymerization to create a poly(3-hydroxybutyrate-co-3-hydroxyvalerate) nanofibrous mat for intrant-ELISA. The polymeric nanofibrous mat is dip-coated with the optimised composition of poly(methylmethacrylate-co-methacrylic acid) to increase the signal intensity of the assay up to 12-fold (Hosseini et al., 2016). Meanwhile, Hu et. al. have developed a reversible fluorescent and colourimetric sensor

for hydrogen chloride gas detection based on a porphyrin doped electrospun polystyrene nanoporous fibre (M. Hu, Kang, Zhao, Shi, & Cheng, 2017).

2.5.1.1 Electrospinning in lateral flow sensor

A porous electrospun nanofibrous material supports lateral flow due to capillary action. Several lateral flow sensors involved electrospun nanofibres in the sensing interface. These electrospun nanofibres are incorporated with biomolecules by functionalizing the resultant nanofibers with ligands or doping the solution before electrospinning. Li et. al. fabricated electrospun nanofibres from poly(lactic acid) (PLA) solution with dispersed biotin molecules that can immobilize streptavidin molecules. The immobilized streptavidin molecules can then bind to biotinylated DNA that further capture target DNA during lateral flow on the nanofibers (D. P. Li et al., 2006). Luo et. al. functionalized the electrospun NC membrane on a lateral flow immunoassay with antibodies to capture *E. coli* O157: H7 and bovine viral diarrhoea virus. In his work, he also utilized polyaniline coated magnetic nanoparticles to isolate the target from the sample and detect target through electric conductivity as polyaniline conduct electricity between the electrodes of the assay (Luo et al., 2012).

Apart from the above, Worsley et. al. integrated electrospun nanofibers as a bio-resorbable scaffold into a theranostic system to enhance tissue repair by supporting autologous cell migration. Together with a thermos-reversible hydrogel and a conventional LFA, the theranostic system detects chronic wound biomarkers, interleukin 6 and tumour necrosis factor alpha with LOD of 48.5 pg mL^{-1} and 55.5 pg mL^{-1}, respectively (Worsley, Attree, Noble, & Horgan, 2012). Another study proposes an alternative to the NC membrane in LFA by introducing a new electrospun nanofiber of mixture polymer that consists of PLA, PEG and polystyrene$_{8K}$-block-poly(ethylene-ran-butylene)$_{25K}$-block-polyisoprene$_{10K}$-Brij76 (K3-Brij76) (KB). The electrospun nanofibres

can support capillary action due to the hydrophilicity of PEG and pre-treatment with methanol-Tris buffered saline while KB enhances specificity due to its anti-fouling property (Reinholt et al., 2014).

Among the applications of electrospun nanofibres in LFA, many have only served as the sensing substrate, where the advantage of the high surface area-to-volume ratio is utilized. Other applications depend on the induction of hydrophilicity to ensure the functionality of capillary action where it is originally feasible in NC membrane. Nevertheless, there is no current application that exploits the hydrophobic property of polymeric nanofibres to enhance detection in lateral flow assay.

2.5.2 Poly(ε-caprolactone)

PCL is a biodegradable petroleum-based biopolyester with a melting point of 65 °C. It can be synthesized by ring opening polymerization of ε-caprolactone in the presence of metal alkoxide catalyst such as tin octoate under heat (Labet & Thielemans, 2009). The chemical structure of PCL is shown below in **Figure 2.1**.

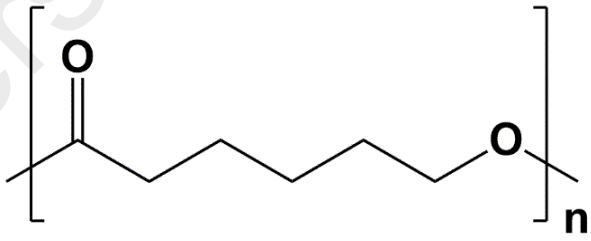

Figure 2.1: Structural formula of polymeric poly(ε-caprolactone)

The biopolymer was initially used as an additive to improve properties in processing resins and a polymer plasticizer for poly(vinyl chloride) (PVC) (Woodruff & Hutmacher, 2010). With its rheological and viscoelastic properties, PCL has shown an outstanding flexibility in undergoing various fabrication techniques, such as electrospinning, phase separation, gravity spinning and rapid prototyping. PCL has frequently been studied for

biomedical applications due to its low-cost synthesis, slow degradation rate (up to 4 years) and mechanical properties that suit various applications.

Notwithstanding, the hydrophobic nature of PCL has become a disadvantage as the reduction in wettability is unfavourable to many biological interactions, particularly in tissue engineering with reduced cell attachment. PCL would be treated to reduce its hydrophobicity. For instance, Gopinathan et. al. has shown that incorporation of galactose to electrospun PCL nanofibrous scaffold for enhanced meniscal cell attachment (Gopinathan et al., 2015). Also, the same issue arises in biosensor applications where the nanofibres are coated with other polymers to support binding of biomolecules or endow functionalities. Zheng et. al. spread the PCL with entrapped haemoglobin on a glassy carbon electrode to detect hydrogen peroxide (H_2O_2). The detection was based on amperometric sensing from the conversion of the heme Fe^{3+}/Fe^{2+} in the haemoglobin with the facilitation of PCL (Zheng, Li, & Zheng, 2008). Meanwhile, Guler et. al coated polypyrrole (PPy) onto electrospun PCL nanofibres by *in situ* polymerisation of pyrrole to endow electrical conduction and enable binding of single-stranded DNA probes. The hybridization of complementary DNA to the single-stranded DNA probes was then detected with EIS based on the changes in the PCL/PPy interfacial electrical properties (Guler, Erkoc, & Sarac, 2015).

As an important parameter of electrospun nanofibres, utilisation of surface tension would also facilitate detection. Falde et. al. has tuned the surface tension of PCL fibres with other hydrophobic and hydrophilic polymers to detect fat content in milk and bile acid content in urine. The sensor meshes have allowed urine with high bile acid and normal milk to wet the meshes and react with pH-indicating dye in the bottom meshes (Falde, Yohe, & Grinstaff, 2015). The biocompatibility, tuneable surface tension and surface functionalization of PCL for both electrochemical and optical sensors has

therefore shown its potential for application in other detection platforms, *e.g.* lateral flow sensors or assays.

2.6 Summary

Gold standards and recent methods developed for water safety assessment and detection of diseases necessitate sensors with complex design or a workstation for analysis. Meanwhile, paper-based sensors for diseases and contamination diagnostics have encountered many challenges, particularly low sensitivity due to limited volume of sample and low concentration of target in the sample. Therefore, there is a necessity to develop a paper-based sensor that requires only simple fabrication and operation for water safety analysis and detection of infection. As the sensor would require low volume of sample, a direct method to enhance the sensitivity of the paper-based sensor should be deliberately explored.

CHAPTER 3: PAPER-BASED CAPACITIVE SENSORS FOR IDENTIFICATION AND QUANTIFICATION OF CHEMICALS AT THE POINT OF CARE

3.1 Introduction

Conventional analysis of chemicals for water safety purposes requires lab-centralized sophisticated equipment that demands skilled personnel to operate. Although miniaturized chemical sensors have been developed, they still require highly complex circuitry and the use of immovable equipment, making *in situ* analyses impossible. This chapter presents the novel development of a simple and lightweight paper-based capacitive sensor (PCS) for identification and quantification of chemical fluids. The geometry of PCS and the conditions during the usage of PCS, *i.e.* loading volume, position of measurement, drying time, load-dry cycle, temperature and relative humidity were optimized. Measurement taken by a portable multimeter was compared to that of an LCR meter. The working principles and concepts of sensing of PCS were discussed. The optimized PCS and conditions were then applied during the assessment of PCS capabilities to identify and quantify chemical fluids (pure liquids and solute-based solutions) at as-prepared and pre-dried conditions using dielectric performances like capacitance and loss tangent. The sensing capabilities of PCS are shown to be beneficial for the development of cheaper, simple sensors for elementary water safety assessment.

3.2 Material and methods

3.2.1 Fabrication of paper-based capacitive sensor (PCS)

The procedures of PCS fabrication are shown in **Figure 3.1**. In the order of top to bottom, the paper-based capacitive sensor (PCS) consists of a stack of 5 layers: aluminium foils (1st and 5th layer), Scotch® Core Series XQ double-sided tapes (2nd and 4th layer) (3M, USA) and No. 201 filter paper (3rd layer) (Whatman-Xinhua Filter Paper

Co., LTD, China). First, the materials were cut to respective shape before assembly: filter paper (55 mm × 100 mm), aluminium foil (40 mm × 100 mm), double-sided tape (2nd) (45 mm × 100 mm) and double-sided tape (4th) (55 mm x 100 mm) **(Figure 3.1a)**. The double-sided tapes at the 2nd and 4th layers held the 3rd layer filter paper firmly with the top and bottom layers of aluminium foil **(Figure 3.1b)**. After assembly, the bulk sensor has a dielectric layer made of filter paper and double-sided tapes, as well as conducting plates of aluminium foil. Subsequently, it was cut into smaller strips (55 mm x 10 mm) using Matrix™ 2360 programmable shear (Kinematic Automation Inc., CA, USA) **(Figure 3.1c)**. The as-prepared PCSs **(Figure 3.1d)** were kept in a dry place at room temperature and protected from direct sunlight until use.

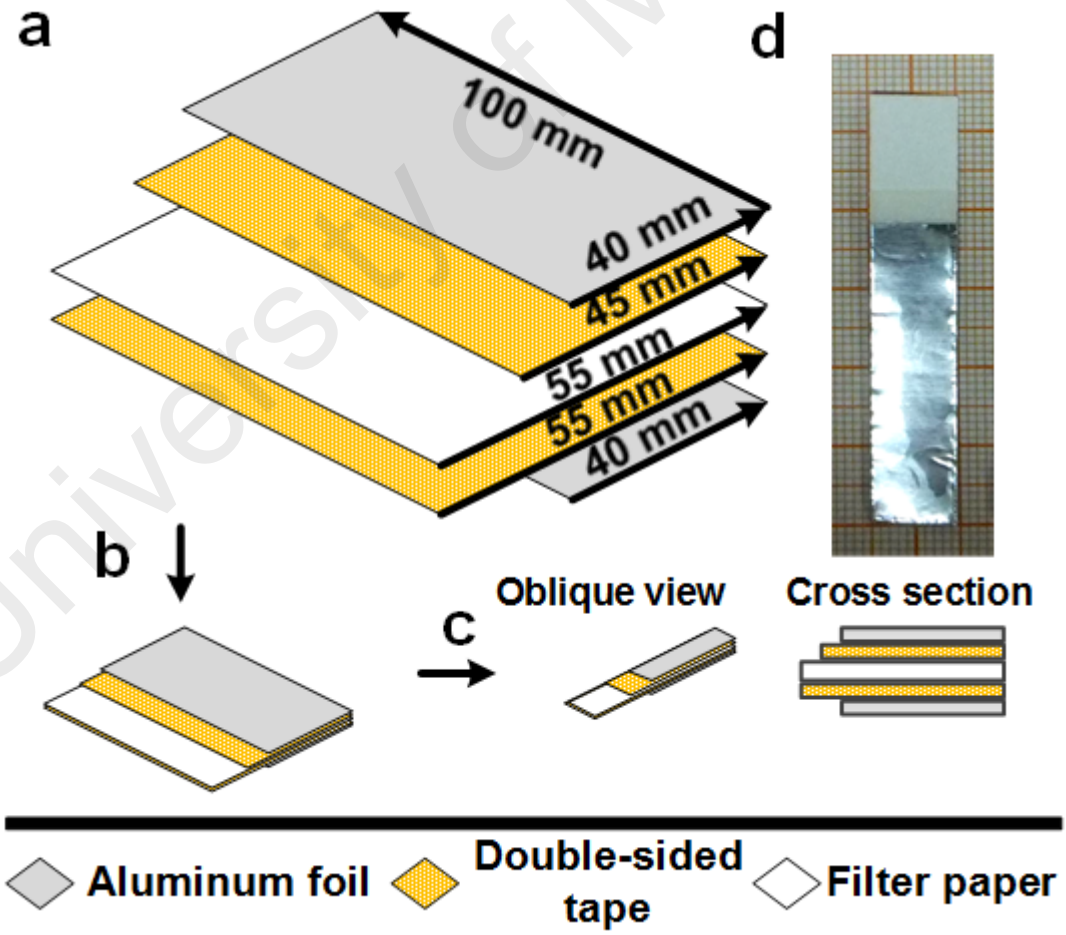

Figure 3.1: Fabrication of PCS

3.2.2 Working principle of PCS

PCS was developed to work as a parallel plate capacitor with fixed shape and tandem layers of double-sided tapes and paper. Such a design can be modelled as a series of capacitors, comprising dielectrics materials of two layers of double-sided tapes (C_t) and a layer of filter paper (C_f). Therefore, the capacitance of PCS (C_p) can be expressed as

$$C_p^{-1} = 2C_t^{-1} + C_f^{-1} \tag{3.1}$$

As filter paper is porous and double-sided tape is not porous, as shown in **Figure 3.2**, the capacitance of filter paper can be further modelled as a series of capacitors, comprising the dielectric materials cellulose fibres (C_c) and air-filling void (C_a).

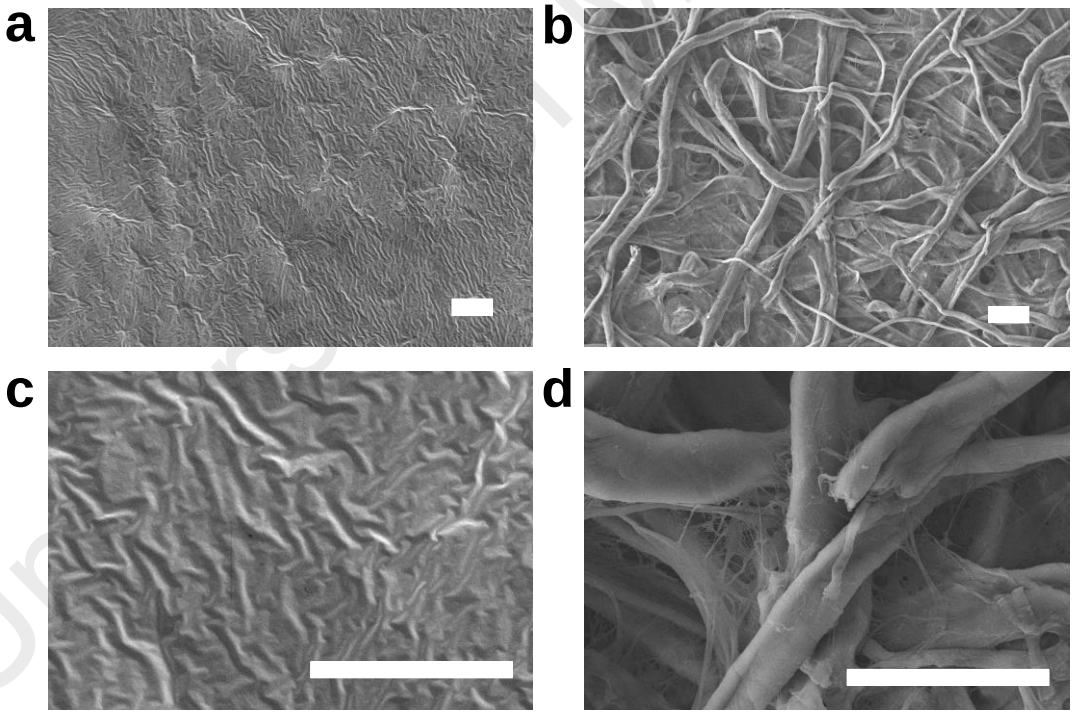

Figure 3.2: The microscopic structure of double sided tape (a,c) and filter paper (b, d) taken by scanning electron microscopy with scale bars represent 50 um

Before the sample fluid is loaded, the PCS would be considered as an idle PCS. Hence, the capacitance of filter paper and the whole idle sensor would be

$$C_f^{-1} = C_c^{-1} + C_a^{-1} \tag{3.2}$$

$$C_p^{-1} = 2C_t^{-1} + C_c^{-1} + C_a^{-1} \tag{3.3}$$

With the assumption of enough volume of sample fluid loaded, the air-filling void in the filter paper would gradually be replaced with the sample fluid by capillary action until it covers all the empty spaces. The sample fluid could be of homogeneous fluid, *i.e.* organic liquid or heterogenous fluid, *i.e.* salt solution. This would induce a change of capacitance from air filling to sample fluid filling (C_{s1}). The capacitance of filter paper and loaded sensor would be

$$C_f^{-1} = C_c^{-1} + C_{s1}^{-1} \tag{3.4}$$

$$C_p^{-1} = 2C_t^{-1} + C_c^{-1} + C_{s1}^{-1} \tag{3.5}$$

For some heterogeneous solutions, i.e. salt solutions, solute based analysis can be done through thorough drying of fluid after loading. Once water is eliminated through evaporation, the void between the cellulose fibres would be now filled with the sample solute and again with air. The capacitance of dried loaded filter paper would be described as a series of capacitors, comprising the cellulose fibres (C_c), sample solute (C_{s2}) and air (C_{a*}). Thus,

$$C_f^{-1} = C_c^{-1} + C_{s2}^{-1} + C_{a*}^{-1} \tag{3.6}$$

$$C_p^{-1} = 2C_t^{-1} + C_c^{-1} + C_{s2}^{-1} + C_{a*}^{-1} \tag{3.7}$$

With the same materials of double-sided tape and filter paper, the dielectric constant and thickness, and the porosity of filter paper would be the same. Thus, the capacitance of cellulose and double-sided tape would remain constant. During fluid based or solute based analysis, the changes of sensor's capacitance (C_p) are expected to vary only with

the change in the loaded sample. Generally, the geometrical capacitance can be described as

$$C = \frac{\varepsilon_r \varepsilon_0 A}{d} \tag{3.8}$$

where ε_r is the dielectric constant of the medium between the conducting plates, ε_0 is the permittivity of space, A is the overlapping area under the conducting plates and d is the distance between the conducting plates. The capacitance of double-sided tape can be expressed as

$$C_t = \frac{\varepsilon_t \varepsilon_0 A_c}{d_t} \tag{3.9}$$

Due to effective porosity of filter paper, η, the capacitance induced by cellulose fibres (C_c), air (C_a) and sample fluid (C_{s1}) can be derived into

$$C_c = \frac{\varepsilon_c \varepsilon_0 A_c}{(1-\eta) d_p} \tag{3.10}$$

$$C_a = \frac{\varepsilon_a \varepsilon_0 A_c}{\eta d_p} \tag{3.11}$$

$$C_{s1} = \frac{\varepsilon_{s1} \varepsilon_0 A_c}{\eta d_p} \tag{3.12}$$

During solute based analysis, when the solvent is eliminated, the effective porosity of filter paper would be modified to η*. Due to the modified effective porosity, the capacitance of air-filling void (C_{a*}) and solute-filling void (C_{s2}) would be

$$\boldsymbol{C_{a*} = \frac{\varepsilon_a \varepsilon_0 A_c}{\eta^* d_p}} \tag{3.13}$$

$$\boldsymbol{C_{s2} = \frac{\varepsilon_{s2} \varepsilon_0 A_c}{(\eta - \eta^*) d_p}} \tag{3.14}$$

Referring to the above equations, the capacitance of idle, loaded and dried loaded sensors can be derived into

$$C_p = \frac{\varepsilon_0 A_c}{\frac{2d_t}{\varepsilon_t}+\frac{(1-\eta)d_p}{\varepsilon_c}+\frac{\eta d_p}{\varepsilon_a}} \tag{3.15}$$

$$C_p = \frac{\varepsilon_0 A_c}{\frac{2d_t}{\varepsilon_t}+\frac{(1-\eta)d_p}{\varepsilon_c}+\frac{\eta d_p}{\varepsilon_{s1}}} \tag{3.16}$$

$$\boldsymbol{C_p = \frac{\varepsilon_0 A_c}{\frac{2d_t}{\varepsilon_t}+\frac{(1-\eta)d_p}{\varepsilon_c}+\frac{\eta^* d_p}{\varepsilon_a}+\frac{(\eta-\eta^*)d_p}{\varepsilon_{s2}}}} \tag{3.17}$$

where ε_{s1} is the dielectric constant of sample fluid. **Figure 3.22** depicts the concept of PCS as a capacitor based on the structures of idle, loaded and dried loaded sensors.

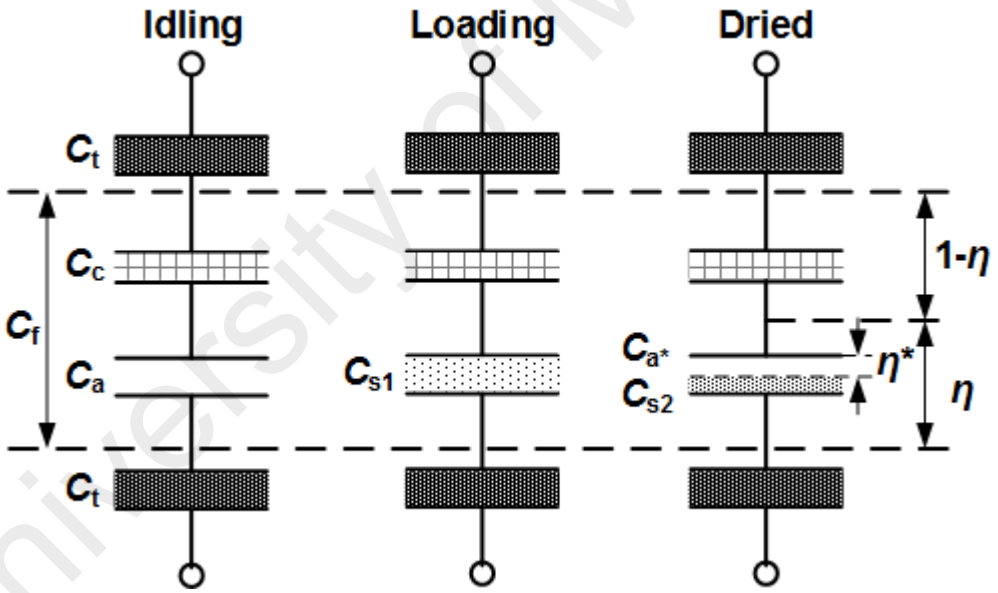

Figure 3.3: Circuitry of PCS based on different conditions in the filter paper

For homogenous fluids, each chemical has its own ε_{s1} according to the condition, thus having different C_p. On the other hand, for heterogenous fluids, *i.e.* salt solutions, ε_{s1} changes according to the amount and species of solutes, thus contributing to the quantifying function using the sensor. Nevertheless, when water comprises the most part of the solution, the dielectric constant of the solution would be close to water due to the

insignificant dielectric constant value of salt or other soluble material compared to the very high value of water, *i.e.* 80.1. When water is eliminated, where $\frac{\eta d_p}{\varepsilon_{s1}}$ turns to $\frac{\eta^* d_p}{\varepsilon_a} + \frac{(\eta-\eta^*)d_p}{\varepsilon_{s2}}$, the capacitance of sensor would relate more to the presence of solute and its amount in the void, and thus decreases due to $\varepsilon_{s1} > \varepsilon_{s2} > \varepsilon_a$ and $\eta \approx \eta^*$. In addition, the basis of solute or fluid is also influenced by frequency and field strength, thus showing differences in its dielectric constant (ε_{s1} or ε_{s2}) and dielectric loss ($tan\ \delta$) in a frequency spectrum.

3.2.3 Optimizations for PCS sensing performance

3.2.3.1 Geometry of PCS

PCS can be divided to 3 areas, *i.e.* loading area, spacer area and capacitance area, as shown in **Figure 3.4**. According to equation (3.9) in section 3.2.2, the capacitance affected by geometrical parameters such as the area of the conducting plates and the distance between them. As all the PCSs used the same materials and layering, they are mainly affected by the area of conducting plates.

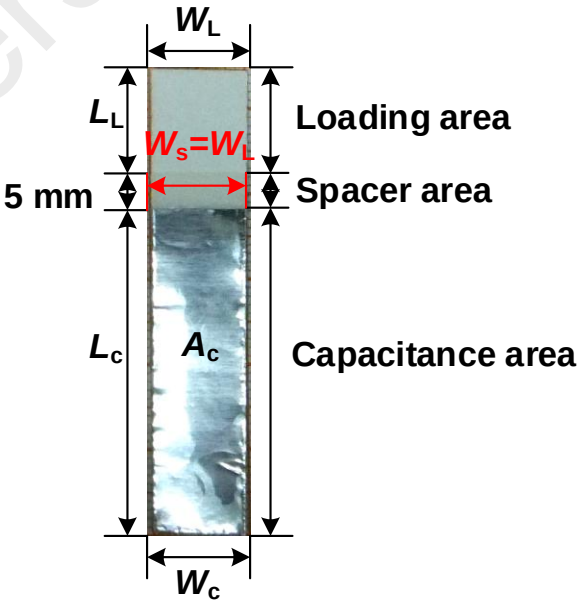

Figure 3.4: Top plan of PCS and geometrical parameters

In **Figure 3.4**, W_C is width of capacitance area, W_S is width of spacer area, W_L is width of loading area, L_C is length of capacitance area, L_L is length of loading area, and A_C is area of capacitance area.

Firstly, by keeping the area constant, PCSs of different geometry (#1 – #7) were fabricated by adjusting the width/length (W_C/L_C) ratio of capacitance area with a pair of scissors to study its effect on the sensing performance (**Figure 3.5a**). Secondly, as sample fluid would be applied to PCS, the loading area was studied by adjusting the L_L (#3, #8 – #10), as shown in **Figure 3.5b**. Thirdly, area of capacitance area of PCSs was studied by adjusting the sensor width (W_C, W_S and W_L altogether, #3, #11 – #12), as shown in **Figure 3.5c**. For instance, when sensor width = 40 mm, W_C = W_S = W_L = 40 mm. All the pre-designed PCSs were loaded at the tip of loading area with adequate ultrapure water (UPW) (>18.2 MΩ·cm) from Milli-Q Integral Water Purification System (Millipore, MA, USA) to fully wet the filter paper. The dimensions of all the PCS designs and the respective volume of loaded UPW (V_{UPW}) were listed **Table 3.1**. The real-time capacitance (C_P) of loaded PCS was measured with Agilent E4982A LCR meter (Agilent Technologies Inc., CA, USA) with AC of 1V peak voltage and 1 kHz frequency. All the results refer to the mean of three independently repeated tests (n=3).

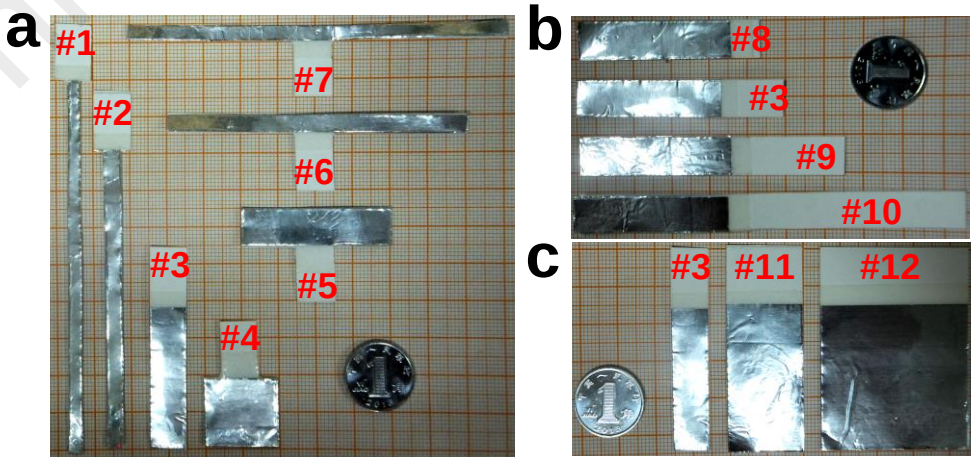

Figure 3.5: PCSs with different geometries

Table 3.1: Dimensions of PCSs in different geometry and respective volume of loaded UPW

No.	W_C (mm)	L_C (mm)	L_L (mm)	W_L (mm)	$W_C \times L_C = A_C$ (mm^2)	V_{UPW} (µL)
#1	4	100	10	10	400	70
#2	5	80	10	10	400	70
#3	10	40	10	10	400	70
#4	20	20	10	10	400	70
#5	40	10	10	10	400	70
#6	80	5	10	10	400	70
#7	100	4	10	10	400	70
#8	10	40	2.5	10	400	60
#9	10	40	25	10	400	90
#10	10	40	55	10	400	120
#11	20	40	10	20	800	130
#12	40	40	10	40	1600	240

3.2.3.2 Sample loading volume

To study the effect of sample loading volume on the sensing performance, different volumes of 1 mM $NaNO_3$ (Tianjin Zhiyuan Chemical Reagent Co., LTD., China) were loaded to the loading area of PCS #3 and left to wet the whole filter paper. Measurement of C_P was done with a UT58 multimeter (UNIT-T, Dongguan, China), as shown in **Figure 3.6** and compared to that of Agilent E4982A LCR meter (Agilent Technologies Inc., CA, USA) with AC of 1V peak voltage at frequency 400 Hz and 1 kHz. Subsequently, all the wet sensors were dried in a 100 °C oven for 15 minutes and capacitance were measured again. All the results refer to the mean of three independently repeated tests (n=3).

Figure 3.6: Measurement of capacitance using multimeter

3.2.3.3 Position of measurement on the capacitance area

When measuring C_P, one electrode tip was touching at a point on one of the conducting plates whereas another electrode tip mirrored to the point on the conducting plate of another side. To study the effect of the location of this measuring point on PCS #3, C_P measurements were taken at 10 different positions on the conducting plates with 4 mm intervals, as depicted in **Figure 3.7**. The measurements were taken when the PCS was as-prepared, loaded with 1mM $NaNO_3$ on its loading area, and dried after loading. All the results refer to the mean of three independently repeated tests (n=3).

Figure 3.7: Position of measurement on the capacitance area

3.2.3.4 Drying time of PCS

Drying is essential to get rid of moisture in the PCS, especially for solute-based analyses, as the high dielectric constant of water would affect the sensor performance. To explore the effect of water content on PCS performance, C_P measurements of as-prepared PCS #3 (idling) and 70 µL 1mM $NaNO_3$-loaded PCS #3 (loading) were taken real-time while drying at 100 °C in an oven. The measurements were taken by multimeter. All the C_P measurements were mean values of three independently repeated tests (n=3).

3.2.3.5 Number of loading and drying cycle

To further study the effect of repeated loading of solution on solute-based analyses, PCS #3 was loaded with sample fluid on its loading area, dried, and its C_P measured. The loading, drying and measuring was defined as 1 cycle. The cycle was repeated up to 6 times to assess the effect on the sensing performance. UPW and 1 mM $NaNO_3$ were used as samples fluid. The measurements were taken by multimeter. All the results refer to the mean of three independently repeated tests (n=3).

3.2.3.6 Surrounding temperature

To examine the effect of temperature on the sensing performance, 1 M $NaNO_3$ and UPW were loaded to the loading area of PCSs #3 and the C_P of the PCSs were measured in a dry oven with preset temperatures (~ 0% RH, 20 – 90 °C). The loaded sensors were dried at first and put into the conditioned oven for at least 15 min before measurement. All the results refer to the mean of three independently repeated tests (n=3).

3.2.3.7 Relative humidity

To study the effect of relative humidity (RH) on the sensing performance at room temperature, two kinds of test were prepared. PCSs #3 were conditioned in a hygrothermostatic chamber for 5 minutes before C_P measurement with multimeter. The first test was using one PCS for 3 repeated tests on the same RH level (repeated use) (n=3). The same PCS was conditioned, measured, dried and reconditioned again at the same RH before measurement. The second test was using three individual PCSs (single use) for 3 repeated tests on the same RH level (n=3). PCS was only conditioned and measured once before disposal. For a different level of RH, new set of PCSs were used for the two kinds of test. No sample fluid was loaded to all the PCSs in the two tests.

3.2.4 Concept of sensing with dielectric performances

As aforementioned in **section 3.2.2**, frequency and field strength can affect the dielectric properties of the dielectric layers and the dispensed sample fluid. When a constant external electric field is applied, each of the conducting plates would be charged, creating an electric field within the conducting plates. The field strength would depend on the external field and distance between the plates. The capacity to store these charges would depend on the dielectric properties of the medium in between the conducting plates. These dielectric properties can be further divided to relative permittivity (a.k.a dielectric constant) and dielectric loss ($tan\ \delta$). Relative permittivity relates to the ability

of the dielectric medium to counteract the established field relative to that of vacuum, thus obstruct the flow of charge and maintaining the field and its strength. On the other hand, dielectric loss relates to the transformed energy that is used to counteract the field.

On the molecular scale, the insulator dielectric medium contains many particles that have a strong attraction to electrons or do not have free electrons to flow in the applied electrical field, thus do not conduct electricity. Even so, these electrons would shift slightly towards the positively charged plates under the applied field, thus causing energy loss during shifting, decrease in field strength and lower capacity to store charge. On the other hand, as protons of the particles would be attracted to the negatively charged plate, it would seem like the particles have slightly moved along its axis to align to the field. An ideal dielectric material would completely resist the applied field without particle movement, thus causing no energy loss, no reduction in field strength and maximum capacity of charge storing.

With AC electric field, the polarity of the field keeps oscillating and the electrons of these particles would oscillate with the field as well. The frequency of the field would affect the ability of the particles to counteract the field. When the frequency of the AC electrical field increases, some features of the particle would start to fade out as the particles unable to react timely to the polarity change of the field. These features, *i.e.* resonance and relaxation, depend on the chemical characteristics of the particles (ionic, polar, atomic and electronic). When the frequency equals to the characteristic frequency, the particles resonate violently and thus imparts an enhanced ability to counteract the applied field and dielectric properties. However, further increasing the frequency would render the particle unable to counteract, and thus weaken its dielectric properties. Meanwhile, the interaction between the particles, be it the same or different species, would also affect this ability (Kirkwood, 1939).

Since the dielectric constant relates to the chemical characteristic, in this study, the type (Lide, 2004) and amount (P. M. Wang & Anderko, 2001) of sample fluid effectively affect the overall dielectric properties and capacitance. Since different materials would give different dielectric – frequency spectra, correspondingly they would also give different capacitance – frequency spectra. As low frequency had been used to generate high capacitance, this method enables the use of a low-frequency handheld measuring instrument, e.g. multimeter that simplifies the application for common people. Moreover, dielectric loss relates to the type and amount of the dielectric material as it is its innate ability to dissipate electromagnetic energy. As both dielectric constant and dielectric loss (*tan δ*) represent the real and imaginary parts of material's dielectric properties, they are used for sample fluid identification and qualification in PCS.

3.2.5 Evaluation of PCS sensing capabilities

Following section 3.2.4 and optimization of PCS conditions, the capabilities of PCS to distinguish and quantify liquid or aqueous chemicals can be evaluated.

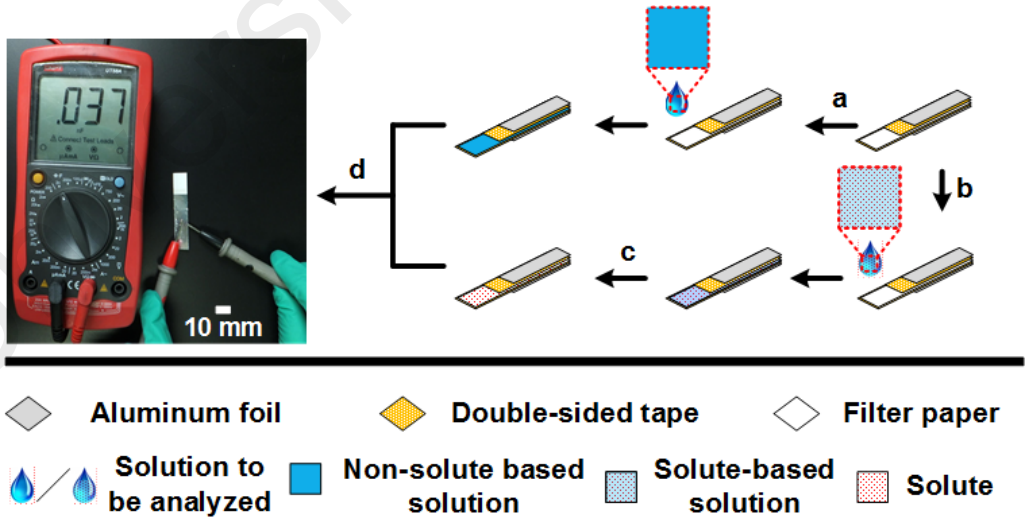

Figure 3.8: Evaluation of PCS sensing capabilities

To evaluate the sensing capabilities of PCSs #3, the PCSs were first laid flat on a clean surface, loaded with sample fluids on the loading area, and then the dielectric

performances (C_P or *tan* δ) were measured using multimeter or LCR meter (AC 1V peak voltage, 100 Hz – 1 MHz), as shown in **Figure 3.8**. Multimeter was used to measure C_P whereas LCR meter was used to measure C_P and *tan* δ. All the analyte sample fluids, their categories and their sources were listed in **Table 3.2**. All the solute-based solutions were prepared with UPW.

Table 3.2: Analyte sample fluids for PCS evaluation

Chemicals	Category	Sources
Air (idling)	Gas	Not applicable
Mineral oil (MO)	Pure liquid	Sigma-Aldrich, China
Oleic acid (OA)	Pure liquid	Tianjin Fuchen Chemical Reagents Factory, China
Toluene	Pure liquid	Tianjin Yongsheng Chemical Reagent Co., LTD., China
Chloroform ($CHCl_3$)	Pure liquid	Tianjin Yongsheng Chemical Reagent Co., LTD., China
Ethyl acetate (EA)	Pure liquid	Tianjin Zhiyuan Chemical Reagent Co., LTD., China
Tetrahydrofuran (THF)	Pure liquid	Tianjin Zhiyuan Chemical Reagent Co., LTD., China
Dichloromethane (CH_2Cl_2)	Pure liquid	Sinopharm Chemical Reagent Co., LTD., China
Isopropyl alcohol (iPrOH)	Pure liquid	Tianjin Zhiyuan Chemical Reagent Co., LTD., China
Ethanol (EtOH)	Pure liquid	Tianjin Zhiyuan Chemical Reagent Co., LTD., China
Diethylene glycol (DEG)	Pure liquid	Tianjin Fuchen Chemical Reagents Factory, China
Ethanolamine (ETA)	Pure liquid	Fuyu Chemical, China
Methanol (MeOH)	Pure liquid	Tianjin Zhiyuan Chemical Reagent Co., LTD., China
Dimethyl formamide (DMF)	Pure liquid	Fuyu Chemical, China
Ethylene glycol (EG)	Pure liquid	Fuyu Chemical, China
Glycerol	Pure liquid	Tianjin Zhiyuan Chemical Reagent Co., LTD., China
Dimethyl sulfoxide (DMSO)	Pure liquid	Tianjin Zhiyuan Chemical Reagent Co., LTD., China

Table 3.2 continued: Analyte sample fluids for PCS evaluation

Chemicals	Category	Sources
Water / UPW (H_2O)	Pure liquid	Milli-Q Integral Water Purification System
Hydrogen peroxide (H_2O_2) (30% v/v)	Aqueous	Tianjin Zhiyuan Chemical Reagent Co., LTD., China
Ammonia (NH3) (25% v/v)	Aqueous	Fuyu Chemical, China
Hydrazine (N_2H_4) (80% v/v)	Aqueous	Fuyu Chemical, China
Acetic acid (AcOH) (1M)	Aqueous	Fuyu Chemical, China
Sodium chloride (NaCl)	Solute-based	Tianjin Tianli Chemical Reagent Co. LTD., China
Sodium bicarbonate ($NaHCO_3$)	Solute-based	Tianjin Tianli Chemical Reagent Co. LTD., China
Sodium dihydrogen phosphate (NaH_2PO_4)	Solute-based	Tianjin Tianli Chemical Reagent Co. LTD., China
Sodium sulphate (Na_2SO_4)	Solute-based	Tianjin Tianli Chemical Reagent Co. LTD., China
Disodium hydrogen phosphate (Na_2HPO_4)	Solute-based	Tianjin Tianli Chemical Reagent Co. LTD., China
Sodium oxalate ($Na_2C_2O_4$)	Solute-based	Tianjin Tianli Chemical Reagent Co. LTD., China
Sodium borate ($Na_2B_4O_7$)	Solute-based	Tianjin Zhiyuan Chemical Reagent Co., LTD., China
Disodium ETDA ($C_{10}H_{16}N_2O_8Na_2$)	Solute-based	Tianjin Shen'ao Chemical Reagent Co., LTD. (Tianjin, China)
Trisodium phosphate (Na_3PO_4)	Solute-based	Tianjin Tianli Chemical Reagent Co. LTD., China
Trisodium citrate ($Na_3C_6H_5O_7$)	Solute-based	Tianjin Shen'ao Chemical Reagent Co., LTD., China
Sodium nitrate ($NaNO_3$)	Solute-based	Tianjin Zhiyuan Chemical Reagent Co., LTD., China
Potassium nitrate (KNO_3)	Solute-based	Tianjin Zhiyuan Chemical Reagent Co., LTD., China
Lead nitrate ($Pb(NO_3)_2$)	Solute-based	Tianjin Guangfu Fine Chemical Research Institute, China
Cadmium nitrate ($Cd(NO_3)_2$)	Solute-based	Chengdu Kelong Chemical Reagent Company, China
Manganese (II) nitrate ($Mn(NO_3)_2$)	Solute-based	Tianjin Guangfu Technology Development Co., Ltd., China
Chromium (III) nitrate ($Cr(NO_3)_3$)	Solute-based	Tianjin Fuchen Chemical Reagents Factory, China

Table 3.2 continued: Analyte sample fluids for PCS evaluation

Chemicals	Category	Sources
Iron (III) nitrate ($Fe(NO_3)_3$)	Solute-based	Tianjin Zhiyuan Chemical Reagent Co., LTD., China

3.2.5.1 Identification of chemical fluids

The PCS capability of identifying chemical fluids was evaluated by loading sample fluids to the loading area of PCS #3 (**Figure 3.8a**) and taking measurements for dielectric performances (C_P or *tan* δ) (**Figure 3.8d**). The sample fluids were loaded to PCSs of two different conditions: pre-dried (Trial 1) and as-prepared (Trial 2). Pre-dried PCS was prepared by drying the as-prepared PCS in 100 °C oven for 15 minutes before loading with sample fluid. C_P was measured before and after loading PCS with sample fluids. C_P differences of PCS before and after loading sample fluids were calculated and compared. The experiments were repeated independently 3 times for each sample fluid (n=3).

3.2.5.2 Quantification of chemical solutions

Quantification of chemical solutions was evaluated with organic solvent-water system and solute-based solutions. For organic solvent-water system, different volume fractions (0% – 100%) of ethanol-water solution were prepared by mixing different volume of ethanol with corresponding volume of UPW. The resultant solutions were loaded onto the loading area of PCS #3 to wet the whole filter paper (**Figure 3.8a**) and C_P was then measured (**Figure 3.8d**). Measurements were taken for PCS of two different conditions: pre-dried (Trial #1) and as-prepared (Trial #2). Pre-dried PCS was prepared by drying the as-prepared PCS in 100 °C oven for 15 minutes before loading with sample fluid. Similarly, different concentrations of various solute-based solutions were prepared by dissolving the salt crystals in UPW. The resultant salt solution was then dispensed onto the loading area of the PCSs (**Figure 3.8b**) and dried in the 100 °C oven for 15 min

(**Figure 3.8c**) before C_P measurements were taken (**Figure 3.8d**). The experiments were repeated independently 3 times for each solution (n=3).

3.3 Results and Discussion

3.3.1 Optimizations for PCS sensing performance

3.3.1.1 Geometry of PCS

The PCSs were being designed and cut into various shapes. These shapes were based on different width (W_c) to length (L_c) ratios of conducting parallel plates (#1 – #7), different length of protruding filter paper (L_L) as loading region (#3, #8 – #10) and different width (W_{PCS}) of the whole PCS (#3, #11, #12) while retaining other parameters. It should be clarified here that the W_{PCS} is the width of the whole sensor, including the width of loading area (W_L), spacer area (W_S) and parallel conducting plates (W_c). Therefore, $W_{PCS} = W_L = W_S = W_c$. Both sensors of different $W_c : L_c$ ratio and different L_L have the same area of parallel conducting plates (A_c) while the sensors with different W_s have different A_c as well. All the design shapes are depicted in the **Figures 3.2a, 3.2c, and 3.2d**. All the geometrical parameters can be referred in **Table 3.1**.

With the same conducting area (A_C), the different W_C/L_C ratio may influence the fluid flow and distribution in the sensor. The effect of different W_C/L_C ratio on the sensing performance (C_P) of PCSs were shown in **Figure 3.9a**. Despite possessing the same area, C_P of PCS #1–3 increased at first and then remained steady with time while C_P of PCS #4–7 increased at first and then decreased with time. Moreover, the peak C_P and the time to achieve it increased with increasing W_C/L_C (#1–6), respectively.

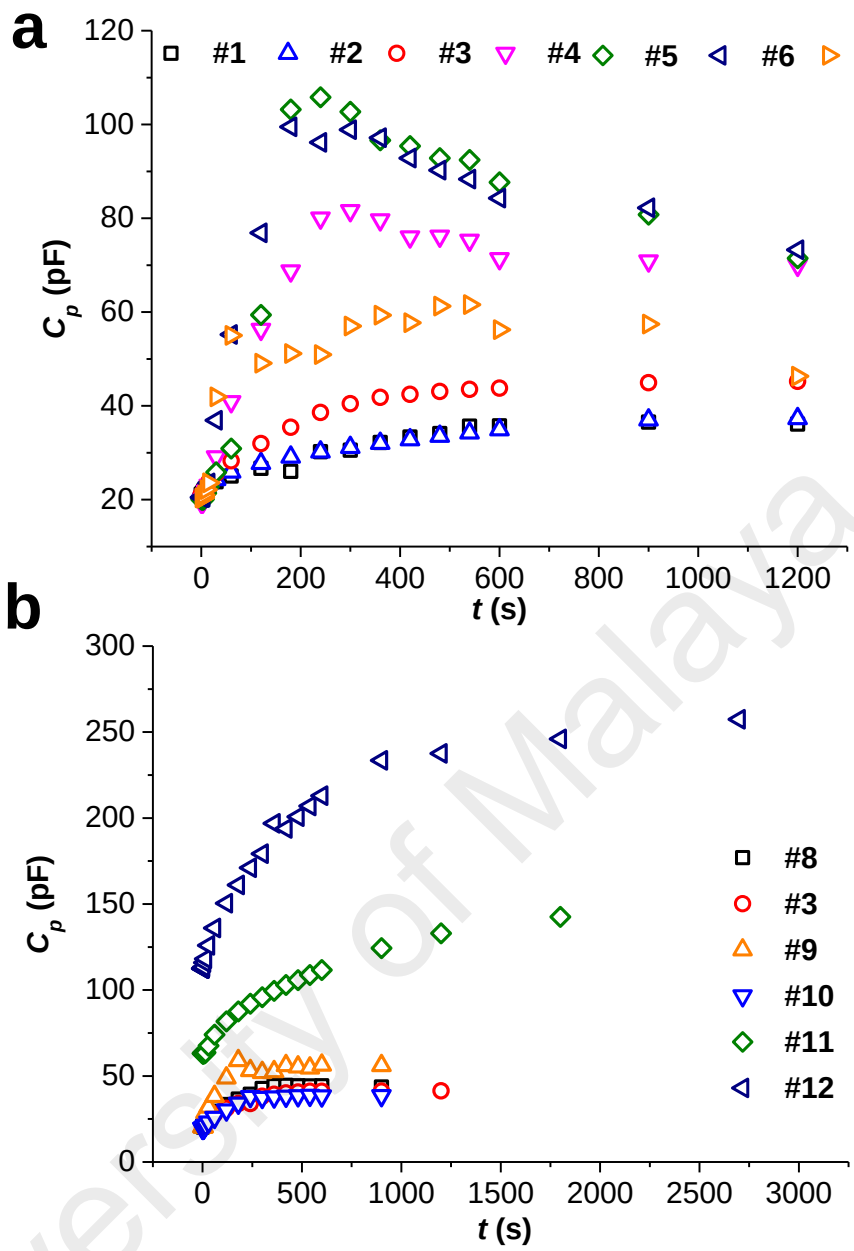

Figure 3.9: Effect of geometry on the sensing performance of PCS

According to Liu et. al., the wicking liquid front height (h) through the derivation of Lucas-Washburn equation (Z. Liu, Hu, Zhao, Qu, & Xu, 2015):

$$h = \sqrt{\frac{4\sigma cos\theta}{\mu}\frac{K}{\varepsilon R}} \cdot t^{1/2} \tag{3.18}$$

While the subsequent theoretical liquid wicking speed (S) would be

$$S = \frac{dh}{dt} = \sqrt{\frac{\sigma cos\theta}{\mu}\frac{K}{\varepsilon R}} \cdot t^{-1/2} \quad (3.19)$$

In both equations (3.18) and (3.19), σ, μ, θ, K, R and t are interfacial tension, viscosity, contact angle, permeability, effective pore radius and time, respectively. With no change of the solution and paper material, $h \propto t^{1/2}$ and $S \propto t^{-1/2}$. In addition, Liu explained that when the width of the paper is completely in contact with water, it has no significant effect on the wicking height.

Hence, water flows unidirectionally in PCS #1–3 and increasing L_c (PCS #1 – #2) would lengthen the time to wet the sensor completely. In PCS #4 – #7, fluid can wick along the length and width of the sensor (bidirectional), therefore covering more spaces at the same timeframe. As the wider and longer the sensor is, lesser water is distributed in the sensor at the same period. Like PCS #1, PCS #7 has a very thin conducting area, hence once fluid was dispensed, it started to wick slowly due to long wicking height. The gradual drop of capacitance in PCS #4 – 7 was hypothesized to be influenced by other factors such as evaporation that would also reduce the amount of fluid and the speed of wicking in the paper. The lower capacitance value of PCS #7 compared to PCS #4 – #6 might suggest the loss of fluid due to evaporation.

To study the effect of loading area on the sensor performance, different length of loading area, L_L was designed and real-time measurement of capacitance was done after dispensing UPW. It is found that when given adequate UPW to wet the sensor, the L_L has little effect to the C_P. PCSs #8 and #10 showed similar C_P with PCS #3 across time while the C_P of PCS #9 was a little higher than PCS #3 in **Figure 3.9b**. It is hypothesized if the fluid volume applied to the sensor was the same as PCS #3, sensors with longer loading region would have dissimilar or even null increment of capacitance due to little or no fluid wetting the capacitance area. Evaporation might also affect the wicking process, as a longer loading region would impose a higher exposure to evaporation and loss of sample

fluid. Therefore, unless sample volume is not limited, a shorter loading region would be preferred.

To assess the effect of capacitance area on the sensor performance, a series of PCSs with different area of capacitance area (A_C) were designed by adjusting the whole width of the sensor (W_{PCS}), which includes W_C, W_L and W_S, and keeping the length of the sensor the same. **Figure 3.9b** showed that C_P increased proportionately with W_{PCS} or A_C. The increment agrees to **equation (3.9)** in section 3.2.2. However, the increasing area renders more sample volume and time to achieve the maximum measurement. Also, the time to reach the peak C_P also increased when W_{PCS} increased, *i.e.* PCS #11 reached the peak at about 1000 s and PCS #12 at about 1250 s. The slower time to achieve maximum measurement might relate to the time taken for the fluid to wick in the paper (Lockington & Parlange, 2003).

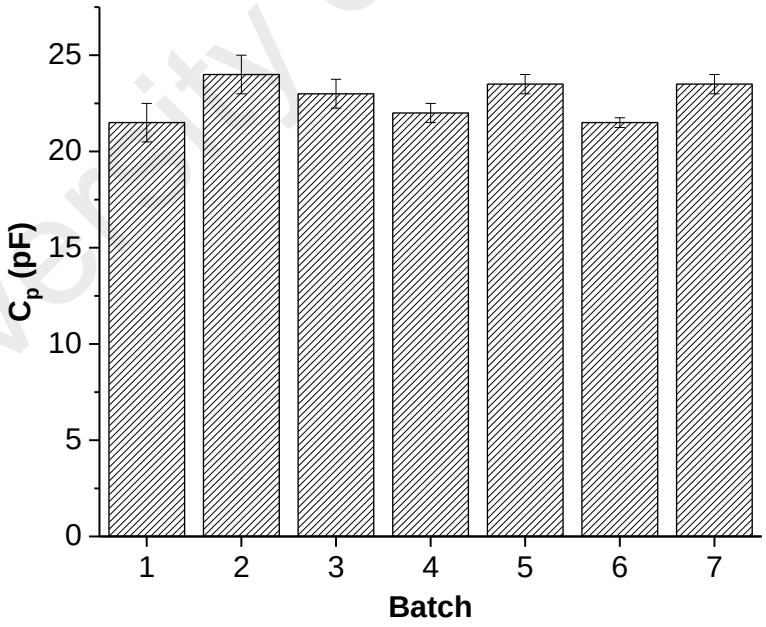

Figure 3.10: Capacitance of different batches of dried PCSs (*n*=8)

For diagnostic purposes, an ideal sensor would be sample conservative, rapid and stable during application. To get a fast measurement with stable results from a small

sample, with the above results, PCS #3 was chosen as the final geometry for further testing. Furthermore, to investigate the stability of PCS #3, 7 batches of PCSs (n=8) were dried and the capacitances were measured. The batches of PCSs do not show significant difference, with an average CP of 23.0 ± 0.3 pF (95% CI), as shown in **Figure 3.10**, thus having a good reproducibility. The parameters of PCS #3 are referred in **Table 3.3.**

Table 3.3: Parameters of #3 PCS

Parameter	Symbol	Value
Dielectric constant of free space	ε_0	8.85 pFm^{-1}
Dielectric constant of double-sided tape	ε_t	2.76 ± 0.08
Dielectric constant of filter paper	ε_p	1.76 ± 0.10
Dielectric constant of cellulose	ε_c	7.45
Thickness of double-sided tape	d_t	1.0×10^{-4} m
Thickness of filter paper	d_p	1.8×10^{-4} m
Effective porosity of filter paper	η	0.57
Capacitance area	A_c	4×10^{-4} m^2

The dielectric constants of double-sided tape and filter paper (at 400 Hz) are measured by broadband dielectric spectroscopy (Novocontrol Concept 80, n=6), respectively. The dielectric constant of cellulose is an estimated value according to the two provided values of cellophane (Clarke, n.d.). The thickness of the double-sided tape is obtained from the manufacturer's instruction, and the thickness of filter paper is an average value of 10 sheets. The effective porosity of filter paper is acquired from Liu et.al. (Z. Liu et al., 2015).

3.3.1.2 Sample loading volume

To investigate the effect of sample fluid loading volume on sensor performance, PCS #3 was loaded with a serial volume of 1 mM $NaNO_3$ and capacitance was measured with a multimeter. Furthermore, to assess the accuracy of the multimeter, its measurement was compared to that by LCR at 400 Hz and 1 kHz. When wet, the multimeter C_P roughly doubled when the loaded volume increased from 10 µL to 60 µL and was almost stable

for higher volume, as shown in **Figure 3.11**. During loading, the dispensed volume of sample fluid determines the amount of sample fluid occupying the void in the filter paper, which corresponds to capacitance.

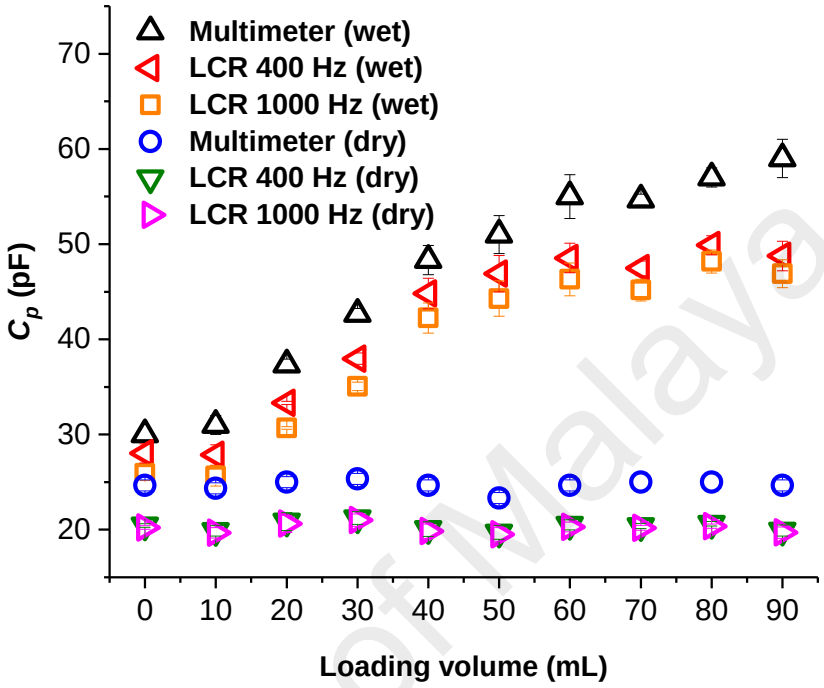

Figure 3.11: Loading volume of sample fluid affecting capacitance measured by multimeter and LCR meter (on 400 Hz and 1000 Hz) before (wet) and after (dry) the sensor was dried

The stable C_P relates to the void volume (V_{void}) that the filter paper has, which is computed as

$$V_{void} = V_p \eta \tag{3.20}$$

where V_p is the total volume of filter paper ($V_p = A_p \times d_p$) and η is the effective porosity of filter paper. For PCS #3, the volume of the void, V_{void} = 56.43 µL, which is 6% lesser than 60 µL. A sample volume beyond 90 µL would result in overflow of sample fluid due to the slow wicking of sample fluid in the filter paper. In consideration of sample evaporation and consumption, we chose to dispense 70 µL sample onto the sensor prior

measurement instead of 60 µL, which takes about 5 min to wet the entire PCS. When comparing the measuring instrument, although CP of multimeter > LCR 400 Hz > LCR 1 kHz, they have similar trend along increasing loading volume. Thus, multimeter makes a good candidate for measuring capacitance.

When dried completely, C_P did not show any trend of change, even though PCSs had been loaded with increasing volume of sample ($p > 0.05$). In the previous wet condition, the measured C_P was mainly affected by the existence of water as the amount of salt was too little, thus extending the need of drying during analysis of heterogenous solution. Notably, when no fluid was applied on the sensor (0 µL), the capacitance before drying (wet) was slightly higher than the one after drying (dry). It is hypothesized that there was moisture in the filter paper before drying that leads to lighter weight after drying, as shown in **Figure 3.12**. Thus, storage humidity or drying may be considered before usage.

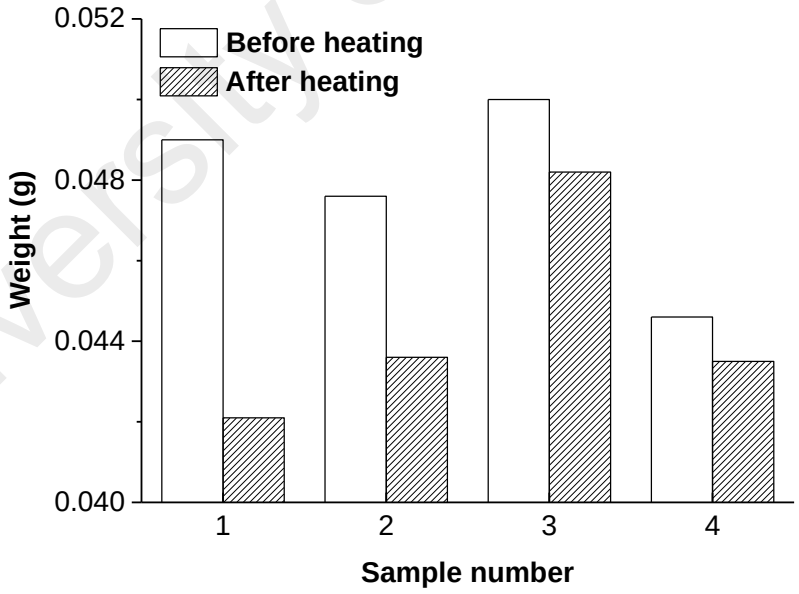

Figure 3.12: The weight of rectangle filter paper with an area of 10 mm×40 mm before and after heating in the oven at 100 ºC for 10 min

3.3.1.3 Position of measurement on the capacitance area

To study the effect of the location of this measuring point, capacitance measurements were taken at 10 different positions on the conducting plates. As shown in **Figure 3.13**,

it is found that C_P for the three situations were showing little or no change at all across the 10 positions. In addition, the higher C_P of as-prepared PCSs than the dried-loaded PCSs relates to the presence of moisture in the as-prepared PCS. Measurements were also taken with LCR at 400 Hz and 1000 Hz after loading. Notably, the lower C_P by multimeter than by LCR after loading with 1mM $NaNO_3$ was due to the incomplete wetting of PCS when it was measured with multimeter first.

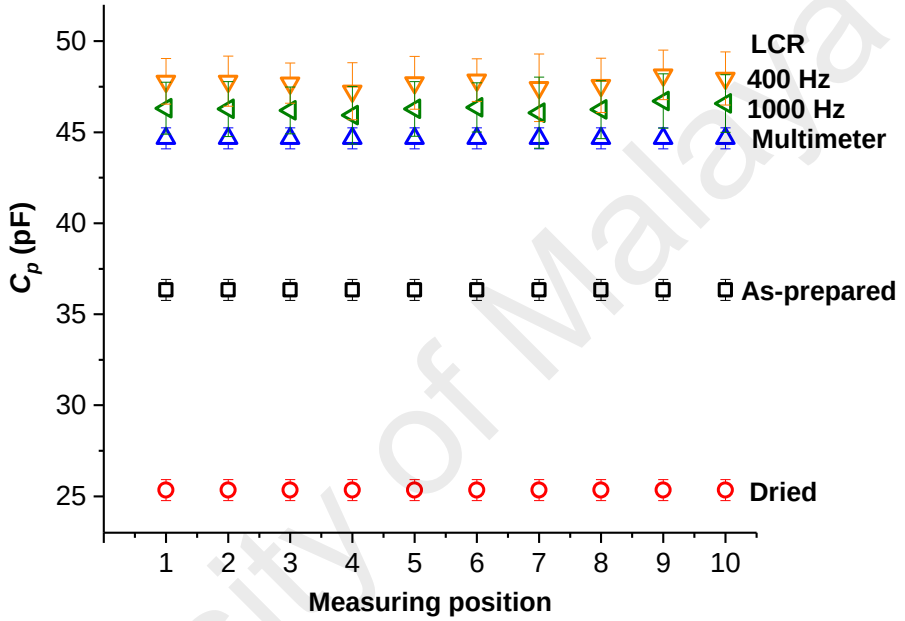

Figure 3.13: Capacitance at 10 different positions on the conducting plates measured with multimeter and LCR meter (400 Hz and 1000 Hz) at different conditions

3.3.1.4 Drying time of PCS

PCS may need drying before sample loading and during solute-based analysis. The drying process eliminates the presence of moisture in PCSs, as the high dielectric constant of water would affect the sensor performance. **Figure 3.14** shows that the C_P across time for idling PCSs has a slight reduction within 10 min. On the other hand, the capacitance of loaded PCS reduced substantially and become stable after about 15 min. To carry on the experiment, 15 min was chosen as the optimized drying time for idle and loaded PCSs. The optimized 15 min of drying time assures the elimination of moisture in filter paper.

Although drying idle sensors has little change in capacitance, it is highly influential to the identification of chemicals and solute-based analyses.

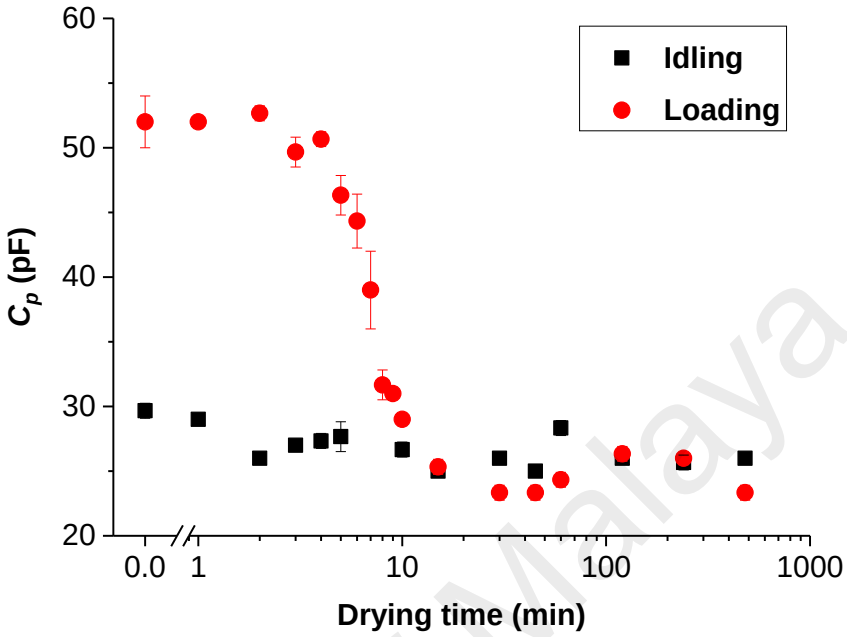

Figure 3.14: Drying time for idle and loaded PCS based on capacitance

3.3.1.5 Number of loading and drying cycle

Theoretically, by repeating the loading of solute-based solution and drying procedures for solute-based analyses, the accumulation of solute particle in the filter paper would change the dielectric properties of filter paper and thus reflect on the C_P measurement. Here in **Figure 3.15**, when UPW (water) was loaded as sample, the C_P remains stable with a little reduction in the third cycle, even though high deviation in measurement was acquired during more load-dry cycles. For 1mM $NaNO_3$, similarly, the C_P reduced after reaching the peak at second cycle, even though the deviation increases after the second cycle. The increase of C_P for 1mM NaNO3 may be due to amount of solute building up in the filter paper of PCS. However, the C_P reduction and increase in deviation may be due to the process of loading and the drying cycle itself. During each cycle of loading and drying, the cellulose fibres undergo hornification that affects the distribution of the fluid (Fernandes Diniz, Gil, & Castro, 2004). Moreover, the ageing process during repeated

drying of filter paper and double-sided tape affects their chemical and dielectric properties. To avoid the frequent effect of cellulose fibres realigning and material degradation, one cycle of load and dry was done for successive tests before measurement.

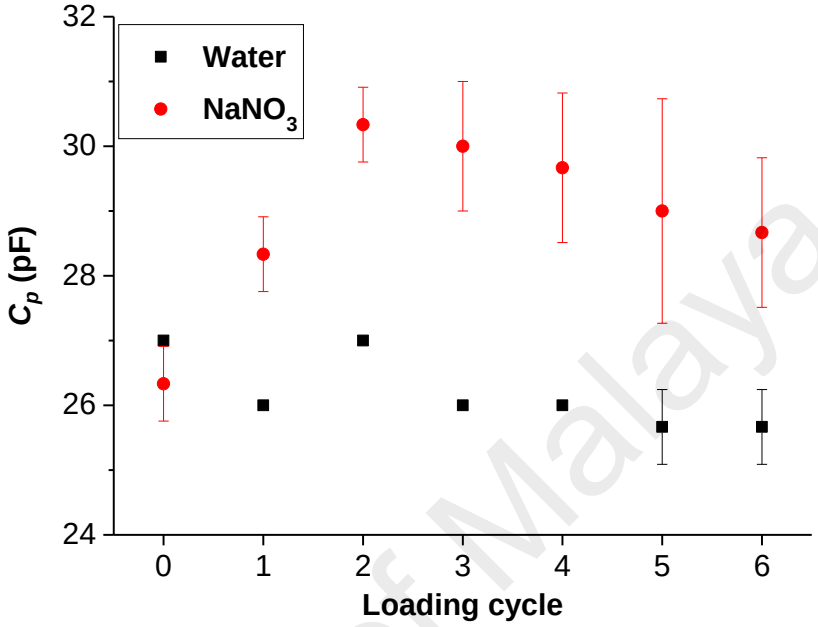

Figure 3.15: Number of loading and drying cycle of fluid affecting capacitance

3.3.1.6 Surrounding temperature

Effects of temperature and RH on the dielectric constant of paper were often discussed in the past studies (Mraovic et al., 2014; Setayeshmehr, Fofana, Akbari, Borsi, & Gockenbach, 2008). In this study, the capacitance for PCSs loaded with UPW were lower than the PCSs loaded with 1M $NaNO_3$, which due to the presence of solute particle in the sensor **(Figure 3.16)**. Different temperature does not significantly affect C_P, when compared to the 0* °C (paired t-test, $p>0.05$, $n=3$), thus showing its feasibility in 20 °C to 90 °C. To clarify, the extrapolated 0* °C was the mean of all the measurements at ambient temperature ($n=3\times8=24$).

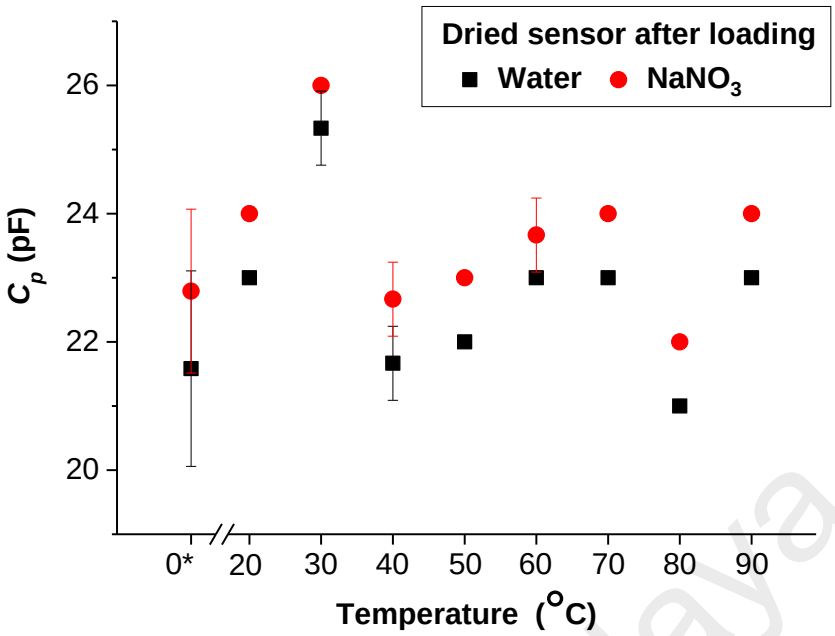

Figure 3.16: Effect of temperature on sensor capacitance during measurement

3.3.1.7 Relative humidity

As filter paper absorbs moisture easily, the dielectric properties of PCS would be greatly affected by different level of relative humidity (RH). By observing differently conditioned PCS, the repeated-use PCSs have a higher C_P than single-use PCS, as shown in **Figure 3.17**. The higher C_P suggests higher water content and dielectric constant, which may be due to enhanced moisture absorbability of filter paper in the PCS after repeated-use.

The C_P of both repeated-use and single-use increased in a linear manner with increasing RH reaching 80%. The R^2 value of repeated use is 0.933 and the R^2 value of single-use is 0.964. At 90% RH, both repeated use and single-use sensors had the highest capacitance that defied the linearity. This high C_P is similar to the measurement achieved by directly dispensing water to the sensor.

In this study, sample volume, time of drying and cycle of loading and drying were optimized to 70 µL, >10 min and 1, respectively, while the position of measurement on

sensor and temperature does not give observable effect to the measurement. While RH cannot be controlled and affects the measurement heavily, the effect can be corrected by normalising the measurements with the base measurement before analysis. Application in an air-conditioned room can also avoid the effect of extreme humidity.

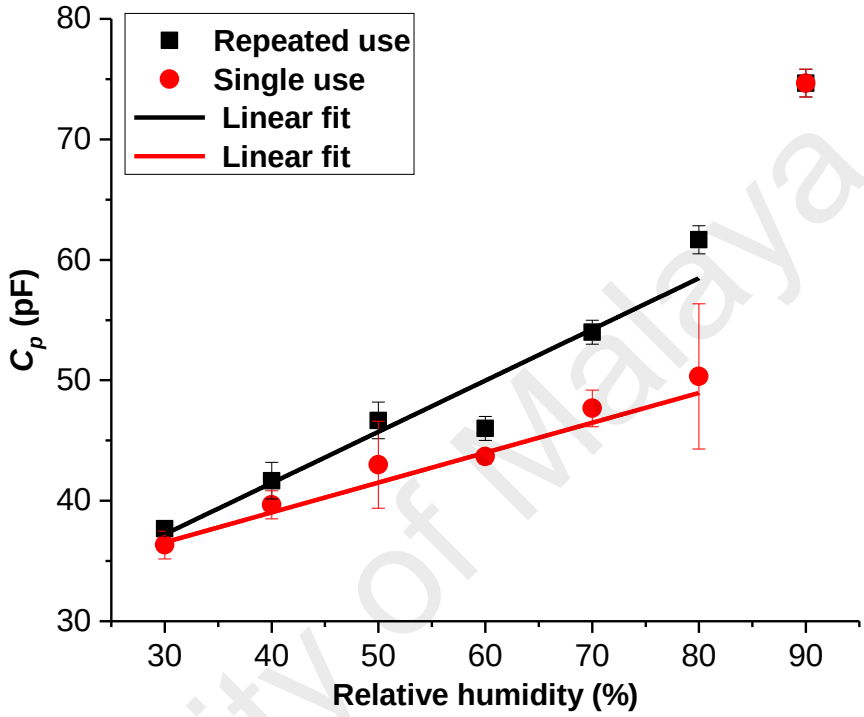

Figure 3.17: Effect of relative humidity to the capacitance during measurement when an unloaded PCS was repeatedly use or singly use

3.3.2 Evaluation of PCS sensing capabilities

Using the previously optimized geometry (PCS #3) and conditions (70 µL sample volume, >15 min of drying and 1 load-dry cycle per PCS), the sensing capabilities of PCSs were assessed through identification of liquid chemicals and quantification of chemical solutions.

3.3.2.1 Identification of liquid chemicals

According to section 3.2.4, the change in PCS's capacitance can be due to the change in dielectric constant of the filter paper.

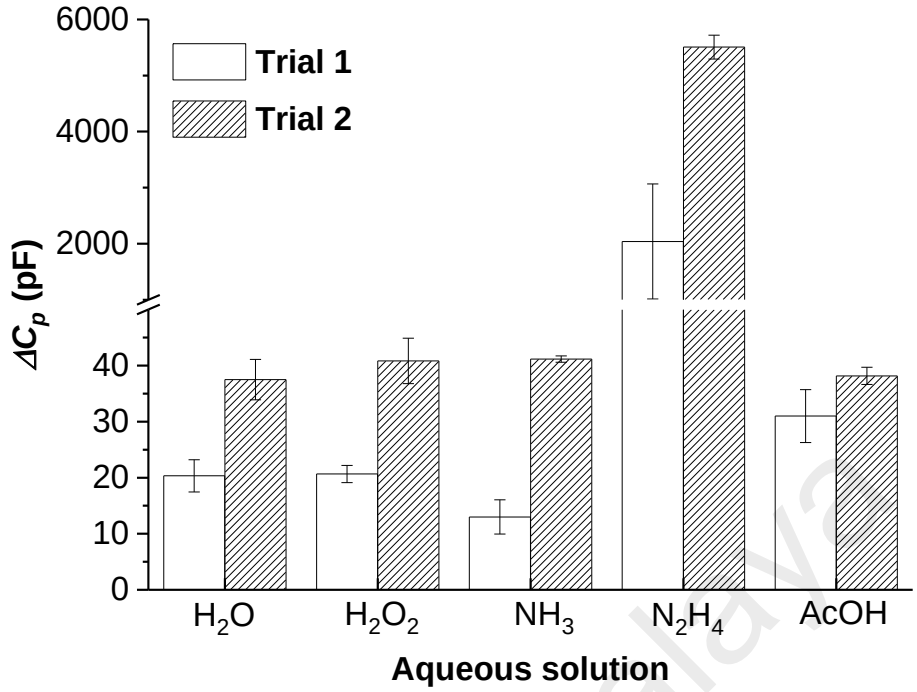

Figure 3.18: Capacitance difference between aqueous solution-loaded PCS and unloaded PCS at pre-dried (trial 1) and no pre-dried (trial 2) conditions

With aqueous non-ionic chemicals (*i.e.* UPW (H_2O), 30% H_2O_2, 25% NH_3, 80% N_2H_4 and 1M AcOH), the trial 2 sensors have higher ΔC_P than trial 1 sensors as shown in **Figure 3.18**. While N_2H_4 had extremely high capacitance, the other chemicals showed similar ΔC_P with trial 2 sensors (Student's t-test, $p>0.05$). With trial 1 sensors, the ΔC_P of the chemicals were distinguishable, especially for AcOH and NH_3.

In **Figure 3.19**, the ΔC_P of liquid organic chemicals (*i.e.* MO, OA, toluene, $CHCl_3$, EA, THF, CH_2Cl_2, iPrOH, EtOH, DEG, ETA, MeOH, DMF, EG, glycerol, DMSO and UPW) were shown with their dielectric constants in an increasing order. The trial 2 sensors have higher ΔC_P than trial 1 sensors for every chemical. The higher ΔC_P of trial 2 sensor than that in the trial 1 sensors is assumingly due to the presence of moisture that affects the measurement. Expected ΔC_P (red circle) of the chemicals was calculated using their standard dielectric constant value. The data and order of chemicals can be referred in **appendix A**. Here, many measured ΔC_P values were lower than expected ΔC_P, possibly

due to loss during the rapid evaporation of the volatile chemicals. Similar to N_2H_4, there were some other chemicals that produced higher ΔC_P than their expected ΔC_P. The ΔC_P decreased significantly when trial 1 sensors were used, especially with N_2H_4 and ETA having extreme value. In overall, an increasing trend can be observed over the increasing dielectric constant, which suit the theoretical expectation. Based on these analyses, it is seen that trial 1 sensor is suitable to identify aqueous fluids with lower capacitance while trial 2 sensor is suitable for identifying organic fluids with higher capacitance. Despite the feasibility of multimeter in chemical identification, some chemicals were having similar ΔC_P on very near dielectric constants, for *e.g.* EtOH, MeOH and DEG. To further distinguish these similar chemicals, $C_P - f$ spectrum of each chemical was produced using LCR meter.

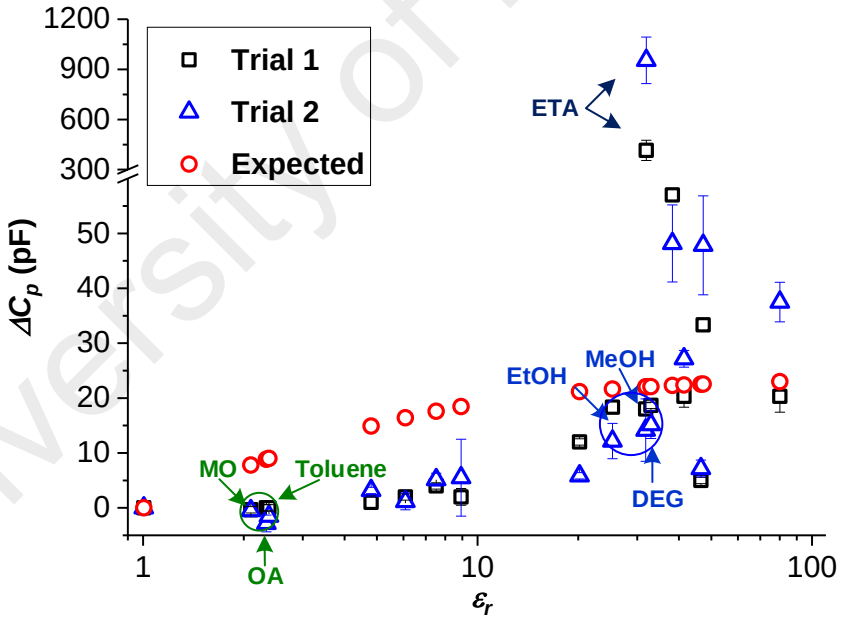

Figure 3.19: Capacitance difference of pre-dried (trial 1) and as-prepared (trial 2) PCSs loaded with pure liquids-loaded unloaded PCS, according to respective dielectric constants (ε_r)

Figure 3.20 shows the capacitance spectra of chemicals at trial 1 (**a, b and c**) and trial 2 (**d, e, and f**) conditions, between 100 Hz to 1 MHz. **Figure 3.20b** and **c** are zoom-ins of y-axis in **Figure 3.20a** while **Figure 3.20e** and **f** are zoom-ins of y-axis in **Figure**

3.20d. While $CHCl_3$ and CH_2Cl_2, and MO and OA were difficult to differentiated with trial 1 sensors (**Figure 3.20c**), N_2H_4, ethanolamine, DEG, EG, DMF, DMSO and glycerol were easily distinguishable with trial 2 sensors (**Figure 3.20d**). It is assumed that these chemicals are very hygroscopic fluids and therefore exhibiting high capacitance. Nevertheless, the aqueous solutions (**Figure 3.20e**) and organic liquids (**Figure 3.20f**) were also hard to distinguish with trial 2 sensors.

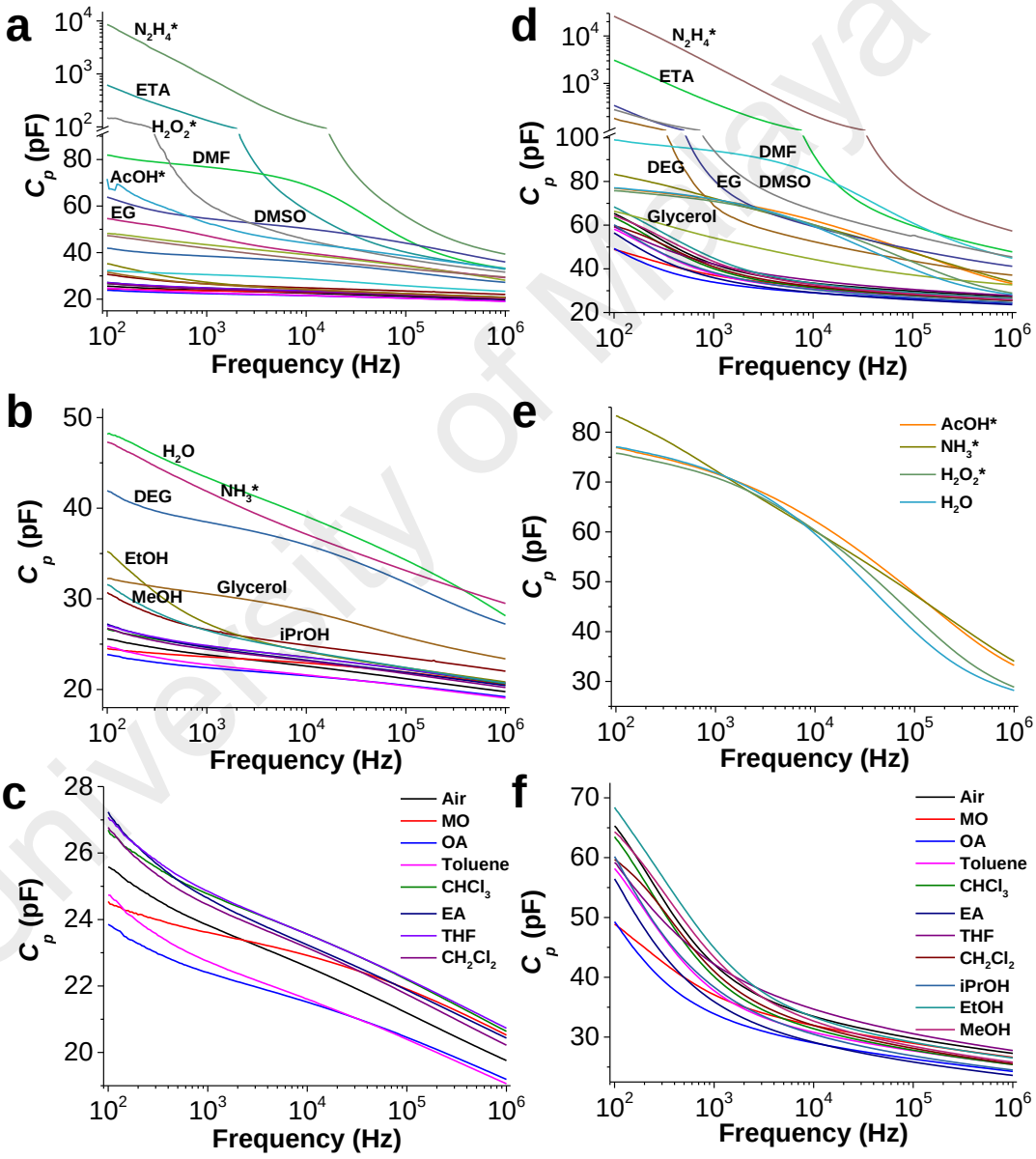

Figure 3.20: Capacitance – frequency spectra of various sample fluids loaded on pre-dried (trial 1) (a, b and c) and no pre-dried (trial 2) (d, e and f) PCSs

Although the C_P–f spectra were able to distinguish DEG from EtOH and MeOH, as shown **Figure 3.21**, the C_P–f spectra of EtOH and MeOH were still hardly distinguishable. Moreover, the C_P–f spectra of two-repeated test for DEG (#1 and #2) were not the same, thus showing a weak repeatability in frequency-based analysis. Improvement may be further studied.

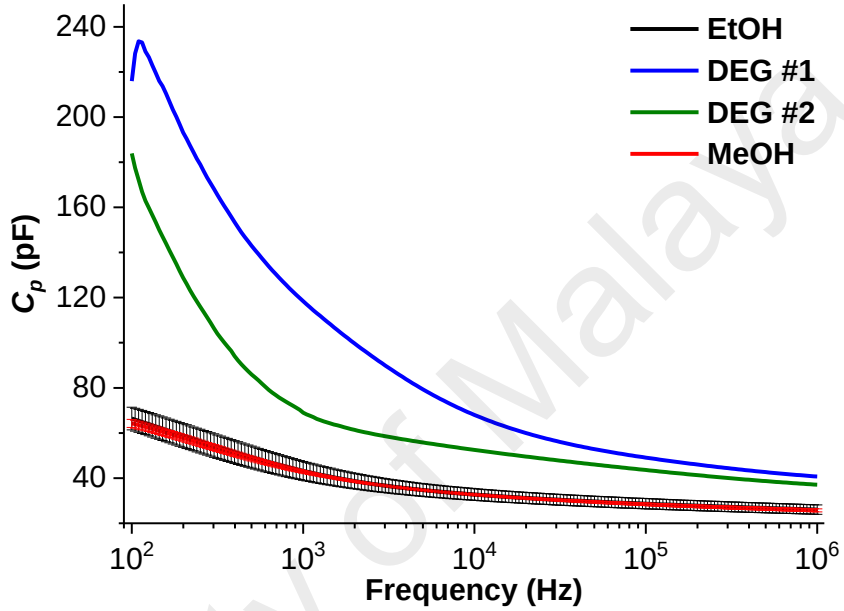

Figure 3.21: Capacitance-frequency spectra of ethanol, methanol, and two repeats of diethylene glycol

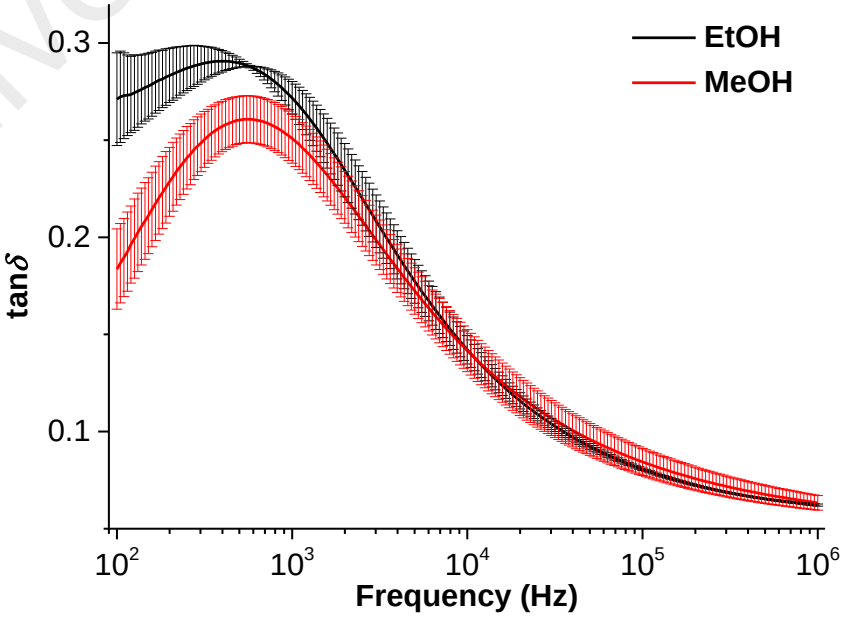

Figure 3.22: Dielectric loss (tan δ) – frequency spectra of ethanol and methanol

To further distinguish MeOH and EtOH, the dielectric loss tangent δ – frequency (*tan δ – f*) spectra of both chemicals at 100 Hz – 1MHz were also acquired. **Figure 3.22** shows that the *tan δ – f* spectra of MeOH and EtOH had different peak *tan δ* and corresponding *f*.

All other chemicals were distinguishable when their *tan δ – f* spectra (*n*=3) were analysed for their peak *tan δ* and corresponding *f*, especially chemicals that were not distinguishable, as shown in **Figure 3.23**. Here it is shown that both MO and OA or CH_2Cl_2 and $CHCl_3$ had different peak values at different frequency points. At this point, dielectric loss – frequency spectroscopy could give a clearer differentiation among the similar fluid chemicals.

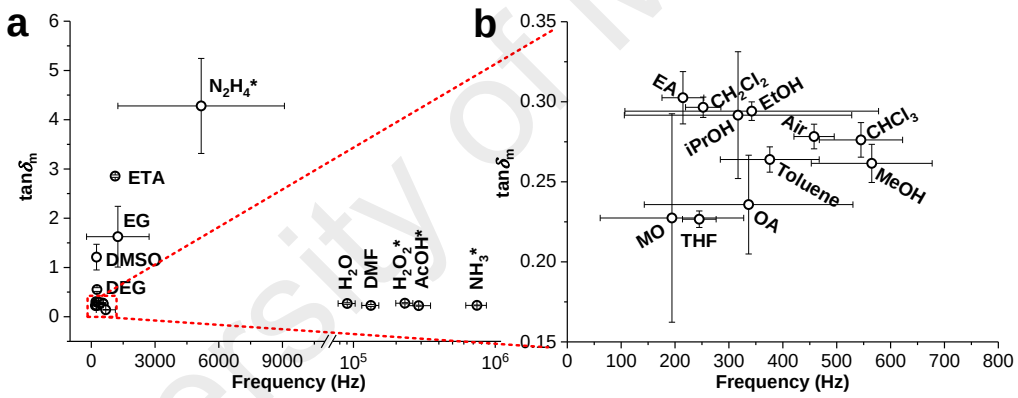

Figure 3.23: Peak value of dielectric loss (tan δ_m) – frequency spectra of various fluid chemicals

3.3.2.2 Quantification of chemical solutions

In the present study, quantification of pure liquid solution (EtOH-water) and solute-based solutions (various sodium and nitrate salts) was done using PCS. For EtOH-water solution, **Figure 3.24** shows the decreasing normalized capacitance value measured by multimeter when the volume fraction of EtOH increases (*n*=3). The decreasing of the overall dielectric constant of the mixture due to the low dielectric constant of EtOH and high dielectric constant of water may lead to the reduction of capacitance. The expected

values were calculated using the dielectric constant value obtained by Wohlfarth (Wohlfarth, 2008). The measured #1 PCSs had a higher normalized capacitance than measured #2 PCSs, however they share a similar increasing trend with the computed expected results.

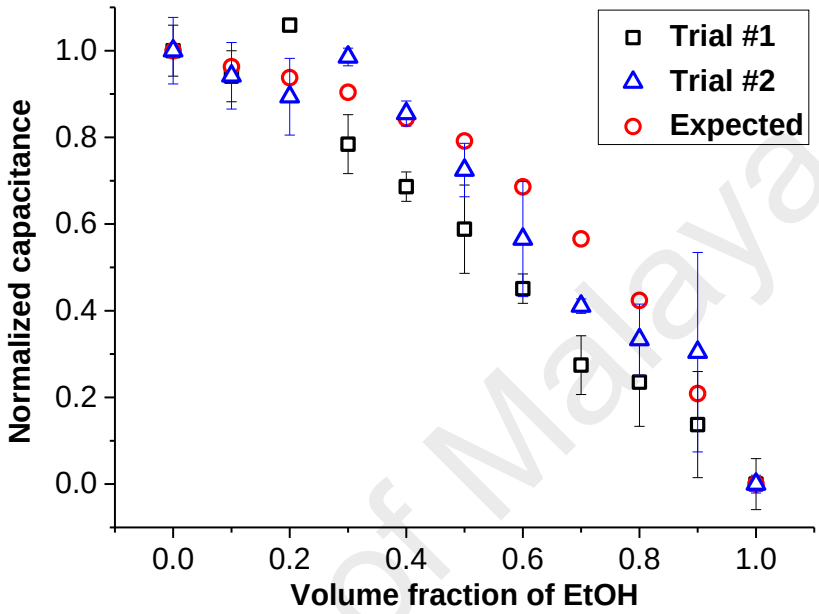

Figure 3.24: Normalized capacitance of ethanol-water solution with different volume fractions on pre-dried (measured #1) and no pre-dried (measured #2) PCS

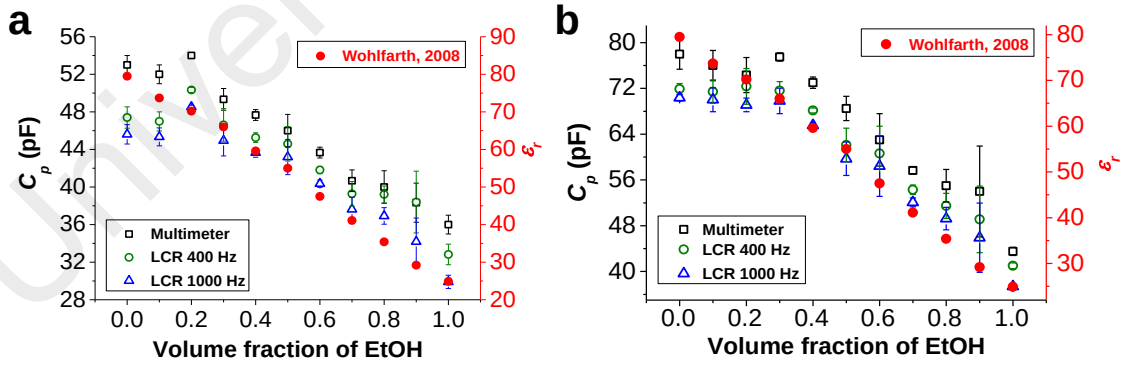

Figure 3.25: Capacitance of ethanol-water solution with different volume fractions on pre-dried PCS (a) and PCS without pre-drying (b) compared to dielectric constant data (red dots) obtained by Wohlfarth

The C_P of EtOH-water solutions by different instruments was compared to the dielectric constants of the solution obtained by Wohlfarth (Wohlfarth, 2008) in **Figure**

3.25. There was no increase of C_P by LCR meter when the volume fraction of EtOH was below 30% whereas it increased when measured by multimeter. Nevertheless, the difference between the measured and calculated capacitance using Wohlfarth's data might still be influenced by evaporation and fluidic factors. The capacitance measured by multimeter was also comparable to that by LCR meter, thus showing similar feasibility in quantifying.

For solute-based or salt solutions, the change in capacitance (ΔC_P) was calculated by subtracting the measurement of loading UPW (0 mM) from that of salt solution. **Figure 3.26** shows an increase in the ΔC_P of sodium salt solutions when the of salt concentration increases from 0.01 to 100 mM. However, the variation trends for the anions and corresponding LOD were dissimilar, thus showing weak recognizability and less sensitivity of PCS to many anions. Similarly, for various cations of nitrate salts, **Figure 3.27** shows that ΔC_P increases with increasing salt concentration. The change in capacitance from 0.01 mM to 1M categorises the nitrate salt solutions into groups based on the increasing valency, *i.e.* Na^+ and K^+, Pb^{2+} and Cd^{2+}, Mn^{2+} and Cr^{3+}, and Fe^{3+}. The capacitance of salts from the same valency tended to increase similarly with rising concentration.

Since the strength of ionic bonding and field strength could affect the dielectric properties of a material (Friedenman & Shuler, 1947; Roberts, 1950), having a higher valency or charge would impart smaller ionic radius and contributes to the higher strength of ionic bonding. With the higher strength of ionic bonding, the ions resist the applied AC electrical field at low frequency, e.g. 400 Hz, easily, hence showing high dielectric properties. In this study, at 1 M of nitrate salt solution, the capacitance increased in the order $Fe^{3+} > Cr^{3+} > Mn^{2+} > Cd^{2+} > Pb^{2+} > Na^+ > K^+$, which is comparable to their

decreasing valency and increasing ionic radius. Among the limited metal nitrates salt in the analysis, Fe^{3+} salt solution shows the greatest difference in capacitance.

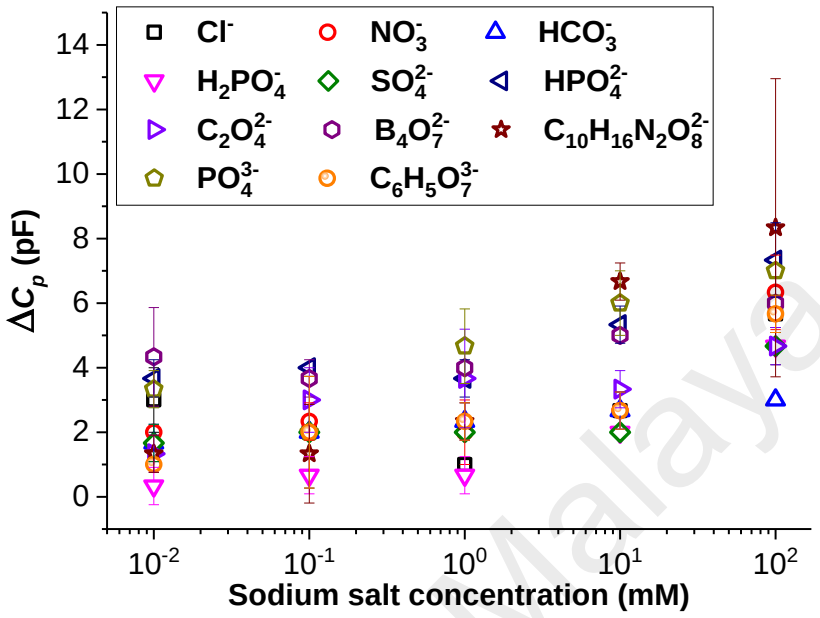

Figure 3.26: Capacitance difference between PCS loaded with various anionic sodium salt solutions and unloaded PCS at different concentrations

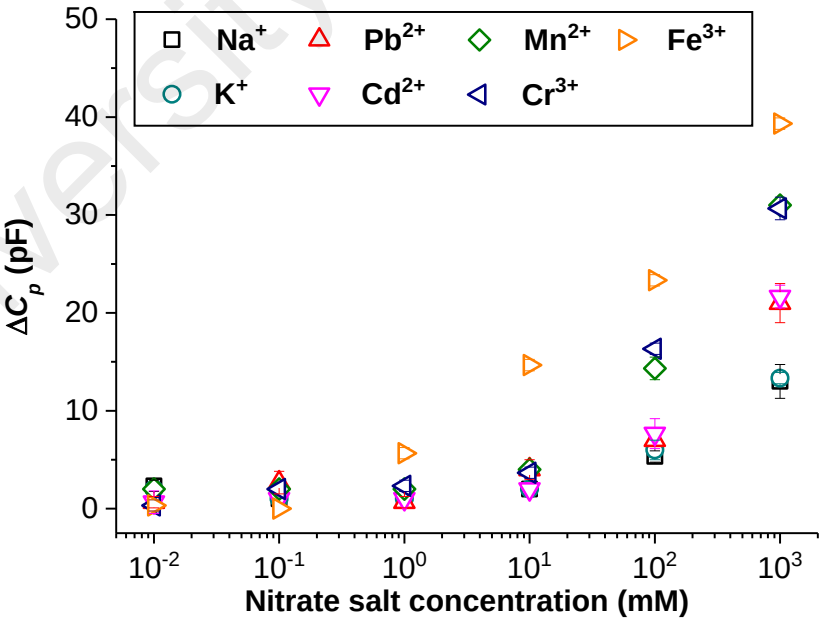

Figure 3.27: Capacitance difference between PCS loaded with various cationic nitrate salt solutions and unloaded PCS at different concentrations

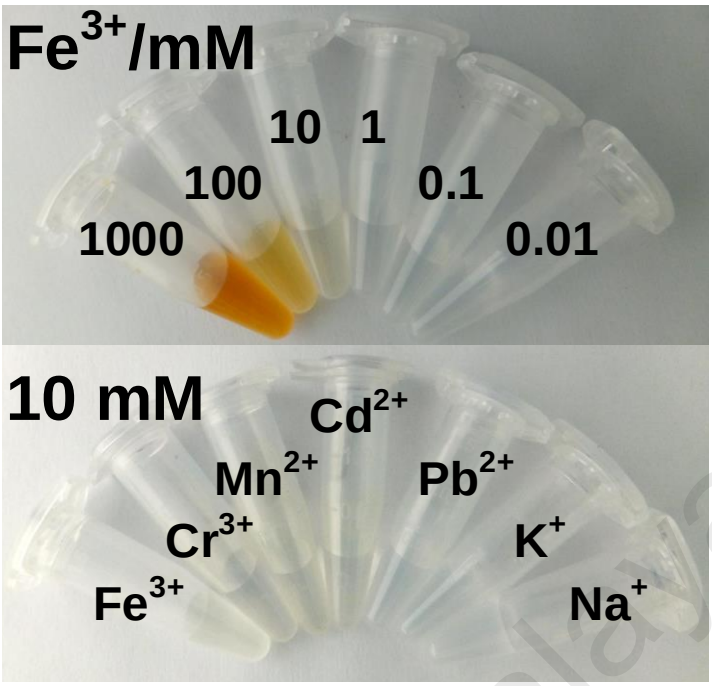

Figure 3.28: Iron (III) nitrate salt solution at different concentrations (top) and various cationic nitrate salt solutions at 10mM (bottom)

The LOD of PCS for Fe^{3+} is 1 mM, where the solution could not be differentiated by the naked eyes from lower concentration or plain water. Visually, when the concentration of the salt solution increases, the colour of Fe^{3+} nitrate solution becomes darker, as shown in the top image in **Figure 3.28**. The bottom image in **Figure 3.28** shows different cationic nitrate salt solutions in 10 mM concentrations that do not show any obvious difference in colour.

With regards to the analyses of the EtOH-water solution and salt solutions with different cations, PCS is feasible for quantifying binary fluids and concentrations of salt solutions. Moreover, PCS could roughly distinguish monovalent, divalent and trivalent cations at high concentrations.

3.3.3 Summary

A low-cost paper-based capacitive sensor (PCS) for chemical identification and quantification has been developed. The sensor leverages the beneficial properties of

paper, i.e. its light weight and wickability, while adapting to the working principle of a simple parallel plates capacitor. The sensor has no specificity and is therefore unable to specify the substance if an unknown solution is given. To detect low level of target analytes in limited clinical and water samples, a direct and easier method to enhance sensitivity of paper-based platform is needed. The following chapter elucidates the novel sensitivity enhancement method on a paper-based lateral flow sensor, i.e. lateral flow assay (LFA).

CHAPTER 4: ELECTROSPIN-COATING OF NITROCELLULOSE MEMBRANE ENHANCES SENSITIVITY IN LATERAL FLOW ASSAY FOR NUCLEIC ACID TESTING

4.1 Introduction

The present chapter showcases the application of electrospun fibres to a conventional nucleic acid-based LFA as a proof of concept to improve the sensitivity of paper-based sensors. Since the fibres can be directly deposited on nitrocellulose (NC) membranes, the fabrication process is simple and straightforward. PCL nanofibers are directly electrospun onto the NC membrane at different duration of time to explore the conditions, *i.e.* flow time and contact angle for improved sensitivity and signal intensity. The microstructure of the electrospun fibrous layer was also observed. This electrospin-coating strategy holds great promise in high detection of various targets in paper-based diagnostic platform.

4.2 Materials and methods

4.2.1 Far-field electrospin-coating nitrocellulose membrane

A 10% (w/v) PCL (M_n=80,000, Sigma Aldrich, USA) solution was prepared in a co-solvent system consisting 9 parts of chloroform (Friedemann Schmidt, Australia) and 1 part of DMF (Merck, USA) (9:1 v/v) in a condensed flask under stirring conditions at room temperature to obtain the spinning dope. The electrospinning was carried out using an electric field of 12 kV (Gamma High Voltage Research, Ormond Beach, FL, USA), a blunt 20 G needle (Terumo), needle to aluminium collector distance of 18cm while the feeding rate was kept constant at 3 ml/h with a syringe pump (KD Scientific, Inc., Holliston, MA, USA). The HFB 13500 NC membrane (Millipore, USA) were stuck on the aluminium collector using double-sided tape and electrospun fibres were directly deposited on them at different time duration. The electrospin-coated NC was then left to dry at least overnight in 37 °C before assembly into the LFA test strip. The setup for

electrospinning and the resultant electrospin-coated NC membrane is depicted in **Figure 4.1**.

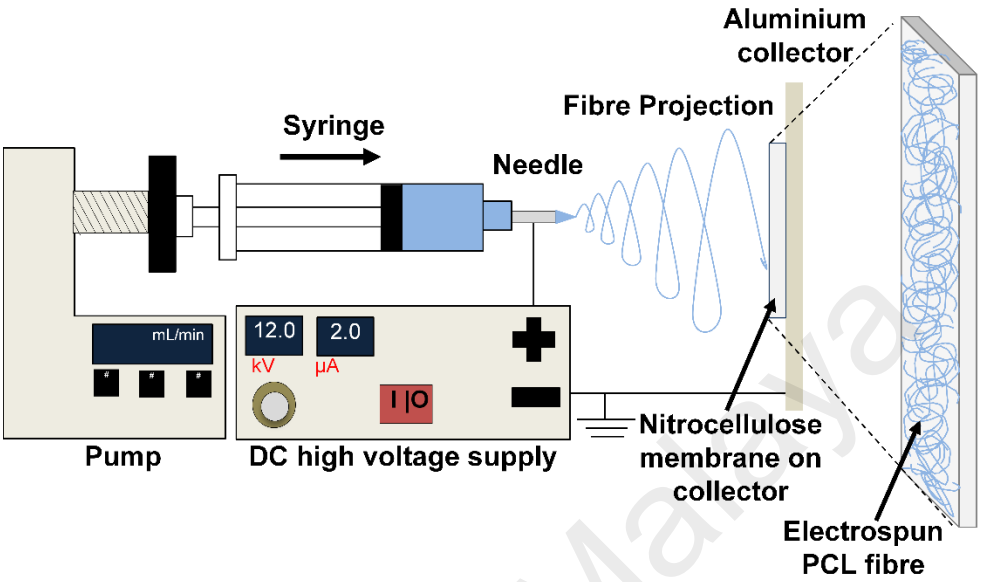

Figure 4.1: Schematics of electrospinning PCL fibres onto the NC membrane

4.2.2 Designation of oligonucleotide probes and target DNA

All the oligonucleotides were synthesized by SBS Genetech Co., Ltd (Beijing, PRC). Designation of the sequences for each probe can be referred to **Table 4.1**.

Table 4.1: Sequences of oligonucleotide probes and target

Oligonucleotide Name	Sequence
Detecting probe	5′-SH-ATCATCgAAgTggCTTCA-biotin-3′
Capture probe	5′-AATgCTTTTCCgCC-biotin-3′
Target DNA	5′-ggAAAAgCATTTgAAgCCACTgTgAgA-3′

The 27 bp target DNA used in the LFA is designed and based on the envelope gene in zika virus. The query of the sequence was done using the website of National Centre for Biotechnology Information (NCBI) search database for virus variation. We referred to the sequence with the accession number of **KY921911** (Hapuarachchi, Koo, & Ng, n.d.). Our target DNA is a copy of a partial CDS sequence from Zika Virus isolate 09410

envelope protein gene starting at 1222 to 1248. The detecting probe was designed to bind partially to the 3′ end of the target DNA. The thiol group was modified at the 5′ to conjugate with AuNPs while biotin at 3′ was to bind with streptavidin at the control line on the LFA. Meanwhile, capture probe was designed to bind partially to the 5′ end of the target DNA and the biotin at 3′ was to bind with streptavidin before being dispensed onto the NC membrane to serve as the test line on the LFA.

4.2.3 Preparation of gold nanoparticles (AuNP) and AuNP-Detecting Probe (AuNP-DP) conjugates

Preparation of AuNP of diameter 13 nm was based on previous study with some modifications (J. Hu et al., 2013). To prepare 13 nm AuNP, 100 mL UPW was boiled at 100 °C under an oil bath with a condenser to avoid the loss of water content. To this was then added 4.5 mL of 1 % (w/v) trisodium citrate (Sigma Aldrich, USA) under continuous stirring (1500 rpm) and heating (100 °C). Subsequently, 1.2 mL of 0.825 % (w/v) gold (III) chloride (Sigma Aldrich, USA) was added to the continuously heated (100 °C) and stirred (1500 rpm) solution to be reduced to AuNP. The solution would gradually turn from yellow to blue and finally to a stable wine red. The heating was then stopped, and the solution was kept stirring until it cooled to room temperature. The resultant AuNP solution was used to prepare AuNP-DP conjugates.

To prepare AuNP-DP conjugates, about 1 mL of the prepared AuNP was conjugated with the addition of 6 µL of 100 µM detecting probe. After 16 h or more, the solution was added with 1% SDS (Sigma Aldrich, USA) and 2 M NaCl (Merck, USA) in an amount that achieved 0.01% SDS and 0.16 M NaCl as the final concentration in the solution. The solution was then allowed to age for at least 24 h before being centrifuged at 14000g for 25 min. Following centrifugation, the pellet was resuspended in 100 µL eluent buffer, comprised of 5% BSA (AMRESCO, USA), 0.25% Tween-20 (Sigma Aldrich, USA),

10% sucrose (Ajax Finechem Pty. Ltd, Australia) and 20 mM Na_3PO_4 (Sigma Aldrich, USA) and the resultant AuNP-DP conjugates solution was kept in 4°C for future use. The DP was prepared by adding in 42.2 µL of 500 mM acetate buffer, pH 4.68, which consists of 1 M acetic acid (Fisher Scientific, Malaysia) and 0.21 M sodium acetate (Ajax Finechem Pty. Ltd, Australia), to the lyophilized detecting probe and topped up to 100 µM with UPW.

4.2.4 Characterizations of electrospin-coated nitrocellulose membrane

4.2.4.1 Microscopy

The surface morphology of the electrospin-coated NC membrane was examined with a Nikon Eclipse E100 upright microscope (Nikon, Japan), and a field emission scanning electron microscope (FESEM) (Carl Zeiss Auriga, Germany) after sputter-coating with gold. Fibre diameter and distribution were obtained using ImageJ software.

4.2.4.2 Water contact angle

Water contact angle on electrospin-coated NC membrane was measured after dispensing a 10 µL ultrapure water droplet (UPW) from an Aquinity P30 LS ultrapurification water system (membraPure GmbH, Germany) using a micropipette tip. Due to swift absorption of water on the membrane, a video of the whole process of dispensing a water droplet was recorded using a Canon EOS 5D Mark III camera. The framed image when the droplet contacted the electrospin-coated NC membrane and just left the micropipette tip was selected for measurements using VLC video player. The contact angle of the water droplet was analysed using ImageJ software.

4.2.4.3 Flow rate measurement

A strip of electrospin-coated NC membrane (3.0 cm x 0.25 cm) was dipped vertically into a well of 96 well plates containing 20 µL AuNP solution. The time taken for the lateral flow in the strip was observed and measured every 0.5 cm travelled using a CT-20

digital timer (Canon, Japan). A ruler was set at the side as a reference to the travelled distance. The AuNP solution used for this measurement was produced by centrifuging 1 mL prepared AuNP, discarding the supernatant and resuspending the pellet in 100 µL eluent buffer. Then, the resuspended AuNP solution was freeze-dried and resuspended again in 500 µL SSC x4 solution.

4.2.5 Fabrication of LFA test strip with electrospin-coated NC membrane

Paper materials included H-1 cellulose pad (JNBio Co., Ltd, Shanghai, PRC) as absorbent pad, Pall 8964 glass fibre (Pall Corporation, Saint Germain-en-Laye) as sample pad and J-B6 backing card (JNBio Co., Ltd). Electrospin-coated NC membrane (2.0 cm x 0.25 cm), sample pad/conjugate pad (2.0 cm x 0.25 cm) and absorbent pad (2.5 cm x 0.25 cm) were tailored using a guillotine paper cutter and assembled together by mounting on a piece of PVC backing card (6.0 cm x 0.25 cm), as shown in **Figure 4.2**.

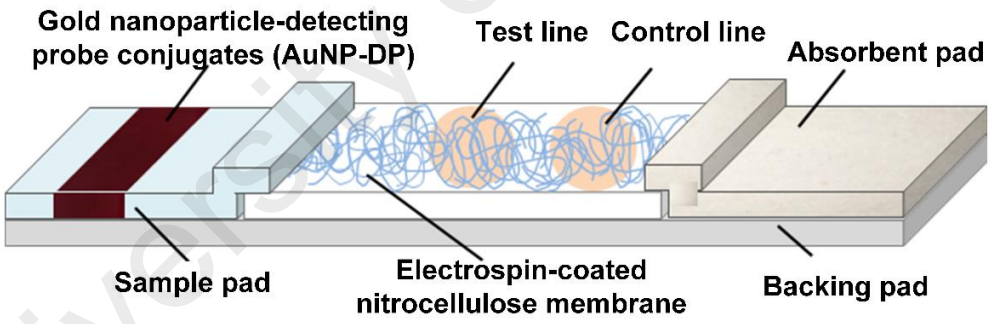

Figure 4.2: Structure of electrospin-coated LFA

The sample pad was soaked wet in 0.1% of Tween-20 and dried in the oven before assembly. On the test strip, 4 µL of AuNP-DP were added to the middle of the conjugate/sample pad while 0.5 µL of control probe and capture probe were dispensed onto the NC membrane using a micropipette to produce a control line and a test line, respectively. The test strip was then dried at 37°C for at least 30 min before using. The control probe was prepared by dissolving 2 mg streptavidin (Promega, USA) in 500 µL

of 10 mM PBS (Sigma Aldrich, USA). The capture probe was prepared by adding 269.5 µL of the 2 mg mL^{-1} streptavidin-PBS solution and 47.1 µL of 10 mM PBS. The solution was then left for 1 h before 36.2 µL 95% ethanol (Systerm, Classic Chemical Sdn Bhd, Malaysia) was added.

4.2.6 Concept of electrospin-coated LFA

Figure 4.3 shows the schematics of LFA with electrospin-coating NC membrane. In LFA, when sample fluid is applied, the target particles bind to the AuNP-DP and the bound target will be captured by the capture probe at test lines in NC membrane (J. Hu et al., 2014). Thus, the number of bound targets would affect the signal intensity (Sajid et al., 2015). Meanwhile, the time taken for the target solution to reach the test zone is vital for binding reactions. The complexity in the capillary action will be the main factor to the flow rate of the solution (Washburn, 1921), affecting the number of labels present in the test line and ultimately the intensity of the signal. Here, the integration of electrospun fibres by electrospin-coating PCL onto NC membrane renders delays in the capillary rate of LFA. Since there is no additional installation of shunts or devices, the original setup of the assay was unchanged, and the simplicity of the strip fabrication is retained.

We chose PCL as our candidate for electrospin-coat material due to its potential hydrophobicity, good mechanical properties and slow degradation rate that make it a good blending material for tissue engineering (Gopinathan et al., 2015), drug delivery platforms (Coombes et al., 2004) and biosensors (Zheng et al., 2008). As shown in **Figure 4.4**, when the number of electrospun PCL fibres on the NC membrane increases, this renders a change in hydrophobicity at the coated region that will reduce the flow rate. This, in turn, causes a rise in signal intensity.

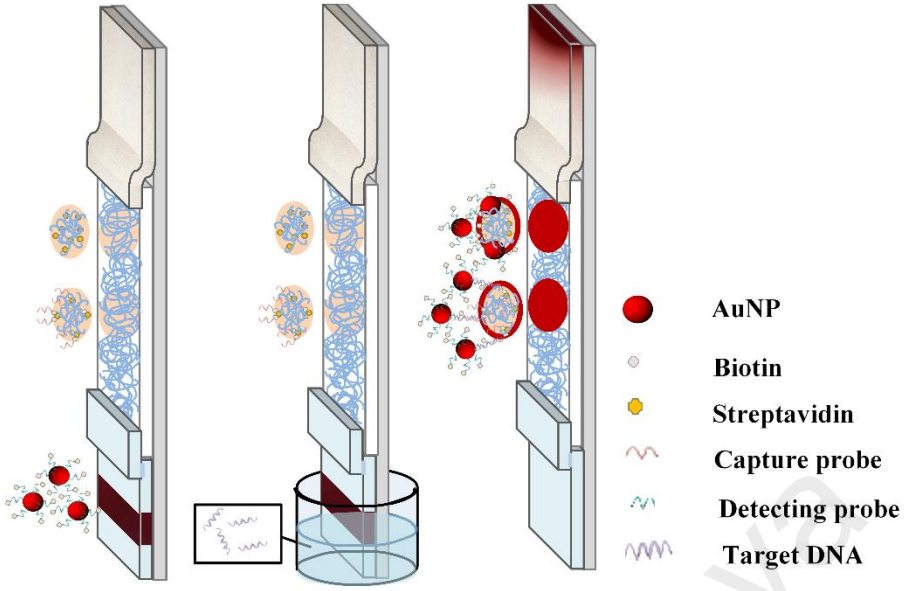

Figure 4.3: Schematics of LFA with electrospin-coating NC membrane

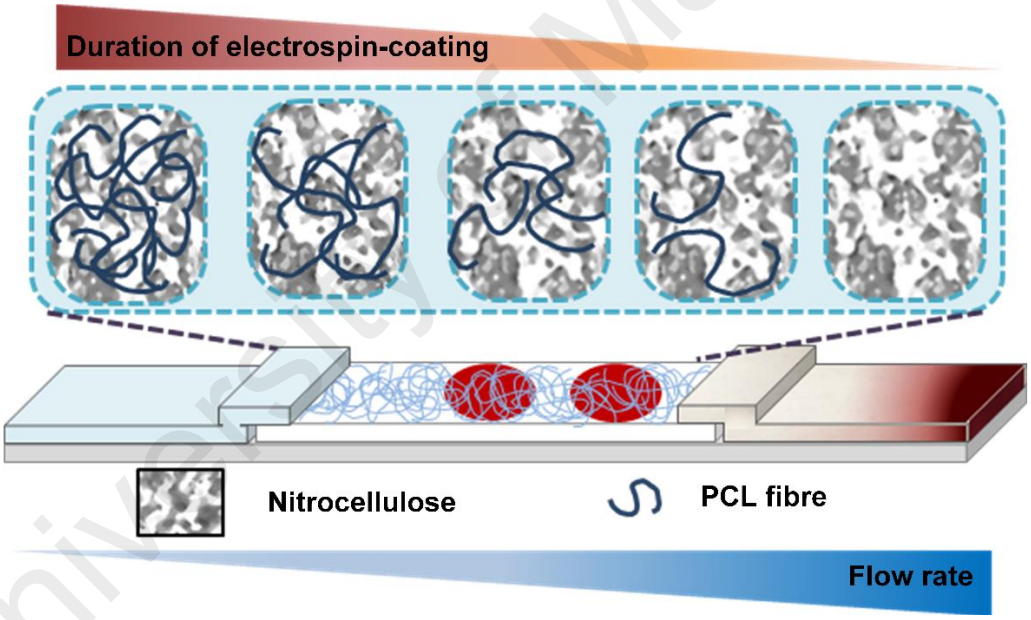

Figure 4.4: Flow control in LFA with electrospin-coating

4.2.7 Colorimetric analysis of lateral flow assay

Synthetic target DNA used was designed according to zika viral cDNA. Target DNA was diluted using 4× SSC buffer pH 7.4 (Roche Diagnostics, USA). The prepared LFA test strips were dipped into the 96 well plate pre-dispensed with the target DNA solution. Comparison between different durations of electrospin-coating was tested with 5 nM

target solution. The sensitivity of the assay was tested at the target's concentration range of 5 nM to 0.1 nM. 4× SSC buffer was used as negative control samples. When the signals at control line and test line were stable, the resultant LFA test strips were scanned at 600 dpi using a Canon LiDE 110 scanner. The mean intensity was analysed using Image Pro Plus 6.0 software (Media Cybernetics. Inc. Bethesda, MD).

4.2.8 Statistical Analysis

Data are tested using IBM SPSS Statistics 24 software. All tests are based on n=3 and results of $p \leq 0.05$ are considered significant or otherwise stated. Data are represented as mean ± standard mean error.

4.3 Results and Discussion

4.3.1 Characterizations of electrospin-coated nitrocellulose membrane

4.3.1.1 Microscopy

Microscopic structures of pre- and post-electrospin-coating PCL on NC membrane are observed using optical microscopy and FESEM. The porous structure of NC membrane in **Figure 4.5a and 4.5b** provides capillary action for fluid to travel in the membrane.

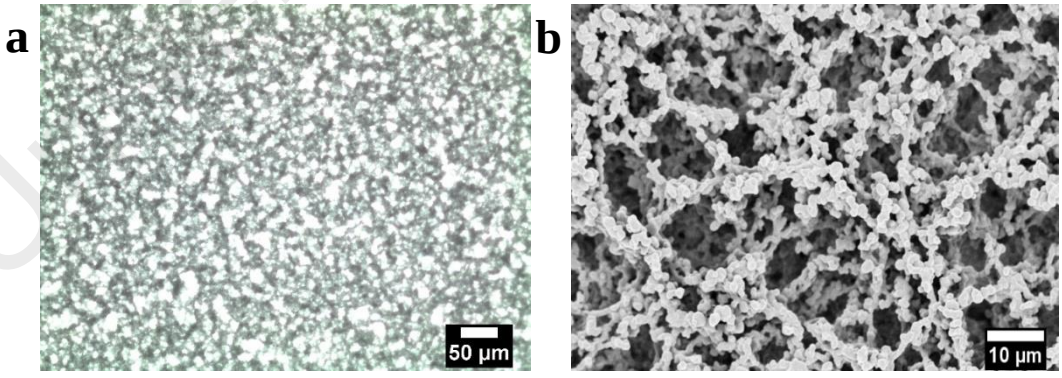

Figure 4.5: Optical microscopic (a) and FESEM (b) images of NC membrane at 100× and 1000× magnification, respectively.

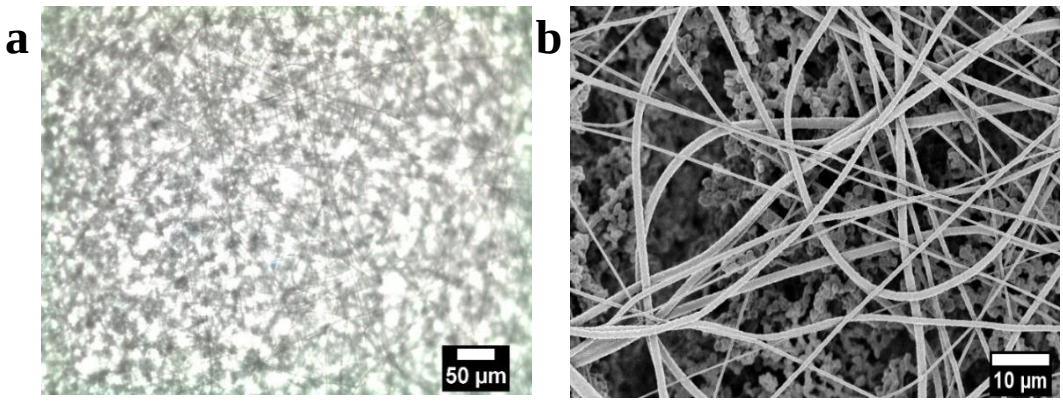

Figure 4.6: Optical microscopic (a) and FESEM (b) images of PCL electrospin-coated NC membrane at 100× and 1000× magnification, respectively.

Electrospin-coated NC membrane after 60 s of electrospinning is shown in **Figure 4.6a and 4.6b**. The fibres are bead free and some fibre bending could be observed. When PCL is electrospin-coated onto NC membrane, the nanofibres cover the NC membrane with a thin layer. Although this layer of PCL nanofibres does not obscure the NC membrane completely, interfibrillar pores provide spaces for the fluid to reach the bottom layer of NC membrane.

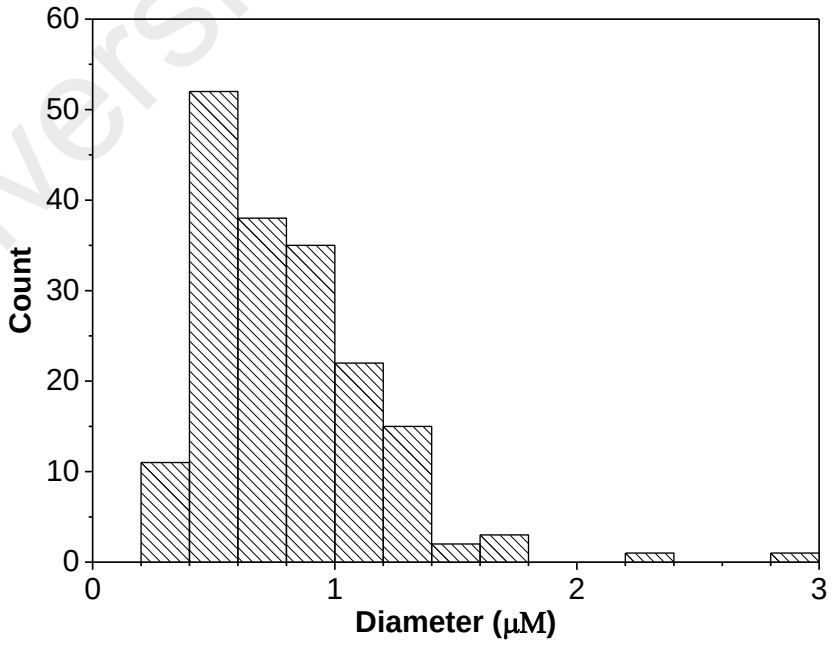

Figure 4.7: Diameter of PCL nanofibres distributed on electrospin-coated NC membrane

From the distribution of fibre diameter in **Figure 4.7**, the nanofibres range from 250 nm to 2.85 µm with an average diameter of 799 nm and standard deviation of 363 nm (*n*=180). The diameter of most fibres ranges from 400 nm to 600 nm. The electrospun PCL nanofibres are only deposited on top of the NC membrane, without any penetration, as shown in the side view of the edge of electrospun-coated NC membrane in **Figure 4.8**.

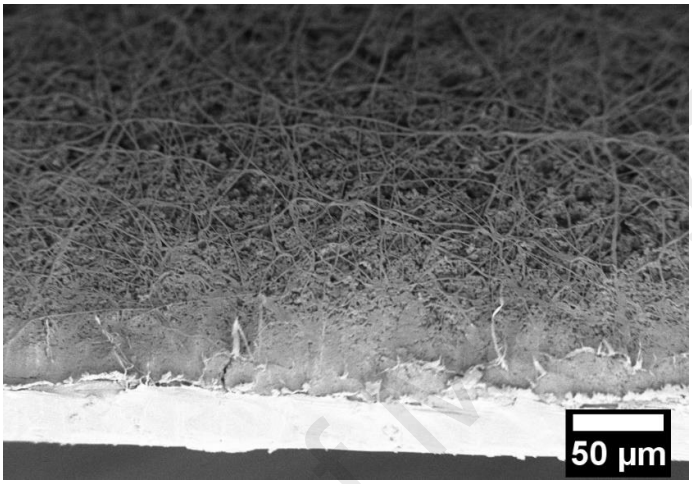

Figure 4.8: Side view on the edge of electrospin-coated NC membrane at 600×

4.3.1.2 Water contact angle

Due to the hydrophobicity of PCL nanofibres, the flow of liquid on the NC membrane is likely to be affected by the presence of PCL nanofibres. We evaluated the PCL effect by electrospin-coating NC membrane for durations of 30 s, 60 s, 180 s, 300 s, 420 s, and 540 s, and comparing those with the uncoated membrane (0 s).

A longer duration of electrospin-coating PCL on NC membrane increases water contact angle on the surface of the coated membrane **(Figure 4.9)**. It is worth noting that without electrospin-coating (0 s), the water droplet was absorbed by the membrane rapidly and thus no water contact angle can be measured. The contact angle of water droplet increases abruptly with the existence of electrospun PCL fibre. As electrospin-coating time increases from 15 s to 60 s, the contact angle increases gradually. When

electrospin-coating extends longer than 60 s, the water contact angle reaches more than 90°. As PCL nanofibres deposit over the spinning time, the fibre density and the area of contact with the water droplets increase. The rising contact angle indicates the reduced wettability of the surface thus becomes more hydrophobic. Additionally, a thicker layer of PCL nanofibres due to long electrospin-coating time may hinder the absorption of water droplets into the NC layer. The extreme timespan for absorption shows hindering of the capture probe and control probe spreading and immobilisation on the NC membrane, which hampers the signalling and detecting process. Therefore, the electrospun coating duration time was maintained at less than 10 min.

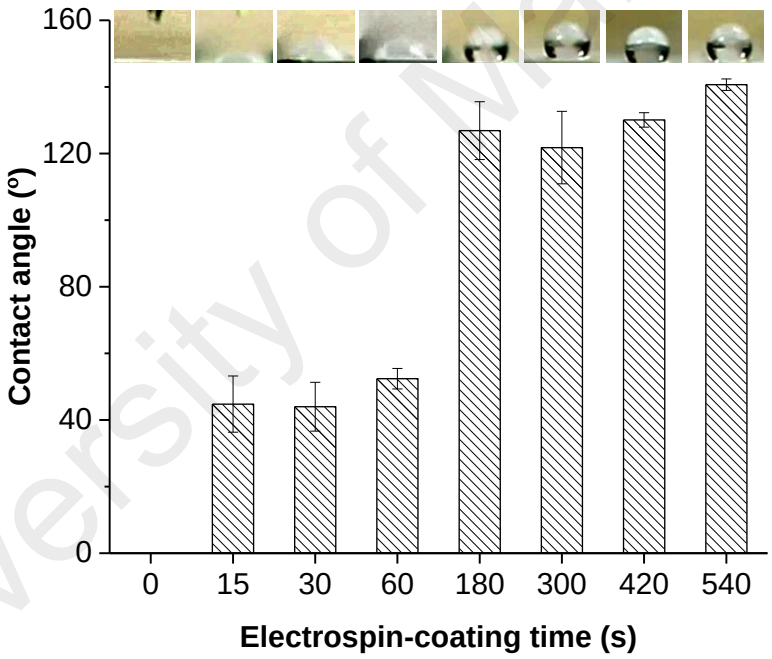

Figure 4.9: Contact angle of water droplet on the surface of NC membrane with different electrospin-coating durations

4.3.1.3 Flow rate measurement

Since sample solution flows laterally in the NC membrane, the rate of the flow determines the signal strength of the assay with respect to the duration of binding between the target particles and all the probes. In **Figure 4.10**, the overall time taken by the lateral flow of solution on NC membrane strip increases with the travelled distance. This is as

presumed according to the relationship in Washburn's equation (Washburn, 1921) (Eq. 4.1),

$$L^2 = \frac{\gamma D \cos\theta}{4\eta} \cdot t \tag{4.1}$$

where L is the length of the liquid has advanced, γ and η are surface tension and viscosity of the liquid respectively, D is the pore diameter, θ is the contact angle between liquid and solid, and t is the time taken for the liquid to advance. Due to capillary forces in NC membrane, the solution travels faster at the beginning (0 cm) and slows down when it reaches the end (3.0 cm).

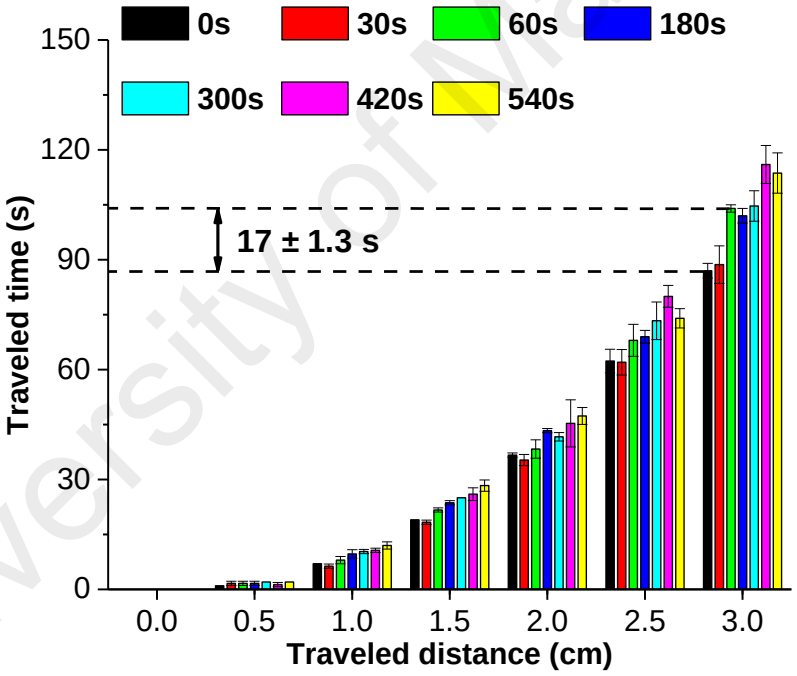

Figure 4.10: Travelling time taken by the liquid on the 3cm long NC membrane with different period of electrospin-coating

The time of travel gradually increases when the solution is reaching the end of the strip. However, the solution takes a longer duration to travel until the end of the strip as the time of electrospin-coating of NC membrane increases. NC membrane, which is electrospin-coated for at least 60 s, takes 17±1.3 s more than an uncoated NC membrane

to travel a 3.0 cm distance ($p<0.05$). According to Washburn's equation (Eq. 4.1), the penetrability of a fluid is derived from $\gamma / \eta \cdot (\cos \theta) /2$ and it equals to the velocity or penetrated distance of a fluid per unit time (Washburn, 1921). By assuming no variations in the liquid properties, the distance travelled by the liquid, L under given time span, t decreases when the liquid-membrane contact angle, θ increases toward 90° due to reducing value of cos θ. In other words, the flow rate reduces due to the increase in liquid-membrane contact angle (**Figure 4.9**). At $\theta > 90°$, the negative value would suggest an opposite motion that represents resistance of flow in both lateral and vertical directions. Therefore, we assume that there is flow resistance caused by the hydrophobic PCL nanofibres on the electrospin-coated NC membrane.

To examine the effect of flow rate on the signal intensity of LFA, we tested the test line optical density (OD) on the LFA strips of different electrospin-coating durations by detecting 5 nM synthetic Zika virus DNA fragment. **Figure 4.11a** indicates the increased signal intensity of test line on LFA with electrospin-coating duration longer than 15s. Among all, the OD of test line for strips with 60 s ($t=8.599$, $p=0.010$), 180 s ($t=14.189$, $p=0.002$) and 300 s ($t=7.228$, $p=0.015$) electrospin-coating have shown significant differences from the strip without electrospin-coating (Student's t-test, $n=3$, relative to 0 s) in **Figure 4.11b**. The OD measured by imaging software has increased about threefold while comparing the test lines of the strip with 60 s electrospin-coating to the strip without coating (0 s). With such results, the enhanced signal OD is relatable to the delayed flow rate that is driven by the presence of PCL nanofibres electrospin-coated on the NC membrane. Because of the hampered water absorption in the highly hydrophobic surface of electrospin-coated membrane, we proceed to sensitivity test with 60 s as our optimum electrospin-coating duration for the LFA.

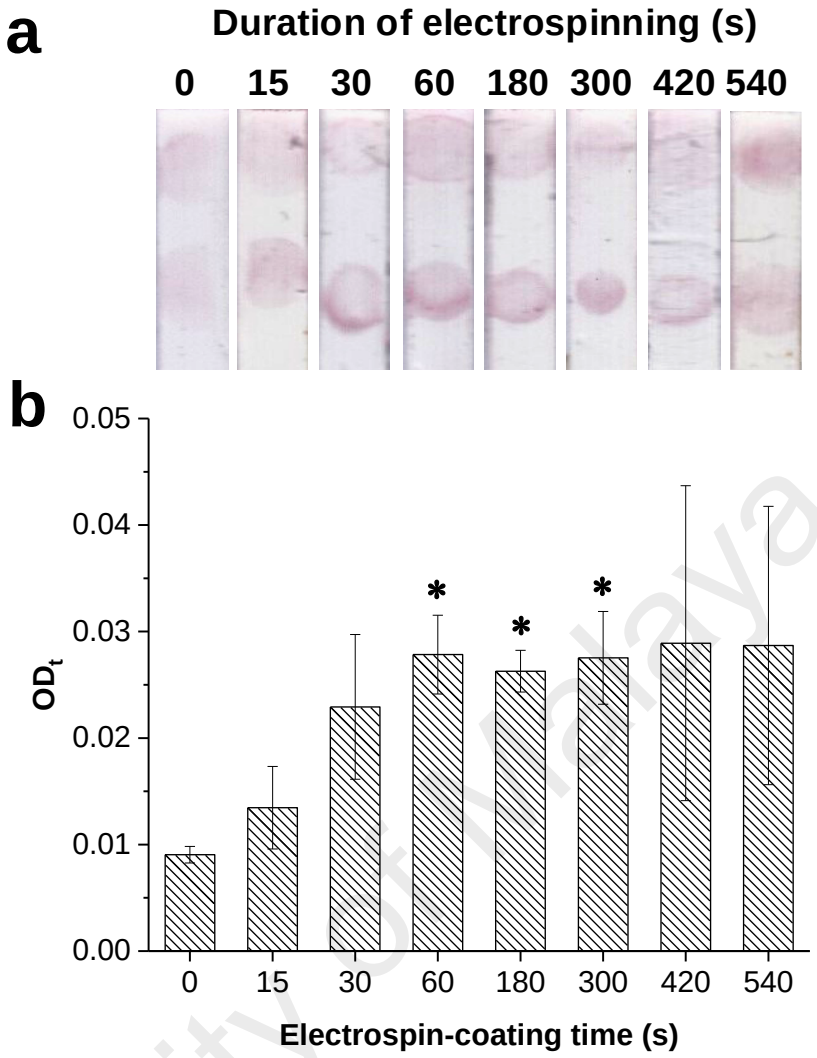

Figure 4.11: Effect of electrospin-coating duration on the optical signal intensity (a) or measured optical density (b) of LFA based on nucleic acid testing

4.3.2 Sensitivity test of electrospin-coated lateral flow assay

To confirm the enhanced sensitivity effect, uncoated and electrospin-coated NC membrane were examined by LFA for synthetic zika virus oligonucleotide at 0 nM (negative control), 0.1 nM, 0.25 nM, 0.5 nM, 1.0 nM and 5 nM. Visually, the signal intensity increases when the target concentration increases as more target particles were captured at the test lines (**Figure 4.12a, b**).

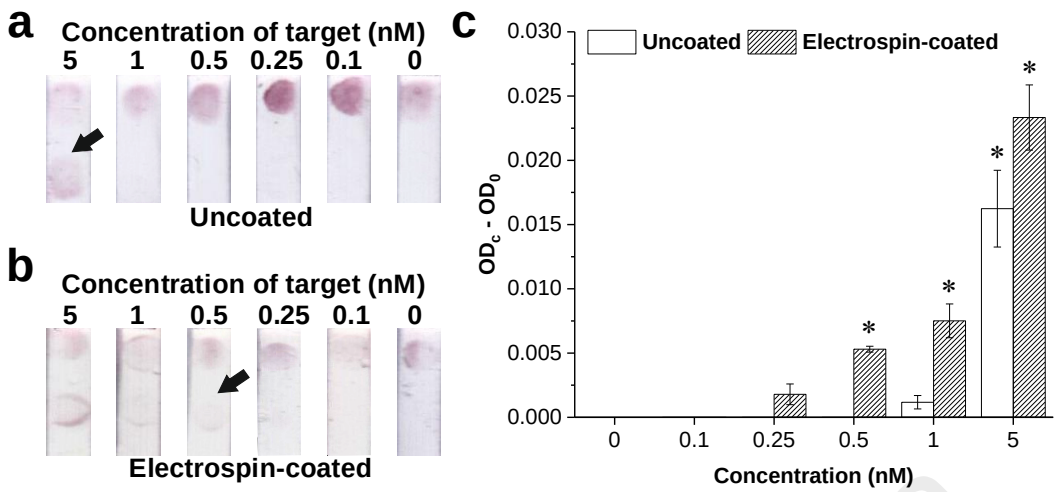

Figure 4.12: Enhancement in sensitivity in LFA with PCL electrospin-coated NC membrane of 60 s

By the naked eye, the LOD of uncoated NC membrane observed in **Figure 4.12a** is 5 nM while the LOD of LFA with electrospin-coated NC membrane observed in **Figure 4.12b** is 0.5 nM. Notably, the designed LFA has produced a tenfold signal enhancement based on the naked eye observation. The OD difference of test lines with the negative control for electrospin-coated and uncoated NC membranes was compared in **Figure 4.12c**. Using software analysis, the LOD of LFA with electrospin-coated ($t=23.20$, $p=0.00185$) and uncoated ($t=5.43$, $p=0.03223$) NC membrane are 0.50 nM and 5.0 nM, respectively. This increase in LOD is consistent with the naked eye observation.

We have demonstrated the electrospin-coating of PCL on NC membrane as a proof of improving signal intensity and sensitivity of LFA by detecting target of low concentration. By electrospin-coating PCL on nitrocellulose membrane, we have exhibited electrospinning as a simple method to modify paper for detection purposes. It neither requires delicate handling during preparation nor additional installation to the assay, such as extra sample volumes, pre-treatment steps, or power supply.

CHAPTER 5: CONCLUSION AND FUTURE WORK

5.1 Conclusions

In the present study, two objectives were set to ameliorate the limit of current paper-based sensors:

i. To develop and optimize a PCS for chemical identification and quantification
ii. To enhance the sensitivity of paper-based assay, *i.e.* LFA by flow manipulation over NC membrane

These two objectives have been fully achieved through the course of the present study. Firstly, a novel paper-based capacitive sensor (PCS) was developed for chemical identification and quantification for water safety purpose. The optimized PCS's geometry had a 40 mm × 10 mm capacitance area, 10 mm × 10 mm loading area and 5mm × 10 mm spacer area. Optimization of conditions during usage of PCSs includes 70 µL of loading volume, 15 minutes of drying and 1 cycle of loading and drying. The usage of PCS was not affected by the location of measurement on the capacitance area and surrounding temperature. Although highly affected by relative humidity, drying was able to get rid of moisture before usage. Capacitance measurement by multimeter has been shown to be comparable to that of LCR meter at 400 Hz and 1 kHz. Identification of standard pure liquid and aqueous chemicals by PCS was possible when as-prepared PCS and pre-dried PCS were used with multimeter, respectively. In-depth differentiation of chemicals was possible by analyzing the peak values of capacitance-frequency spectrum and loss tan-frequency spectrum using LCR meter. On the other hand, quantification of volume fraction of ethanol in ethanol-water solution and concentration of cations in nitrate solutions. Using PCS, the differentiation of cation was possible based on number of valency. Among cations, PCS was most sensitive to Fe(III) solution, which achieved the limit of detection of 1 mM.

Secondly, by using nucleic acid testing in LFA as a model paper-based assay for disease diagnostics, sensitivity is enhanced by manipulating flow in NC membrane with electrospinning PCL. Electrospinning PCL nanofibres onto a 3 cm piece of NC membrane for 60 s creates a hydrophobic layer that slows down the flow of the sample solution by 17±1.3 s. Moreover, this delay time of flow gives an optimal increase in signal intensity for the detection of 5 nM zika virus DNA. In sensitivity assay, a tenfold increase in LOD has been achieved when compared to uncoated NC membrane in LFA. The LOD increases from 5 nM to 0.5 nM, which has been evaluated by software analysis.

5.2 Future work

For the paper capacitive model, it would be of benefit to increase the specificity beyond roughly distinguishing monovalent, divalent and trivalent cations at high concentration, as at present. Future work for the electrospin-coating may include optimising conditions, material selection and functionalization for enhanced detection of different targets in LFA. Due to low degradability of polymeric materials, future work should also be focused on the assessment of long-term storage towards functionality using real clinical samples. Progress is anticipated to be brought by electrospun polymeric materials to enhance sensitivity for a broad range of targets in LFA or other paper-based platforms.

REFERENCES

Acuna-Hidalgo, R., Veltman, J. A., & Hoischen, A. (2016). New insights into the generation and role of de novo mutations in health and disease. *Genome Biol, 17*(1), 241.

Akhgari, A., Heshmati, Z., Afrasiabi Garekani, H., Sadeghi, F., Sabbagh, A., Sharif Makhmalzadeh, B., & Nokhodchi, A. (2017). Indomethacin electrospun nanofibers for colonic drug delivery: In vitro dissolution studies. *Colloids Surf B Biointerfaces, 152*, 29-35.

Allibai Mohanan, V. M., Kacheri Kunnummal, A., & Biju, V. M. N. (2016). Electrochemical sensing of hydroxylamine using a wax impregnated graphite electrode modified with a nanocomposite consisting of ferric oxide and copper hexacyanoferrate. *Microchimica Acta, 183*(6), 2013-2021.

Alothman, Z. A., Unsal, Y. E., Habila, M., Tuzen, M., & Soylak, M. (2014). A membrane filtration procedure for the enrichment, separation, and flame atomic absorption spectrometric determinations of some metals in water, hair, urine, and fish samples. *Desalination and Water Treatment, 53*(13), 3457-3465.

Anfossi, L., Di Nardo, F., Giovannoli, C., Passini, C., & Baggiani, C. (2013). Increased sensitivity of lateral flow immunoassay for ochratoxin A through silver enhancement. *Anal Bioanal Chem, 405*(30), 9859-9867.

Apilux, A., Dungchai, W., Siangproh, W., Praphairaksit, N., Henry, C. S., & Chailapakul, O. (2010). Lab-on-paper with dual electrochemical/colorimetric detection for simultaneous determination of gold and iron. *Anal Chem, 82*(5), 1727-1732.

Arslan, O., & Uyar, T. (2017). Multifunctional electrospun polymeric nanofibrous mats for catalytic reduction, photocatalysis and sensing. *Nanoscale, 9*(27), 9606-9614.

Berney, H., West, J., Haefele, E., Alderman, J., Lane, W., & Collins, J. K. (2000). A DNA diagnostic biosensor: development, characterisation and performance. *Sensors and Actuators B-Chemical, 68*(1-3), 100-108.

Bernhoft, R. A. (2012). Mercury toxicity and treatment: a review of the literature. *J Environ Public Health, 2012*, 460508.

Bhunia, A. K. (2014). One day to one hour: how quickly can foodborne pathogens be detected? *Future microbiology, 9*(8), 935-946.

Bruno, J. G. (2014). Application of DNA Aptamers and Quantum Dots to Lateral Flow Test Strips for Detection of Foodborne Pathogens with Improved Sensitivity versus Colloidal Gold. *Pathogens, 3*(2), 341-355.

Buchko, C. J., Chen, L. C., Shen, Y., & Martin, D. C. (1999). Processing and microstructural characterization of porous biocompatible protein polymer thin films. *Polymer, 40*(26), 7397-7407.

Carabali, M., Hernandez, L. M., Arauz, M. J., Villar, L. A., & Ridde, V. (2015). Why are people with dengue dying? A scoping review of determinants for dengue mortality. *BMC Infect Dis, 15*, 301.

Castaneda, M. T., Alegret, S., & Merkoci, A. (2007). Electrochemical sensing of DNA using gold nanoparticles. *Electroanalysis, 19*(7-8), 743-753.

Chatterjee, A., Santra, M., Won, N., Kim, S., Kim, J. K., Kim, S. B., & Ahn, K. H. (2009). Selective fluorogenic and chromogenic probe for detection of silver ions and silver nanoparticles in aqueous media. *J Am Chem Soc, 131*(6), 2040-2041.

Chen, L., Liu, L., Guo, Q., Wang, Z., Liu, G., Chen, S., & Hou, H. (2017). Preparation of Ni(OH)2nanoplatelet/electrospun carbon nanofiber hybrids for highly sensitive nonenzymatic glucose sensors. *RSC Adv., 7*(31), 19345-19352.

Chen, M., Yu, Z., Liu, D., Peng, T., Liu, K., Wang, S., . . . Lai, W. (2015). Dual gold nanoparticle lateflow immunoassay for sensitive detection of Escherichia coli O157:H7. *Anal Chim Acta, 876*, 71-76.

Cho, I. H., Bhunia, A., & Irudayaraj, J. (2015). Rapid pathogen detection by lateral-flow immunochromatographic assay with gold nanoparticle-assisted enzyme signal amplification. *Int J Food Microbiol, 206*, 60-66.

Choi, J. R., Hu, J., Feng, S., Wan Abas, W. A., Pingguan-Murphy, B., & Xu, F. (2016). Sensitive biomolecule detection in lateral flow assay with a portable temperature-humidity control device. *Biosens Bioelectron, 79*, 98-107.

Choi, J. R., Hu, J., Tang, R., Gong, Y., Feng, S., Ren, H., . . . Xu, F. (2016). An integrated paper-based sample-to-answer biosensor for nucleic acid testing at the point of care. *Lab Chip, 16*(3), 611-621.

Choi, J. R., Liu, Z., Hu, J., Tang, R., Gong, Y., Feng, S., . . . Xu, F. (2016). Polydimethylsiloxane-Paper Hybrid Lateral Flow Assay for Highly Sensitive Point-of-Care Nucleic Acid Testing. *Anal Chem, 88*(12), 6254-6264.

Choi, J. R., Yong, K. W., Tang, R., Gong, Y., Wen, T., Li, F., . . . Xu, F. (2017). Advances and challenges of fully integrated paper-based point-of-care nucleic acid testing. *TrAC Trends in Analytical Chemistry, 93*, 37-50.

Choi, J. R., Yong, K. W., Tang, R., Gong, Y., Wen, T., Yang, H., . . . Xu, F. (2017). Lateral Flow Assay Based on Paper-Hydrogel Hybrid Material for Sensitive Point-of-Care Detection of Dengue Virus. *Adv Healthc Mater, 6*(1).

Clarke, R. N. (n.d.). Dielectric properties of materials 2.6.5. from (http://www.kayelaby.npl.co.uk/general_physics/2_6/2_6_5.html)

Coombes, A. G., Rizzi, S. C., Williamson, M., Barralet, J. E., Downes, S., & Wallace, W. A. (2004). Precipitation casting of polycaprolactone for applications in tissue engineering and drug delivery. *Biomaterials, 25*(2), 315-325.

Cordeiro, M., Ferreira Carlos, F., Pedrosa, P., Lopez, A., & Baptista, P. V. (2016). Gold Nanoparticles for Diagnostics: Advances towards Points of Care. *Diagnostics (Basel), 6*(4).

Dasbasi, T., Sacmaci, S., Ulgen, A., & Kartal, S. (2015). A solid phase extraction procedure for the determination of Cd(II) and Pb(II) ions in food and water samples by flame atomic absorption spectrometry. *Food Chem, 174*, 591-596.

Dawan, S., Kanatharana, P., Wongkittisuksa, B., Limbut, W., Numnuam, A., Limsakul, C., & Thavarungkul, P. (2011). Label-free capacitive immunosensors for ultra-trace detection based on the increase of immobilized antibodies on silver nanoparticles. *Anal Chim Acta, 699*(2), 232-241.

de la Monte, S. M., & Kril, J. J. (2014). Human alcohol-related neuropathology. *Acta Neuropathol, 127*(1), 71-90.

de Oliveira, W. K., de Franca, G. V. A., Carmo, E. H., Duncan, B. B., de Souza Kuchenbecker, R., & Schmidt, M. I. (2017). Infection-related microcephaly after the 2015 and 2016 Zika virus outbreaks in Brazil: a surveillance-based analysis. *Lancet*.

Deitzel, J. M., Kleinmeyer, J., Harris, D., & Tan, N. B. (2001). The effect of processing variables on the morphology of electrospun nanofibers and textiles. *Polymer, 42*(1), 261-272.

Delbeke, S., Ceuppens, S., Holvoet, K., Samuels, E., Sampers, I., & Uyttendaele, M. (2015). Multiplex real-time PCR and culture methods for detection of Shiga toxin-producing Escherichia coli and Salmonella Thompson in strawberries, a lettuce mix and basil. *Int J Food Microbiol, 193*, 1-7.

Dickson, R. P., & Luks, A. M. (2009). Toluene Toxicity as a Cause of Elevated Anion Gap Metabolic Acidosis. *Respiratory Care, 54*(8), 1115-1117.

Dieguez-Acuna, F. J., Polk, W. W., Ellis, M. E., Simmonds, P. L., Kushleika, J. V., & Woods, J. S. (2004). Nuclear factor kappaB activity determines the sensitivity of kidney epithelial cells to apoptosis: implications for mercury-induced renal failure. *Toxicol Sci, 82*(1), 114-123.

Falde, E. J., Yohe, S. T., & Grinstaff, M. W. (2015). Surface Tension Triggered Wetting and Point of Care Sensor Design. *Adv Healthc Mater, 4*(11), 1654-1657.

Fang, Z., Huang, J., Lie, P., Xiao, Z., Ouyang, C., Wu, Q., . . . Zeng, L. (2010). Lateral flow nucleic acid biosensor for Cu2+ detection in aqueous solution with high sensitivity and selectivity. *Chem Commun (Camb), 46*(47), 9043-9045.

Feng, L., Li, H., Niu, L. Y., Guan, Y. S., Duan, C. F., Guan, Y. F., . . . Yang, Q. Z. (2013). A fluorometric paper-based sensor array for the discrimination of heavy-metal ions. *Talanta, 108*, 103-108.

Fernandes Diniz, J. M. B., Gil, M. H., & Castro, J. A. A. M. (2004). Hornification—its origin and interpretation in wood pulps. *Wood Science and Technology, 37*(6), 489-494.

Fongaro, G., Do Nascimento, M. A., Rigotto, C., Ritterbusch, G., da Silva, A. D. A., Esteves, P. A., & Barardi, C. R. (2013). Evaluation and molecular characterization of human adenovirus in drinking water supplies: viral integrity and viability assays. *Virology journal*, *10*(1), 166.

Freidman, E., Greenburg, J., Merrill, J., & Dammin, G. (1962). Consequences of ethylene glycol poisoning. *Am J Med, 32*, 891-902.

Friberg, L., & Vostal, J. (1972). Mercury in the environment: A toxicological and epidemiological appraisal.

Friedenman, H., & Shuler, K. E. (1947). Evidence for the ionic nature of certain crystal lattices. *Journal of Chemical Education*, *24*(1), 11.

Ge, L., Wang, S., Song, X., Ge, S., & Yu, J. (2012). 3D origami-based multifunction-integrated immunodevice: low-cost and multiplexed sandwich chemiluminescence immunoassay on microfluidic paper-based analytical device. *Lab Chip*, *12*(17), 3150-3158.

Gopinathan, J., Mano, S., Elakkiya, V., Pillai, M. M., Sahanand, K. S., Rai, B. K. D., . . . Bhattacharyya, A. (2015). Biomolecule incorporated poly-ε-caprolactone nanofibrous scaffolds for enhanced human meniscal cell attachment and proliferation. *RSC Adv.*, *5*(90), 73552-73561.

Gould, L. H. (2012). Update: Recommendations for Diagnosis of Shiga Toxin-Producing Escherichia coli Infections by Clinical Laboratories. *Clinical Microbiology Newsletter*, *34*(10), 75-83.

Govindhan, M., Lafleur, T., Adhikari, B. R., & Chen, A. C. (2015). Electrochemical Sensor Based on Carbon Nanotubes for the Simultaneous Detection of Phenolic Pollutants. *Electroanalysis*, *27*(4), 902-909.

Goyer, R. A. (1990). Lead toxicity: from overt to subclinical to subtle health effects. *Environ Health Perspect, 86*, 177-181.

Guler, Z., Erkoc, P., & Sarac, A. S. (2015). Electrochemical impedance spectroscopic study of single-stranded DNA-immobilized electroactive polypyrrole-coated electrospun poly(<I>ε</I>-caprolactone) nanofibers. *Materials Express*, *5*(4), 269-279.

Gupta, P., Elkins, C., Long, T. E., & Wilkes, G. L. (2005). Electrospinning of linear homopolymers of poly (methyl methacrylate): exploring relationships between fiber formation, viscosity, molecular weight and concentration in a good solvent. *Polymer*, *46*(13), 4799-4810.

Han, J. W., Kim, B., Li, J., & Meyyappan, M. (2012). Carbon Nanotube Based Humidity Sensor on Cellulose Paper. *Journal of Physical Chemistry C*, *116*(41), 22094-22097.

Hao, J. L., Lei, G. T., Li, Z. H., Wu, L. J., Xiao, Q. Z., & Wang, L. (2013). A novel polyethylene terephthalate nonwoven separator based on electrospinning technique for lithium ion battery. *Journal of Membrane Science*, *428*, 11-16.

Hapuarachchi, H. C., Koo, C., & Ng, L. C. (n.d.). Zika virus isolate 09410 envelope protein gene, partial cds - Nucleotide - NCBI. 2017, from https://www.ncbi.nlm.nih.gov/nuccore/KY921911

Hassell, J. M., Begon, M., Ward, M. J., & Fevre, E. M. (2017). Urbanization and Disease Emergence: Dynamics at the Wildlife-Livestock-Human Interface. *Trends Ecol Evol, 32*(1), 55-67.

Hawkins, K. R., & Weigl, B. H. (2010). Microfluidic diagnostics for low-resource settings. *Microfluidics, bioMEMs, and medical microsystems VIII, 7593*, 75930L75931-75915.

He, S., Liu, D. B., Wang, Z., Cai, K. Y., & Jiang, X. Y. (2011). Utilization of unmodified gold nanoparticles in colorimetric detection. *Science China-Physics Mechanics & Astronomy, 54*(10), 1757-1765.

Hocevar, S. B., Wang, J., Deo, R. P., & Ogorevc, B. (2002). Potentiometric stripping analysis at bismuth‐film electrode. *Electroanalysis, 14*(2), 112-115.

Hossain, S. M., & Brennan, J. D. (2011). beta-Galactosidase-based colorimetric paper sensor for determination of heavy metals. *Anal Chem, 83*(22), 8772-8778.

Hosseini, S., Azari, P., Aeinehvand, M. M., Rothan, H. A., Djordjevic, I., Martinez-Chapa, S. O., & Madou, M. J. (2016). Intrant ELISA: A Novel Approach to Fabrication of Electrospun Fiber Mat-Assisted Biosensor Platforms and Their Integration within Standard Analytical Well Plates. *Applied Sciences-Basel, 6*(11), 336.

Hu, J., Wang, L., Li, F., Han, Y. L., Lin, M., Lu, T. J., & Xu, F. (2013). Oligonucleotide-linked gold nanoparticle aggregates for enhanced sensitivity in lateral flow assays. *Lab Chip, 13*(22), 4352-4357.

Hu, J., Wang, S., Wang, L., Li, F., Pingguan-Murphy, B., Lu, T. J., & Xu, F. (2014). Advances in paper-based point-of-care diagnostics. *Biosens Bioelectron, 54*, 585-597.

Hu, M., Kang, W. M., Zhao, Y. X., Shi, J., & Cheng, B. W. (2017). A fluorescent and colorimetric sensor based on a porphyrin doped polystyrene nanoporous fiber membrane for HCl gas detection. *Rsc Advances, 7*(43), 26849-26856.

Huang, X., Zhan, S., Xu, H., Meng, X., Xiong, Y., & Chen, X. (2016). Ultrasensitive fluorescence immunoassay for detection of ochratoxin A using catalase-mediated fluorescence quenching of CdTe QDs. *Nanoscale, 8*(17), 9390-9397.

Jagner, D. (1978). Instrumental approach to potentiometric stripping analysis of some heavy metals. *Anal Chem, 50*(13), 1924-1929.

Jamal, I., Sam, C., Chan, Y. F., Vythilingam, I., & Sulaiman, W. Y. W. (2016). Zika virus and its potential re-emergence in Malaysia. *Med J Malaysia, 71*(2).

Jiao, H. Z., Zhang, L., Liang, Z. H., Peng, G. H., & Lin, H. W. (2014). Size-controlled sensitivity and selectivity for the fluorometric detection of Ag+ by homocysteine capped CdTe quantum dots. *Microchimica Acta, 181*(11-12), 1393-1399.

Kamsari, S. A. (2014, 23 December). Sungai tercemar teruk, *Utusan Online*. Retrieved from http://www.utusan.com.my/berita/wilayah/kl-putrajaya/sungai-tercemar-teruk-1.40116

Karim, F. N., & Shah, A. (2015, 8 October). Depts confirm contamination, *News Straits Times Online*. Retrieved from http://www.nst.com.my/news/2015/10/depts-confirm-contamination

Karlsson, E. K., Kwiatkowski, D. P., & Sabeti, P. C. (2014). Natural selection and infectious disease in human populations. *Nat Rev Genet, 15*(6), 379-393.

Kim, C. H., Jung, Y. H., Kim, H. Y., Lee, D. R., Dharmaraj, N., & Choi, K. E. (2006). Effect of collector temperature on the porous structure of electrospun fibers. *Macromolecular Research, 14*(1), 59-65.

Kim, H. N., Ren, W. X., Kim, J. S., & Yoon, J. (2012). Fluorescent and colorimetric sensors for detection of lead, cadmium, and mercury ions. *Chem Soc Rev, 41*(8), 3210-3244.

Kirkwood, J. G. (1939). The Dielectric Polarization of Polar Liquids. *The Journal of Chemical Physics, 7*(10), 911-919.

Kumar Reddy, D., & Lee, S. (2012). Water pollution and treatment technologies. *Journal of Environmental & Analytical Toxicology, 2*, e103.

Kwoun, S., Lec, R., Han, B., & Ko, F. (2001). *Polymer nanofiber thin films for biosensor applications.* Paper presented at the Bioengineering Conference, 2001. Proceedings of the IEEE 27th Annual Northeast.

Labet, M., & Thielemans, W. (2009). Synthesis of polycaprolactone: a review. *Chem Soc Rev, 38*(12), 3484-3504.

Lan, M., Guo, Y., Zhao, Y., Liu, Y., Gui, W., & Zhu, G. (2016). Multi-residue detection of pesticides using a sensitive immunochip assay based on nanogold enhancement. *Anal Chim Acta, 938*, 146-155.

Li, D. P., Frey, M. W., & Baeumner, A. J. (2006). Electrospun polylactic acid nanofiber membranes as substrates for biosensor assemblies. *Journal of Membrane Science, 279*(1-2), 354-363.

Li, M., Cao, R., Nilghaz, A., Guan, L., Zhang, X., & Shen, W. (2015). "Periodic-table-style" paper device for monitoring heavy metals in water. *Anal Chem, 87*(5), 2555-2559.

Li, W., Qian, D., Wang, Q., Li, Y., Bao, N., Gu, H., & Yu, C. (2016). Fully-drawn origami paper analytical device for electrochemical detection of glucose. *Sensors and Actuators B: Chemical, 231*, 230-238.

Li, Z. D., Liu, H., Ouyang, C., Wee, W. H., Cui, X. Y., Lu, T. J., . . . Xu, F. (2016). Recent Advances in Pen-Based Writing Electronics and their Emerging Applications. *Advanced Functional Materials, 26*(2), 165-180.

Liana, D. D., Raguse, B., Gooding, J. J., & Chow, E. (2012). Recent advances in paper-based sensors. *Sensors (Basel), 12*(9), 11505-11526.

Lide, D. (2004). *DR 2003–2004 CRC Handbook of Chemistry and Physics*.

Lin, G. Z., Wu, F., Yan, C. H., Li, K., & Liu, X. Y. (2012). Childhood lead poisoning associated with traditional Chinese medicine: a case report and the subsequent lead source inquiry. *Clin Chim Acta, 413*(13-14), 1156-1159.

Lin, Z., Li, X., & Kraatz, H. B. (2011). Impedimetric immobilized DNA-based sensor for simultaneous detection of Pb2+, Ag+, and Hg2+. *Anal Chem, 83*(17), 6896-6901.

Liu, D., Wang, Z., & Jiang, X. (2011). Gold nanoparticles for the colorimetric and fluorescent detection of ions and small organic molecules. *Nanoscale, 3*(4), 1421-1433.

Liu, H., Li, X., & Crooks, R. M. (2013). Paper-based SlipPAD for high-throughput chemical sensing. *Anal Chem, 85*(9), 4263-4267.

Liu, S. J., Nie, H. G., Jiang, J. H., Shen, G. L., & Yu, R. Q. (2009). Electrochemical sensor for mercury(II) based on conformational switch mediated by interstrand cooperative coordination. *Anal Chem, 81*(14), 5724-5730.

Liu, Z., Hu, J., Zhao, Y., Qu, Z., & Xu, F. (2015). Experimental and numerical studies on liquid wicking into filter papers for paper-based diagnostics. *Applied Thermal Engineering, 88*, 280-287.

Lockington, D. A., & Parlange, J. Y. (2003). Anomalous water absorption in porous materials. *Journal of Physics D-Applied Physics, 36*(6), 760-767.

Lötters, J. C., Groenesteijn, J., van der Wouden, E., Sparreboom, W., Lammerink, T. S., & Wiegerink, R. J. (2015). *Fully integrated microfluidic measurement system for real-time determination of gas and liquid mixtures composition.* Paper presented at the Solid-State Sensors, Actuators and Microsystems (TRANSDUCERS), 2015 Transducers-2015 18th International Conference on.

Louvet, A., & Mathurin, P. (2015). Alcoholic liver disease: mechanisms of injury and targeted treatment. *Nat Rev Gastroenterol Hepatol, 12*(4), 231-242.

Luo, Y. L., Nartker, S., Wiederoder, M., Miller, H., Hochhalter, D., Drzal, L. T., & Alocilja, E. C. (2012). Novel Biosensor Based on Electrospun Nanofiber and Magnetic Nanoparticles for the Detection of E. coli O157:H7. *IEEE transactions on nanotechnology, 11*(4), 676-681.

Macagnano, A., Perri, V., Zampetti, E., Bearzotti, A., De Cesare, F., Sprovieri, F., & Pirrone, N. (2017). A smart nanofibrous material for adsorbing and detecting elemental mercury in air. *Atmospheric Chemistry and Physics, 17*(11), 6883-6893.

Makaremi, M., De Silva, R. T., & Pasbakhsh, P. (2015). Electrospun Nanofibrous Membranes of Polyacrylonitrile/Halloysite with Superior Water Filtration Ability. *Journal of Physical Chemistry C, 119*(14), 7949-7958.

Megelski, S., Stephens, J. S., Chase, D. B., & Rabolt, J. F. (2002). Micro-and nanostructured surface morphology on electrospun polymer fibers. *Macromolecules, 35*(22), 8456-8466.

Moghadam, B. Y., Connelly, K. T., & Posner, J. D. (2015). Two orders of magnitude improvement in detection limit of lateral flow assays using isotachophoresis. *Anal Chem, 87*(2), 1009-1017.

Mraovic, M., Muck, T., Pivar, M., Trontelj, J., & Pletersek, A. (2014). Humidity sensors printed on recycled paper and cardboard. *Sensors (Basel), 14*(8), 13628-13643.

Needleman, H. L., & Bellinger, D. (1991). The health effects of low level exposure to lead. *Annu Rev Public Health, 12*(1), 111-140.

Nie, Z., Nijhuis, C. A., Gong, J., Chen, X., Kumachev, A., Martinez, A. W., . . . Whitesides, G. M. (2010). Electrochemical sensing in paper-based microfluidic devices. *Lab Chip, 10*(4), 477-483.

Park, J. H., Byun, J. Y., Yim, S. Y., & Kim, M. G. (2016). A Localized Surface Plasmon Resonance (LSPR)-based, simple, receptor-free and regeneratable Hg(2+) detection system. *J Hazard Mater, 307*, 137-144.

Parolo, C., Medina-Sanchez, M., de la Escosura-Muniz, A., & Merkoci, A. (2013). Simple paper architecture modifications lead to enhanced sensitivity in nanoparticle based lateral flow immunoassays. *Lab Chip, 13*(3), 386-390.

Patel, S. V., Mlsna, T. E., Fruhberger, B., Klaassen, E., Cemalovic, S., & Baselt, D. R. (2003). Chemicapacitive microsensors for volatile organic compound detection. *Sensors and Actuators B-Chemical, 96*(3), 541-553.

Peeling, R. W., Artsob, H., Pelegrino, J. L., Buchy, P., Cardosa, M. J., Devi, S., . . . Yoksan, S. (2010). Evaluation of diagnostic tests: dengue. *Nat Rev Microbiol, 8*(12 Suppl), S30-38.

Peng, J., Wang, Y. W., Liu, L. Q., Kuang, H., Li, A. K., & Xu, C. L. (2016). Multiplex lateral flow immunoassay for five antibiotics detection based on gold nanoparticle aggregations. *Rsc Advances, 6*(10), 7798-7805.

Peterson, G. W., Lu, A. X., & Epps Iii, T. H. (2017). Tuning the Morphology and Activity of Electrospun Polystyrene/ UiO-66-NH2 Metal-Organic Framework Composites to Enhance Chemical Warfare Agent Removal. *ACS Appl Mater Interfaces*.

Pieper, I., Wehe, C. A., Bornhorst, J., Ebert, F., Leffers, L., Holtkamp, M., . . . Schwerdtle, T. (2014). Mechanisms of Hg species induced toxicity in cultured human astrocytes: genotoxicity and DNA-damage response. *Metallomics, 6*(3), 662-671.

Piriya, V. S. A., Joseph, P., Daniel, S. C. G. K., Lakshmanan, S., Kinoshita, T., & Muthusamy, S. (2017). Colorimetric sensors for rapid detection of various analytes. *Mater Sci Eng C Mater Biol Appl, 78*, 1231-1245.

Posthuma-Trumpie, G. A., Korf, J., & van Amerongen, A. (2009). Lateral flow (immuno)assay: its strengths, weaknesses, opportunities and threats. A literature survey. *Anal Bioanal Chem, 393*(2), 569-582.

Qureshi, A., Niazi, J. H., Kallempudi, S., & Gurbuz, Y. (2010). Label-free capacitive biosensor for sensitive detection of multiple biomarkers using gold interdigitated capacitor arrays. *Biosens Bioelectron, 25*(10), 2318-2323.

Rajawat, D. S., Srivastava, S., & Satsangee, S. P. (2012). Electrochemical Determination of Mercury at Trace Levels Using Eichhornia Crassipes Modified Carbon Paste Electrode. *International Journal of Electrochemical Science, 7*(11), 11456-11469.

Reinholt, S. J., Sonnenfeldt, A., Naik, A., Frey, M. W., & Baeumner, A. J. (2014). Developing new materials for paper-based diagnostics using electrospun nanofibers. *Anal Bioanal Chem, 406*(14), 3297-3304.

Reneker, D. H., & Yarin, A. L. (2008). Electrospinning jets and polymer nanofibers. *Polymer, 49*(10), 2387-2425.

Reneker, D. H., Yarin, A. L., Fong, H., & Koombhongse, S. (2000). Bending instability of electrically charged liquid jets of polymer solutions in electrospinning. *Journal of applied physics, 87*(9), 4531-4547.

Rivas, L., Medina-Sanchez, M., de la Escosura-Muniz, A., & Merkoci, A. (2014). Improving sensitivity of gold nanoparticle-based lateral flow assays by using wax-printed pillars as delay barriers of microfluidics. *Lab Chip, 14*(22), 4406-4414.

Roberts, S. (1950). A Theory of Dielectric Polarization in Alkali-Halide Crystals. *Physical Review, 77*(2), 258-263.

Rodriguez, M. O., Covian, L. B., Garcia, A. C., & Blanco-Lopez, M. C. (2016). Silver and gold enhancement methods for lateral flow immunoassays. *Talanta, 148*, 272-278.

Ros-Lis, J. V., Marcos, M. D., Martinez-Manez, R., Rurack, K., & Soto, J. (2005). A regenerative chemodosimeter based on metal-induced dye formation for the highly selective and sensitive optical determination of Hg2+ ions. *Angew Chem Int Ed Engl, 44*(28), 4405-4407.

Rozila, I., Azari, P., Munirah, S., Wan Safwani, W. K., Gan, S. N., Nur Azurah, A. G., . . . Chua, K. H. (2016). Differential osteogenic potential of human adipose-derived stem cells co-cultured with human osteoblasts on polymeric microfiber scaffolds. *J Biomed Mater Res A, 104*(2), 377-387.

Sajid, M., Kawde, A. N., & Daud, M. (2015). Designs, formats and applications of lateral flow assay: A literature review. *Journal of Saudi Chemical Society, 19*(6), 689-705.

Samanman, S., Kanatharana, P., Chotigeat, W., Deachamag, P., & Thavarungkul, P. (2011). Highly sensitive capacitive biosensor for detecting white spot syndrome virus in shrimp pond water. *J Virol Methods, 173*(1), 75-84.

Setayeshmehr, A., Fofana, I., Akbari, A., Borsi, H., & Gockenbach, E. (2008). *Effect of temperature, water content and aging on the dielectric response of oil-impregnated paper.* Paper presented at the Dielectric Liquids, 2008. ICDL 2008. IEEE International Conference on.

Shafie, A., Roslan, M. A., Ngui, R., Lim, Y. A. L., & Sulaiman, W. Y. W. (2016). Mosquito Biology and Mosquito-Borne Disease Awareness among Island Communities in Malaysia. *Journal of the American Mosquito Control Association, 32*(4), 273-281.

Shannon, M. (2003). Severe lead poisoning in pregnancy. *Ambul Pediatr, 3*(1), 37-39.

Shrestha, S., Yeung, C. M., Mills, C. E., Lewington, J., & Tsang, S. C. (2007). Chemically immobilized single-stranded oligonucleotides on praseodymium oxide nanoparticles as an unlabeled DNA sensor probe using impedance. *Angew Chem Int Ed Engl, 46*(21), 3855-3859.

Shuster, G., Baltianski, S., Tsur, Y., & Haick, H. (2011). Utility of Resistance and Capacitance Response in Sensors Based on Monolayer-Capped Metal Nanoparticles. *Journal of Physical Chemistry Letters, 2*(15), 1912-1916.

Subbiah, T., Bhat, G., Tock, R., Parameswaran, S., & Ramkumar, S. (2005). Electrospinning of nanofibers. *Journal of Applied Polymer Science, 96*(2), 557-569.

Sun, J., Xianyu, Y., & Jiang, X. (2014). Point-of-care biochemical assays using gold nanoparticle-implemented microfluidics. *Chem Soc Rev, 43*(17), 6239-6253.

Tang, R., Yang, H., Choi, J. R., Gong, Y., Hu, J., Feng, S., . . . Xu, F. (2016). Improved sensitivity of lateral flow assay using paper-based sample concentration technique. *Talanta, 152*, 269-276.

Tang, R., Yang, H., Gong, Y., Liu, Z., Li, X., Wen, T., . . . Xu, F. (2017). Improved Analytical Sensitivity of Lateral Flow Assay using Sponge for HBV Nucleic Acid Detection. *Sci Rep, 7*(1), 1360.

Taranova, N. A., Byzova, N. A., Zaiko, V. V., Starovoitova, T. A., Vengerov, Y. Y., Zherdev, A. V., & Dzantiev, B. B. (2013). Integration of lateral flow and microarray technologies for multiplex immunoassay: application to the determination of drugs of abuse. *Microchimica Acta, 180*(11-12), 1165-1172.

Tariq, Q. (2015, 30 December 2015). Kuantan residents wake up to a crimson tide after heavy rain, *The Star Newspaper*. Retrieved from http://www.thestar.com.my/news/nation/2015/12/30/black-stone-beach-turns-red-kuantan-residents-wake-up-to-a-crimson-tide-after-heavy-rain/

Thenmozhi, S., Dharmaraj, N., Kadirvelu, K., & Kim, H. Y. (2017). Electrospun nanofibers: New generation materials for advanced applications. *Materials*

Science and Engineering B-Advanced Functional Solid-State Materials, 217, 36-48.

Tobin, R. (2014). Detection of Pesticide Residues in Organic and Conventional Fruits and Vegetables Available in Ireland Using Gas Chromotography/Tandem Mass Spectrometry (GC-MS/MS) and Liquid Chromotography/Tandem Mass Spectrometry (LC-MS/MS) Detection. *Journal of Nutritional Health & Food Science, 2*(1).

Tobin, R., Walsh, T., Garvey, J., & Larkin, T. (2014). Detection of Pesticide Residues in Organic and Conventional Fruits and Vegetables Available in Ireland Using Gas Chromotography/Tandem Mass Spectrometry (GC-MS/MS) and Liquid Chromotography/Tandem Mass Spectrometry (LC-MS/MS) Detection. *J Nutrition Health Food Sci, 2*(1), 7.

Toley, B. J., McKenzie, B., Liang, T., Buser, J. R., Yager, P., & Fu, E. (2013). Tunable-delay shunts for paper microfluidic devices. *Anal Chem, 85*(23), 11545-11552.

Tripatanasuwan, S., Zhong, Z., & Reneker, D. H. (2007). Effect of evaporation and solidification of the charged jet in electrospinning of poly (ethylene oxide) aqueous solution. *Polymer, 48*(19), 5742-5746.

USEPA. (2017a). National Primary Drinking Water Regulations | Ground Water and Drinking Water | US EPA. Retrieved 29 September 2017, from https://www.epa.gov/ground-water-and-drinking-water/national-primary-drinking-water-regulations#Inorganic

USEPA. (2017b, 8 March 2017). Secondary Drinking Water Regulations: Guidance for Nuisance Chemicals | Drinking Water Contaminants – Standards and Regulations | US EPA. Retrieved 29 September 2017, from https://www.epa.gov/dwstandardsregulations/secondary-drinking-water-standards-guidance-nuisance-chemicals#table-of-secondary

Valentine, K., Mastropietro, C., & Sarnaik, A. P. (2009). Infantile iron poisoning: challenges in diagnosis and management. *Pediatr Crit Care Med, 10*(3), e31-33.

Waggoner, J. J., & Pinsky, B. A. (2016). Zika Virus: Diagnostics for an Emerging Pandemic Threat. *J Clin Microbiol, 54*(4), 860-867.

Wang, H., Li, Y. J., Wei, J. F., Xu, J. R., Wang, Y. H., & Zheng, G. X. (2014). Paper-based three-dimensional microfluidic device for monitoring of heavy metals with a camera cell phone. *Anal Bioanal Chem, 406*(12), 2799-2807.

Wang, H., Wang, D., Peng, Z., Tang, W., Li, N., & Liu, F. (2013). Assembly of DNA-functionalized gold nanoparticles on electrospun nanofibers as a fluorescent sensor for nucleic acids. *Chem Commun (Camb), 49*(49), 5568-5570.

Wang, H. M., Tang, W., Wei, H. J., Zhao, Y., Hu, S. C., Guan, Y., . . . Liu, F. (2015). Integrating dye-intercalated DNA dendrimers with electrospun nanofibers: a new fluorescent sensing platform for nucleic acids, proteins, and cells. *Journal of Materials Chemistry B, 3*(17), 3541-3547.

Wang, P. M., & Anderko, A. (2001). Computation of dielectric constants of solvent mixtures and electrolyte solutions. *Fluid Phase Equilibria, 186*(1-2), 103-122.

Wang, X. Y., Drew, C., Lee, S. H., Senecal, K. J., Kumar, J., & Sarnuelson, L. A. (2002). Electrospun nanofibrous membranes for highly sensitive optical sensors. *Nano letters, 2*(11), 1273-1275.

Wang, Y., Wang, L., Xue, J., Dong, J., Cai, J., Hua, X., . . . Liu, F. (2017). Signal-Amplified Lateral Flow Test Strip for Visual Detection of Cu2. *PLoS One, 12*(1), e0169345.

Wannatong, L., Sirivat, A., & Supaphol, P. (2004). Effects of solvents on electrospun polymeric fibers: preliminary study on polystyrene. *Polymer International, 53*(11), 1851-1859.

Washburn, E. W. (1921). The Dynamics of Capillary Flow. *Physical Review, 17*(3), 273-283.

Watanabe, E., Kobara, Y., Baba, K., & Eun, H. (2013). Reduction of hazardous organic solvent in sample preparation for hydrophilic pesticide residues in agricultural products with conventional liquid chromatography. *J Agric Food Chem, 61*(20), 4792-4798.

Wohlfarth, C. (2008). Dielectric constant of the mixture (1) water;(2) ethanol *Supplement to IV/6* (pp. 520-523): Springer.

Wong, S. Y., Cabodi, M., Rolland, J., & Klapperich, C. M. (2014). Evaporative concentration on a paper-based device to concentrate analytes in a biological fluid. *Anal Chem, 86*(24), 11981-11985.

Woodruff, M. A., & Hutmacher, D. W. (2010). The return of a forgotten polymer—polycaprolactone in the 21st century. *Progress in polymer science, 35*(10), 1217-1256.

Worsley, G. J., Attree, S. L., Noble, J. E., & Horgan, A. M. (2012). Rapid duplex immunoassay for wound biomarkers at the point-of-care. *Biosens Bioelectron, 34*(1), 215-220.

Wu, L., Ma, C., Ge, L., Kong, Q., Yan, M., Ge, S., & Yu, J. (2015). Paper-based electrochemiluminescence origami cyto-device for multiple cancer cells detection using porous AuPd alloy as catalytically promoted nanolabels. *Biosens Bioelectron, 63*, 450-457.

Xing, C., Liu, L., Song, S., Feng, M., Kuang, H., & Xu, C. (2015). Ultrasensitive immunochromatographic assay for the simultaneous detection of five chemicals in drinking water. *Biosens Bioelectron, 66*, 445-453.

Yang, F., Duan, J., Li, M., Wang, Z. B., & Guo, Z. Y. (2012). Visual and On-site Detection of Mercury(II) Ions on Lateral Flow Strips Using DNA-functionalized Gold Nanoparticles. *Analytical Sciences, 28*(4), 333-338.

Yarin, A. L., Koombhongse, S., & Reneker, D. H. (2001). Taylor cone and jetting from liquid droplets in electrospinning of nanofibers. *Journal of applied physics, 90*(9), 4836-4846.

Yetisen, A. K., Akram, M. S., & Lowe, C. R. (2013). Paper-based microfluidic point-of-care diagnostic devices. *Lab Chip, 13*(12), 2210-2251.

Yu, L., Shi, Z., Fang, C., Zhang, Y., Liu, Y., & Li, C. (2015). Disposable lateral flow-through strip for smartphone-camera to quantitatively detect alkaline phosphatase activity in milk. *Biosens Bioelectron, 69*, 307-315.

Zeng, S., Baillargeat, D., Ho, H. P., & Yong, K. T. (2014). Nanomaterials enhanced surface plasmon resonance for biological and chemical sensing applications. *Chem Soc Rev, 43*(10), 3426-3452.

Zhang, M., Ge, L., Ge, S., Yan, M., Yu, J., Huang, J., & Liu, S. (2013). Three-dimensional paper-based electrochemiluminescence device for simultaneous detection of Pb2+ and Hg2+ based on potential-control technique. *Biosens Bioelectron, 41*, 544-550.

Zhang, Y., Zuo, P., & Ye, B. C. (2015). A low-cost and simple paper-based microfluidic device for simultaneous multiplex determination of different types of chemical contaminants in food. *Biosens Bioelectron, 68*, 14-19.

Zhang, Y. A., Zhong, C., Zhang, Q. Y., Chen, B. B., He, M., & Hu, B. (2015). Graphene oxide-TiO2 composite as a novel adsorbent for the preconcentration of heavy metals and rare earth elements in environmental samples followed by on-line inductively coupled plasma optical emission spectrometry detection. *Rsc Advances, 5*(8), 5996-6005.

Zhao, G. R., Huang, B. S., Zhang, J. X., Wang, A. C., Ren, K. L., & Wang, Z. L. (2017). Electrospun Poly(l-Lactic Acid) Nanofibers for Nanogenerator and Diagnostic Sensor Applications. *Macromolecular Materials and Engineering, 302*(5), 1600476.

Zhao, S., Wu, X., Wang, L., & Huang, Y. (2004). Electrospinning of ethyl–cyanoethyl cellulose/tetrahydrofuran solutions. *Journal of Applied Polymer Science, 91*(1), 242-246.

Zheng, W., Li, J., & Zheng, Y. F. (2008). An amperometric biosensor based on hemoglobin immobilized in poly(epsilon-caprolactone) film and its application. *Biosens Bioelectron, 23*(10), 1562-1566.

Zhu, Z., Su, Y., Li, J., Li, D., Zhang, J., Song, S., . . . Fan, C. (2009). Highly sensitive electrochemical sensor for mercury(II) ions by using a mercury-specific oligonucleotide probe and gold nanoparticle-based amplification. *Anal Chem, 81*(18), 7660-7666.

Zuo, W., Zhu, M., Yang, W., Yu, H., Chen, Y., & Zhang, Y. (2005). Experimental study on relationship between jet instability and formation of beaded fibers during electrospinning. *Polymer Engineering & Science, 45*(5), 704-709.

LIST OF PUBLICATIONS

1. Hu, J., **Yew, C. H. T.**, Chen, X., Feng, S., Yang, Q., Wang, S., ..., Xu, F*. (2017). Paper-based Capacitive Sensors for Identification and Quantification of Chemicals at the Point of Care. *Talanta*, *165*, 419-428.

2. **Yew, C. H. T.**, Azari, P., Choi, J. R., Li, F., & Pingguan-Murphy, B. (2018). Electrospin-coating of nitrocellulose membrane enhances sensitivity in nucleic acid-based lateral flow assay. *Analytica chimica acta*, *1009*, 81-88.